

# Resilience of a precise motor behavior

Thesis by  
Zsofia Torok

In Partial Fulfillment of the Requirements for  
the Degree of  
Doctor of Philosophy in Neurobiology

CALIFORNIA INSTITUTE OF TECHNOLOGY  
Pasadena, California

2023  
(Defended October 25<sup>th</sup>, 2022)

© 2023

Rights statement (All rights reserved)

Zsofia Torok

ORCID: 0000-0001-6298-9940

## ACKNOWLEDGEMENTS

I would like to thank my advisor Carlos Lois, for guidance and support throughout my graduate school years. Thank you to my collaborators on my first paper draft: Shelyn Wongso, Bo Wang, Alison Duffy, Adrienne Fairhall, and David Bell. Thank you to my collaborators on my second manuscript: Laura Luebbert, Walter Gonzalez, Alex Nevue , Jordan Feldman, and Claudio Mello.

Special thanks to my committee members; Marianne Bronner, Lior Pachter, and Athanassios Siapas, who have provided me with great scientific feedback throughout the years.

## ABSTRACT

Motor memory retention is an essential part of survival and reproduction of most species. However, these behaviors are variable and hard to measure. The zebra finch provides a great model organism to study motor behavior on a fine scale and ask fundamentally important questions. Zebra finch males learn their song from their father and once learnt this song remains unchanged for the remainder of the animals' life. This highly stereotypic and precise motor function engages a handful of motor nuclei organized in a spatially spread out manner that allows for precise targeting of each key circuit participant for the production of the behavior. In my studies, I focus on better understanding the role of excitatory and inhibitory neurons in the pre-motor nucleus of the song production system. The goal was to perturb the precision of behavioral execution by collapsing the neuronal circuit responsible for sequential activity. Then, to study if the behavior could re-establish in an adult less plastic state of neuronal organization. After I have shown that motor function recovers to produce the same song post disruption, I investigated the large and small scale changes in neuronal activity and transcriptomics accompanying this degradation and recovery trajectory. I have learned that loss of inhibition leads to hyperactivation which eventually leads to a circuit level homeostatic compensation to shut down the pathological activity level. In addition, the upregulation of MHC1 receptors and microglia points to a homeostatic mechanism for synaptic reorganization and re-establishment. Now that we have the means to execute precise cell-type specific manipulations that are reversible and that we understand the underlying phenomenology of perturbation and recovery, we can ask many questions about the architecture of a highly resilient motor pathway. This could shine light on specific electrophysiological and molecular candidates to study for brain damage repair and neurodegenerative research.

## PUBLISHED CONTENT AND CONTRIBUTIONS

My first manuscript on the project that involved muting projection neurons in a pre-motor area was published on bioRxiv and is currently in review at Nature. In this work, I was responsible for behavioral manipulations to mute projection neurons and for the song prevention experimental paradigm. These key findings showed that an adult pre-motor circuit can recover from the permanent inactivation of a large portion of its excitatory neurons. In addition, I found that re-establishment of the behavior happens mostly offline, meaning without the need to practice the motor action. This work is detailed in Chapter 2, with methodology in Chapter 4 and the full manuscript is attached as Appendix C.

Wang, B.\*, Torok, Z.\*, Duffy, A.\*, Bell, D., Wongso, S., Velho, T., Fairhall, A., Lois, C. *Unsupervised Restoration of a Complex Learned Behavior After Large-scale Neuronal Perturbation*. bioRxiv. DOI: <https://doi.org/10.1101/2022.09.09.507372>.

The second publication was in collaboration with Adrienne Fairhall's lab as well as the first published work. In this project, I contributed behavioral data and behavioral observations to provide the foundation for the modeling work done by my co-authors. The pre-print is attached as Appendix D.

Pang, R., Duffy, A., Bell, D., Torok, Z., Fairhall, A. *Precision motor timing via scalar input fluctuations*. bioRxiv. DOI: <https://doi.org/10.1101/2022.05.18.492498>.

## TABLE OF CONTENTS

Acknowledgements.....	iv
Abstract .....	v
Published Content and Contributions.....	vi
Table of Contents.....	vii
Nomenclature.....	ix
Chapter I: Introduction.....	1
Song motor circuit in zebra finches .....	3
Learning and memory maintenance.....	4
Chapter II: Adult song stability.....	5
Behavioral degradation and recovery .....	6
Circuit level assessment of recovery .....	9
Chapter III: Molecular mechanisms for recovery.....	10
Behavior .....	11
Electrophysiology .....	13
Transcriptomic changes .....	20
Findings and discussion .....	37
Chapter IV: Methodology I.....	38
Methodology II.....	42
Chapter V: Pilot experiments.....	48
Summary and discussion of thesis work.....	51
Bibliography .....	55
Appendix A .....	59
Appendix B.....	75
Appendix C.....	79
Appendix D .....	106

## NOMENCLATURE

**SONG CIRCUIT.** Series of song nuclei in the song bird brain. The bird brain lacks the mammalian cortical layer, therefore many cortical-like areas (like HVC) are organized into nuclei. There is a motor circuit consisting of a series of nuclei that lead to control and innervation of the syringeal muscles to produce sound. There is an anterior forebrain pathway (AFP) that include auditory and motor nuclei that are responsible for proper song learning and adult song maintenance via auditory feedback. The role of AFP decreases with the age of the animals, as the song becomes more stereotyped and less variable.

**SYLLABLE.** The smallest unit of vocalization that song birds produce, these millisecond-long sounds have certain characterizing features that tells them apart. Zebra finches usually sing a handful of different syllables in a fixed order.

**MOTIF.** The unit of vocalization that is made up of a series of syllables in a fixed order. They comprise the motif that is about half a second long.

**INTRODUCTORY NOTES.** The first couple of syllable-like vocalizations leading up to the start of the motif sequence.

**BOUT.** It is the unit of vocally active period, where the zebra finch repeats many motifs that follow each other with some call-like syllables inserted in between most motifs.

**HVC.** The proper name of the pre-motor cortical nuclei responsible for song production in song birds. This is a bilateral nucleus, so both hemispheres has one.

**RA.** The robust nucleus of the archistriatum is the motor nucleus that is being driven by HVC to produce song. It is also a bilateral nucleus so each hemisphere has one. HVC-Ra neurons within HVC fire very precisely only one during adult song production, which is believed to control the stereotypy and accuracy of song production. There is adult neurogenesis of HVC-Ra neurons, which means that older animals have a larger pool of these pre-motor neurons and produce a more accurate song.

**LMAN.** The lateral magnocellular nucleus of the anterior neostriatum. This nucleus is responsible for variable song production during song learning and introduces acoustic variability into adult song syllables.

**Area X.** This bilateral auditory motor area is important for proper song learning. It projects to HVC where HVC-X neurons are born before the animals hatch and they claim to have the function of adjusting the copy of the tutor song based on auditory feedback during practice in juveniles. These HVC-X neurons fire multiple times during adult song production, but there seems to be no essential function associated with them.

*Chapter 1*

## THE SONG MOTOR CIRCUIT IN ZEBRA FINCHES

Song birds lack the mammalian cortical organization, however their motor circuit for song production is organized into distinct nuclei distributed throughout their brain (Reiner et al., 2004). The pre-motor nucleus HVC (actual name) drives the firing in RA (the motor nuclei) that then eventually drives nucleus XVII that innervates the syrinx muscles to give rise to vocalization. This circuitry is only fully functional in adult male animals.

Juvenile male zebra finches learn the song from their father. This learning trajectory has a sensory and a sensorimotor phase (Bohner, 1983). Once the juvenile male hits sexual maturity (90-120 days post hatch), the song crystallizes. Crystallization means that the sounds produced become highly stereotypical with repetition of the same set of syllables in the same order. These syllables form the motif that then gets repeated several times in a bout which is the unit of vocally active periods. This song that was learned from the father through vocal babbling of unstructured vocalizations, once crystallized, stay the same for the life of the animal. As male birds age their songs become more stereotypic and more inviting to females. This means that memory is not only stored but actively updated and improved while the brain ages (Leonardo & Konishi, 1999). This is a remarkable phenomenon of a motor circuit perfecting itself instead of deteriorating in the aging process.

In order to understand the robustness of this adult motor circuitry, I aimed to study the boundaries of restoration of this circuit after major disruption. To this end, I used viral vectors to deliver tetanus toxin into the pre-motor nucleus HVC of the adult male zebra finches. Tetanus toxin is an enzyme that cleaves synaptobrevin which is a protein essential for vesicle docking and neurotransmitter release in neurons. Upon the presence of tetanus toxin in a neuron, the cell will be unable to release neurotransmitter, therefore becoming muted and unable to communicate with its post-synaptic partners (Sweeney et al., 1995). Although this tetanus toxin carrying neuron is unable to communicate with its synaptic partners, it is able to fire action potentials.

To be able to detect the presence of tetanus toxin in the neurons infected with virus, the construct also carries GFP fused to tetanus toxin. This allows for easy detection of neurons affected by the manipulation over long periods of time. The next step was to find the appropriate viruses to deliver our toxin of interest, as well as, to try to use cell-type specific manipulations. First, I started using lentivirus containing tetanus toxin-GFP with a generic promoter to allow for broad labelling of cells. In past experiments conducted in our lab, we saw that lentivirus seems to be selective in infecting excitatory neurons in the pre-motor nucleus HVC. This allowed for specific manipulation of excitatory neurons of this circuit. The advantage of lentivirus is that it does not diffuse very far and that the expression of the construct is very rapid

(within 24-48 hours). In addition, lentiviruses integrate into the genome of the host cell, which means the neurons infected will not be carrying the toxin until they die (Durand & Cimarelli, 2011). The downside of this manipulation is that given the small diffusion and infection rate, one needs to deliver large amount of viral volume with very high infectious particle counts for it to be effective.

Second, to be able to manipulate the inhibitory neurons of the same circuit, we needed to find a virus that is able to infect them, as well as a promoter that is specific for this type of neurons. To this end, I used AAV9-dlx carrying the same tetanus toxin-GFP. There are several differences in this manipulation, one being that AAVs diffuse broadly and label many more cells (Dayton et al., 2012). However, in our case the promoter that is selective for interneurons limits the effect of the virus. Moreover, the amount of viral volume is significantly smaller than with lentiviral manipulation. The timeline for expressing the viral DNA is around 10 days, but in our case one copy of the enzyme tetanus toxin is sufficient per cell so the desired effects could start relatively early in the replication cycle. AAVs do not integrate into the genome of the host, so with time windows of 6 months, it is possible to completely clear the viral DNA out of the neurons.

One fascinating aspect of this distributed organization is that we can manipulate very precisely each point of the motor circuit without concern for potential direct changes caused by diffusion of viruses into brain areas. This is due to the physical distance of the brain nuclei from each other meaning that the downstream motor pathway will be altered due to the local changes induced in higher brain areas as opposed to a side effect of physically being close to the other brain area.

In previous studies using local cooling devices directly on top of the pre-motor nucleus HVC since this is a very superficial brain area,  $\sim 0.2-0.4 \mu\text{m}$  below the dura, it has been proposed that the length (in msec) of the song and its syllables are the information stored in this local circuitry (Long & Fee, 2009). Acute head fixed recordings within the area also showed that HVC-Ra projecting neurons (pre-motor neurons driving song behavior) fire only when the animal sings and only once during the song at the same position in repeated trials (Kozhevnikov & Fee, 2007). This high level precision on the neuronal level and the finding that the timing of the song was distorted by cooling was attributed to this area. In an attempt to disrupt this strict firing pattern of pre-motor neurons, we used the previously described viral delivery of tetanus toxin.

Previously researchers manipulated this pre-motor nuclei and have found that upon small local electrical lesions of HVC, the song of the animal degrades and recovers within 7 days (Thompson & Johnson, 2005). There are some missing aspects of this disruption, one being that the lesion site could damage axonal paths passing by that could have indirect effects on other brain areas that are not the focus of this study. The level of loss of stereotypic song production is also not severe and lasts for very few days. In addition, this manipulation does not address the important role of neuronal cell types in the circuit. Nevertheless, these publications gave a good background and putative expectations, for future experimental design of my studies of the same brain area.

In summary, I aimed to understand the dynamics of the pre-motor nuclei that enables the precise and robust execution of a learned motor behavior that withstands neuronal death and aging. To this end, I first investigated the behavioral level changes upon targeted perturbation of neuronal groups in the pre-motor nucleus, as well as the effect on the neuronal and circuit level electrophysiology and transcriptome.

## Chapter 2

### PERMANENT GENETIC MANIPULATION OF PROJECTION NEURONS IN A PRE-MOTOR AREA

First, I investigated the effect of muting excitatory neurons in the HVC of adult male zebra finches. Animals were injected with a fluorescent retrograde tracer to allow precise targeting with the viral injection based on fluorescent signal in HVC. I used lentivirus to deliver tetanus-GFP into excitatory neurons of this pre-motor nuclei. Within 24 hours after viral injection, the song of the adult male zebra finches started to shift. The acoustic and temporal parameters of the vocalization completely degraded and the vocally active periods lost all stereotypy. After about 10-14 days, the same intact stereotypic song the bird possessed pre-perturbation re-emerged. This is a phenomena that is very surprising, how an adult pre-motor area can re-structure and reform connections, to allow for the precise execution of a learned behavior.

To quantify the changes in song throughout the manipulation, my collaborator Alison Duffy developed, custom Matlab code to look at acoustic and temporal features. Before the vocalizations were analyzed, I manually curated the dataset into segments of vocally active periods (song degradation made identification of bird sound challenging). From this analysis, we see that the acoustic similarity of degraded syllables to pre-manipulation ones severely decreases and then slowly re-establishes. In terms of the length of syllables, we see a significant shift to shorter vocalizations that are disordered. One interesting finding is that the most acoustically complex syllables ( that tend to be in the middle of the song sequence) recover the fastest. However, the acoustically simple call-like syllables have a much harder time to regain their original space in the song. This suggests a model in which the more complex syllables might have a stronger representation in the brain ( more redundant networks of neurons allocated for that same behavior).

In addition, the recovered song seems to be produced with more stereotypy from rendition to rendition. This suggests a network of neurons in which there is a lot of redundancy, meaning many neurons are tasked to produce the same part of the vocalization. Since these neurons are slightly different, you can get similar behavioral output by using many combinations of patterns of activity. However, when we mute a large portion of these excitatory neurons, this redundancy decreases in size, therefore the song is produced the only way it possibly can.

The level of recovery of the behavior is surprising, therefore, I wonder whether the animal needs to re-learn the song or this mechanism of re-establishment of the circuit is completely independent from juvenile learning. To address this question, I prevented the animals from singing after muting a large proportion of excitatory neurons in HVC. The length of the song prevention was 10 days, which is how long it usually takes for the animals to recover the pre-manipulation behavior. The results show that much of the restoration of the circuit happens unsupervised. After 10 days of song prevention the animals were able to produce

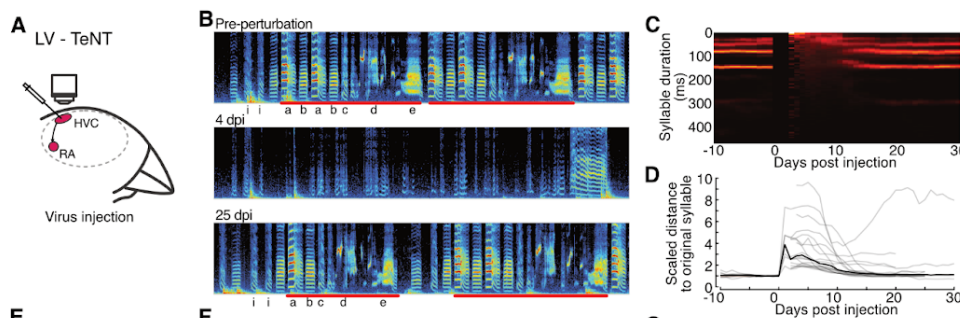
highly stereotypic song similar to their original vocalization. However, the acoustic features needed some fine tuning after song prevention. This could be since we de-coupled the auditory feedback from the circuit for so long that the bird became “rusty” at producing its own song.

While I focused on the behavioral manipulations of this project, a postdoc in my lab Bo Wang performed brain slice patch clamp recordings to assess the changes in connectivity among HVC neurons. His finding showed that the excitatory pre-motor neurons that did not get muted (had no GFP) receive much more excitatory input and much less inhibitory input.

From the two observations we concluded that most of the recovery happens unsupervised and that the neurons unaffected by the manipulation step in to restore the activity. Our collaborator built a computational model based on these experimental observations. This model suggests that within HVC there has to be single cell and homeostatic mechanisms that allow for rapid unsupervised recovery of the motor sequence. In addition, the activation of a pool of neurons that were silent prior to the manipulation are needed to fully restore the circuit level activity.

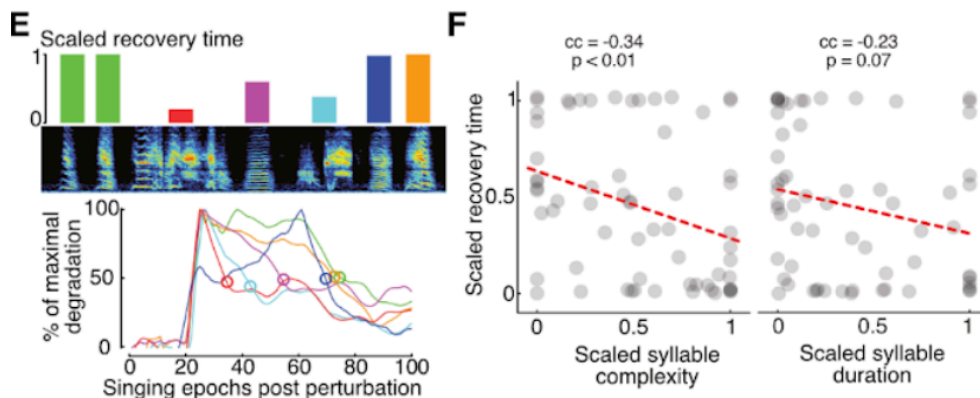
Figures showing the observations detailed in the previous text, all figures are altered or directly taken from Wang et al., 2022:

1. Showing the song degradation and recovery after muting excitatory neurons in the pre-motor nucleus HVC:



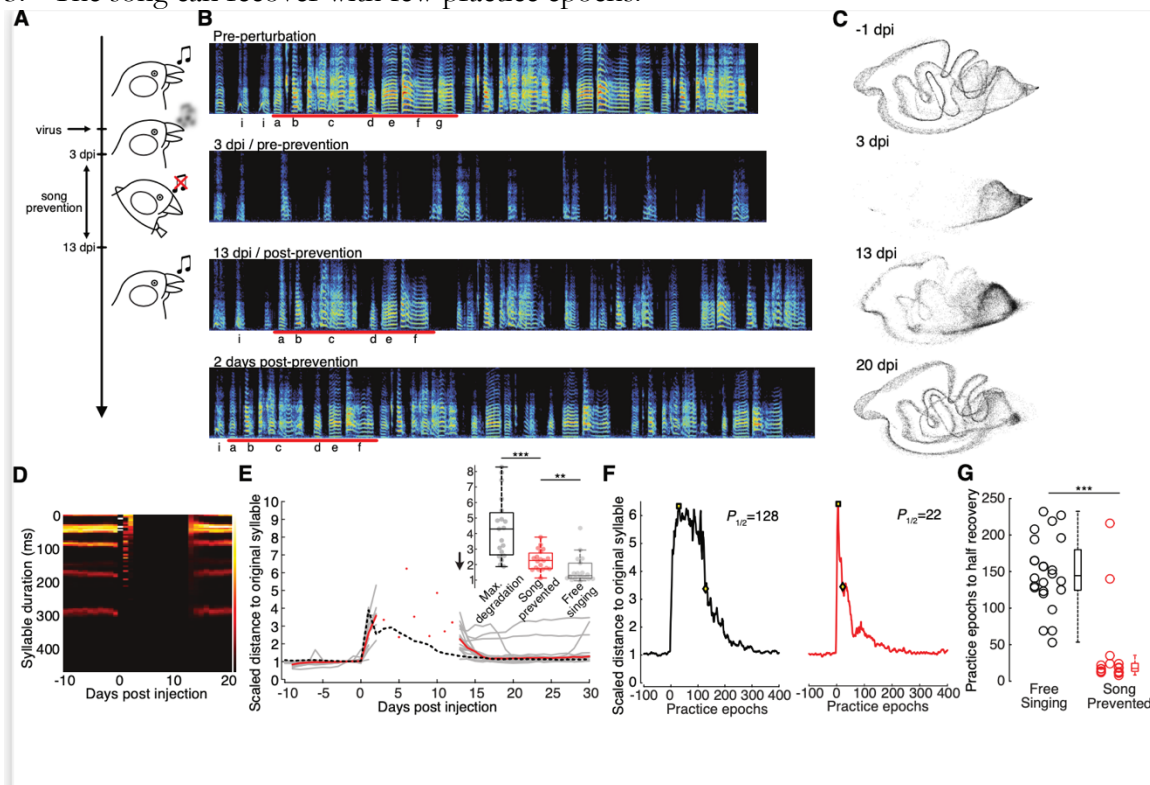
**A**, Schematic drawing illustrating the visual guided virus delivery into HVC (see Methods); **B**, Example spectrograms of the song of a bird injected with LV-TeNT. The song motifs containing the syllables (abcde) are marked by red lines, and can be seen before perturbation and after recovery; **C**, Plot of the distribution of syllable durations (per day) from the bird shown in B; **D**, Plots of scaled distance to original syllables (gray lines) from birds with LV-TeNT ( $n = 4$ ). Black line shows the median of all syllables.

## 2. More acoustically complex syllables recover faster:



**E**, (top) Spectrogram of one song motif and relative recovery time of each of its syllables indicated by the height of the bars. (bottom) Recovery trajectories of the syllables color coded as on top of the spectrogram with the 50% recovery point marked with open circles; **F**, Scatter plots of recovery time against syllable complexity and duration. (Data from LV-TeNT birds combined). Dashed red lines are linear fits.  $cc$  = Pearson correlation coefficient.  $N = 11$ .

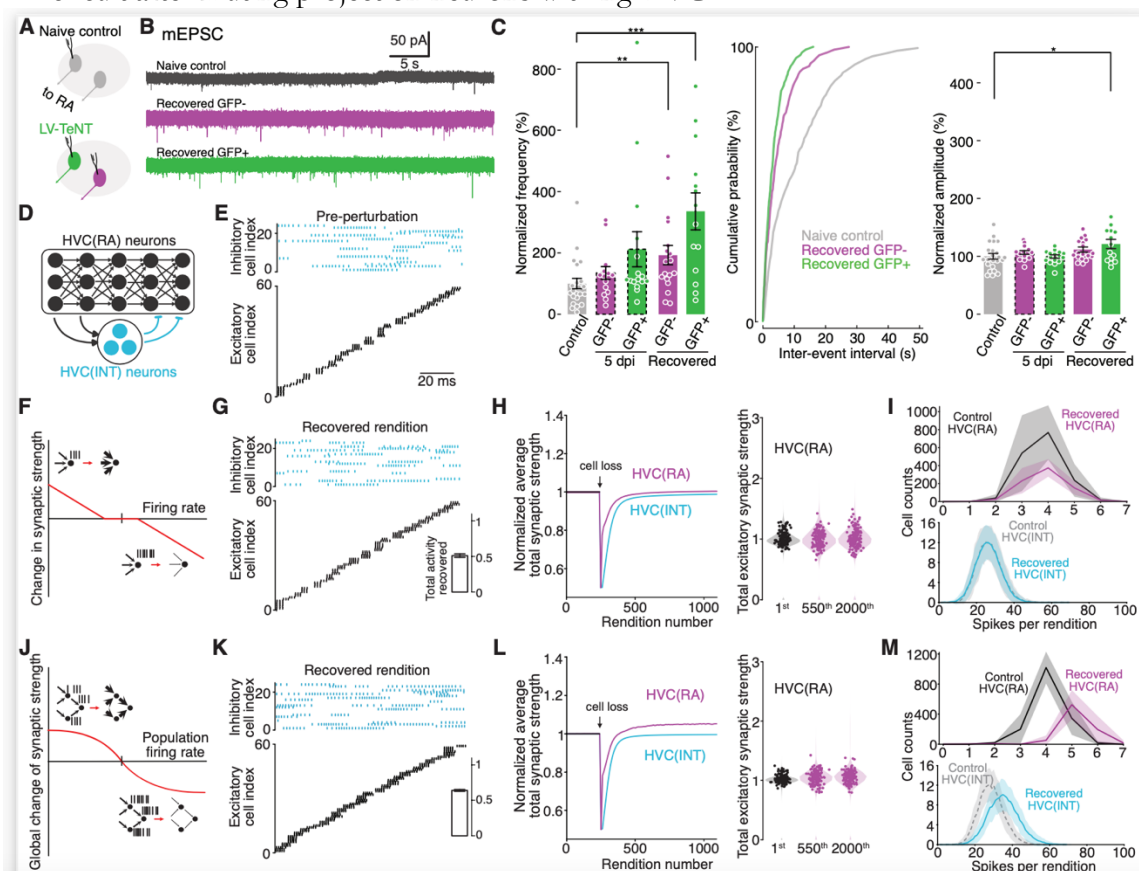
## 3. The song can recover with few practice epochs:



**A**, Schematic illustrating the experimental procedure of perturbation with LV-TeNT and song prevention; **B**, Example spectrograms of a bird injected with LV-TeNT and

prevented from singing for 10 days. On the first day after song prevention (“post-prevention”) the song was partially recovered and syllables were good enough to match to those of unperturbed song (“pre-perturbation”); **C**, UMAP visualizations of songs of the same bird shown in **B**; **D**, Distribution of syllable durations per day; **E**, Plots of distance to original syllables of all birds prevented from singing (gray lines). Red line is the median. The red scattered dots during the song prevention period (3 to 13 dpi) represent the median of syllable distances from the rare occasional songs produced during this time. Prevented animals sang fewer than 8 songs per animal versus more than 5,000 songs per animal for the freely singing animals during the 10 day prevention period. Dashed line shows the song trajectory of freely singing birds, adapted from Fig. 1D. Inset, comparison of syllable recovery at 13 dpi (prevented & free singing) to maximal degradation day; **F**, Example plots of syllable recovery vs number of practice epochs with or without prevention; **G**, Group data of the number of practice epochs to reach half recovery of each syllable.  $n = 4$  (free singing) & 3 (song prevented). \*\*,  $p < 0.01$ . \*\*\*,  $p < 0.001$ . Rank sum test.

4. Electrophysiological changes and modeling showing a suggested route of recovery in the circuit after muting projection neurons with HVC:



**A**, Schematic illustrating whole-cell recordings were made in HVC(RA) neurons in birds injected with LV-TeNT or naive controls (no virus); **B**, Example traces of mEPSC recordings; **C**, Group data of mEPSCs.  $N = 23/4$  (Control),  $15/3$  (5 dpi GFP-),  $16/4$  (5 dpi GFP+),  $18/4$  (Recovered GFP-), &

14/4 (Recovered GFP+). \*,  $p < 0.05$ . \*\*,  $p < 0.01$ . \*\*\*,  $p < 0.001$ ; **D**, Schematic of the neuronal organization in our model; **E**, Spike raster plots showing the sequential dynamics generated by HVC cells; **F-Q**, Recovery of the model network after 50% loss of excitatory cells after implementing different mechanisms. When single-cell homeostatic plasticity was implemented (**F-I**), when both single-cell and population-level homeostatic plasticity were implemented (**J-M**) or when initially inactive neurons were recruited (**N-Q**); **F, J, N**, Schematics illustrating each type of mechanisms implemented; **G, K, O**, Spike raster plots of the recovered dynamics. Insets show the total recovered activity of all functional HVC(RA) neurons normalized to pre-perturbation. Red rasters in panel O represent the firing of originally inactive neurons that were recruited into the network; **H, L, P**, (Left panels) Plots of the averaged total excitatory synaptic input per neuron against renditions. (Right panels) Plots showing the normalized total excitatory synaptic input received by HVC(RA) neurons at three times: before perturbation (1<sup>st</sup> rendition), during reorganization (550<sup>th</sup>), and recovered; **I, M, Q**, Density distribution plots of the number of spikes per neuron per rendition, before perturbation (Control) and after recovery (ina., inactive cells).

These experiments allowed us to understand some fundamental aspects of the circuit, nevertheless, there were some experimental caveats that pushed me to explore other avenues.

One main limitation of this experiment is the inefficiency of lentiviruses to infect neurons in the bird brain. In order to achieve behavioral changes, one has to inject a large volume of virus with a very high infection rate. This also proves how resilient this circuit is since most brain areas microinjected with a bulk of fluid would show behavioral changes.

*Chapter 3*GENETIC MANIPULATION OF INTERNEURONS IN AN ADULT  
PRE-MOTOR AREA

To further investigate the resilience of the pre-motor nucleus, I set out to mute the inhibitory tone to see whether the circuit could overcome the drastic loss of inhibition. Previous work showed that structured inhibition is a key feature of adult song production (Kosche et al., 2015). During juvenile song learning, the emergence of structured inhibition allows for protection of stabilized song segments during the learning process (Vallentin et al., 2016). This phenomena contributes to the stereotypy of the adult song. Muting a large population of interneurons resembles seizure-like activity in brain circuits that are an important aspect of circuit malfunction in humans (Dehghani et al., 2016). The behavioral changes after muting inhibitory neurons in HVC are much more drastic and take longer to recover than muting excitatory neurons of the same circuit. One explanation why this is that the viral vector used to deliver tetanus toxin (that blocks exocytosis and neurotransmitter release in inhibitory neurons) is different. For this manipulation as previously discussed, we needed to use AAV9 (because anecdotally we found that lentiviruses do not efficiently label interneurons). AAV viruses take longer to express in the neurons than lentiviruses, but since tetanus toxin is a very potent enzyme we only need a molecule of it to take effect. The song of interneuron manipulated birds start to degraded within 6 days post injection and recovered in about 60 to a 100 days. There is a catastrophic collapse of the song that stays variable from rendition to rendition for about 40 – 50 days, then the structure and stereotypy of the song rapidly recovers.

I hypothesized that drastic reduction in inhibitory tone to the excitatory neurons in HVC will lead to an extreme hyperexcitation then eventual silencing of the circuitry to re-build the normal architecture. To get a broad look at the dynamics in HVC, I performed freely moving chronic electrophysiology recordings for 120 days, which is twice the length of recovery time needed for the behavior. I performed control experiments in which the birds were injected with a similar AAV9 virus carrying GFP but no tetanus toxin. These recordings are solely measuring LFPs of the brain area given the length of time it takes for the manipulation to recover, single neuronal activity is not feasible to measure on this scale. The animals injected with interneuron muting virus showed an extreme increase in average LFP power (between 2-12 Hz) overnight at the beginning on behavioral degradation compared to control (that had an intact song). This increase in LFPs in the lower frequencies was gradually lost even before the song started to improve. This phenomena is expected, since behavior can only be restored to baseline once the circuit dynamics recovered enough to produce similar levels of activity. I decided to focus on dynamics during sleep since the most robust changes were seen in these periods. In addition, when the song is degraded the LFP signature that usually accompanies renditions of stereotypic song is not feasible to measure reliably (Brown et al., 2021; Markowitz et al., 2015). Animals were recorded 24 hours a day, so awake, sleep and singing data was collected.

Upon the observation that during the loss of behavioral stereotypy the LFP power at low frequencies drastically increases, I set out to study the underlying single neuronal dynamics of the system. To this end I performed head-fixed recordings with high-density silicone probes that record not only for HVC but the motor nuclei RA as well (Jun et al., 2017; Steinmetz et al., 2018).

These head-fixed recordings were performed at the start of song degradation (3-6 days post injection), then at 20 days post injection (song completely lost stereotypy) and at the recovery stage (or at 70 days post injection). The same animals were recorded at day 20 and day 70, however for the earliest recordings separate set of birds were used but with similar level of degradation. As predicted the birds at the start of song degradation have large discharges in HVC that resemble seizure like activity upon acute loss of inhibitory tone (such with drugs that block GABA type A receptors – like Gabazine). To study the difference between chronic and acute removal of inhibitory tone, I used Gabazine in control animals to see circuit responses to acute removal of inhibition.

The head-fixed recordings were done in 4 different brain states at each time point of degradation and recovery per bird. First the birds were awake, then the bird's own song (BOS) was played back (intact and degraded for manipulated animals). According to literature, birds have auditory gating within HVC when they are awake, which abolishes neuronal response to song. However, once the bird is asleep HVC and RA responds to playback of the BOS (Nick & Konishi, 2001). The second set of recordings were in sleep, followed by song playback in sleep. Then, the bird's HVC was infused with 250 $\mu$ M Gabazine while the same protocol was repeated (lights on silence, lights on playback, lights off, lights off playback). In this set of experiments, the overall observation matched the hypothesis that there is hyperactivation of the area for the first couple of days after the song degradation starts, then this results in exhaustion and increase in inhibitory tone that leads to complete silencing of HVC and then slow recovery to a level of activity that is not as high as control but efficient in driving the circuit for normal song production (indicated by the behavior). The most striking finding is these large discharges produced in HVC that are mostly present in RA as well. The length and spike content of these abnormal bursts right after song degradation might be different from bursting that occurs upon acute removal of inhibitions by Gabazine in a control animal. However, there is large variability and small sample size for this phenomena that does not fully allow for assessing whether these observations made by visual inspection are statistically significant or not. One other measure we looked at is the log firing rate of the two distinct clusters of single neurons (based on their waveform) before and after Gabazine administration. This is an interesting question, because if neurons in HVC go through homeostatic regulation during the manipulation the response of the circuit to be pushed to the limit and trigger ictal discharges might be completely different.

We measured overall spiking rate in HVC and RA of control and experimental animals across the timescale of the manipulation. One surprising finding is that while HVC starts out with a heightened state of activity (due to loss of inhibition), this gradually decreases to levels below the control, RA seems to show the opposite trend to compensate for changes in HVC activity. This finding gives us an insight into how the brain attempts to recover circuit level activity between coordinated brain areas for production of motor behavior. According to a previous

study (Kosche et al., 2015), *in vitro* (in brain slices) stimulation of axon collaterals from HVC to Ra leads to increase in the local inhibitory neuron firing. This indicates tight regulation of HVC activity upon indirect feedback from Ra. One hypothesis is that HVC activity in sleep reinforces the maintenance of adult song as well serves to drive song learning (Crandall et al., 2007; Dave & Margoliash, 2000; Elmaleh et al., 2021; Hahnloser et al., 2006; Shank & Margoliash, 2009), therefore our observation of loss of activity in sleep in HVC could mean that the degraded song that is produced in this period needs to be “kicked out” of the memory space therefore there is no consolidation of information at night so no sleep activity is necessary. In addition, Crandall et al. found that HVC sleep bursting arose once the juvenile bird is exposed to the tutor song. This further supports our hypothesis about the reduction of sleep activity in HVC during the song degradation period.

An alternative hypothesis is that during this long perturbation paradigm, we not only disrupt the activity in the motor cortical nuclei but the auditory feedback for a long time. Leonardo and Konishi have shown that even in adult male zebra finches song maintenance is an active process, meaning that disruption to auditory feedback over months leads to drifts in the crystallized song that over time re-adjusts back to the original song. We cannot exclude this possibility that the experimental paradigm that would be needed to disprove this involves deafening of adult animals that by itself could cause shifts in singing behavior over the length of the interneuron muting experimental paradigm. Hence, this is not a possible approach to take. In the prior set of experiments I conducted (Chapter 2), I did prevent animals from singing practice for the length of song degradation and recovery. However muting excitatory neurons only perturbs HVC activity for 14 days, allowing for a biologically possible experimental paradigm. In the latest set of experiments the degradation and recovery occurs over 60 plus days, for that amount of time to prevent an animal from singing would lead to either drifts in song or death of the animal due to the stress of the experiment.

Finally, we found parallels between sharp wave ripples (SWR) in the hippocampus of rodents to sleep bursts in normal and manipulated animals. Sharp wave ripples in the hippocampus have been correlated with memory consolidation and recall (Buzsáki, 2015; Hulse et al., 2017; Joo & Frank, 2018; Lubenov & Siapas, 2009). Therefore, during the song degradation and recovery period the structure and function of these ripple like bursts might change in a consistent way to aid in recovery of the motor circuit. To test this hypothesis we extracted the average LFP signal during sleep bursts in HVC and aligned it with the spiking activity in a burst. We decomposed the LFP signal power content by using continuous wavelet transform. This allowed us to look at the fine scale changes in power during bursts in normal and perturbed circuits of the pre-motor nucleus. We find many single units that fire phase locked to some part of the low frequency oscillation or the ripple in gabazine induced p-waves (Buzsáki, 2015) in the control animals. However, the interneuron muted animals have very broad firing that seem to show no significant trend with any phase of the sharp wave ripple (SWR) like oscillations. As the animals recover their song there seems to be an emergence of phase locking of single units to the large amplitude irregular activity (LIA) or SWR-like oscillations. This potentially could suggest that the circuit assembly is less perturbed and is able to restore and recall the memory of the song. Although, these findings are not in direct relation to sleep replay or active singing activity in the

pre-motor nucleus. Hence, this is just a broad estimation for a putative trend which in future work should be investigated.

In order to understand the changes neurons have to undergo to adjust and repair the circuit I performed single cell RNA sequencing experiments on HVC at day 25 post degradation. This is the mid time point at which the hyperactivity is gone and the behavior is most degraded and the song is the softest (indicating not enough drive from HVC to Ra for louder vocalization). In this experimental paradigm I dissociated the HVC cells of birds injected with the interneuron muting virus as well as control birds that carry the same serotype of AAV but only with GFP, that leads to no change in behavior. There were two biological replicates per experimental group. There are several challenges, one of them is the lack of fully annotated genome for zebra finches, which makes analysis and interpretation of the results difficult. With this caveat I proceeded to look at the transcriptomic changes between control and experimental conditions. There has been one publication with RNA sequencing in the HVC of zebra finches which looked at very different questions but allowed us to have a baseline for neuronal markers (Colquitt et al., 2021).

First, we saw a 3 fold increase in microglia in the experimental group. Previously publications implicate the role of microglia in synaptic plasticity during development (Cheadle et al., 2020; Gunner et al., 2019; Hong et al., 2016) Microglia is associated with clearing nonfunctional synapses between neurons, with a mechanism that is poorly understood. Moreover, microglia is known as the resident immune cell of the central nervous system and we injected virus that could trigger an immune response. This explanation is highly unlikely given that our control animals were injected with the same amount, titer and serotype virus (except it did not carry tetanus toxin). Therefore the immune response level in control and experimental should be fairly comparable.

Second, we observed an overexpression of MHC1, a receptor associated with immune function as well as synaptic plasticity in learning (Turrigiano, 2011). These parallel lines of evidence suggest that neurons are actively reorganizing and dynamically building new synaptic connections to achieve recovery. To support these findings, we performed in situ hybridization of mRNA probes associated with microglia and MHC1. Since the RNA seq experiments give a ballpark resolution image of the transcriptome of individual cells, in situ hybridization could show with more certainty the expression changes of the candidate genes as well as topography of neurons in HVC and other brain areas.

Third, we found that previously used marker genes (genes that are restricted in expression to a specific population of neurons) for HVC-Ra (pre-motor neurons) and HVC-X (X projecting neurons important for song learning in juveniles) are lacking in the experimental data. The first step was to ensure these marker genes are not affected by changes in activity levels, which according to previously publications is unlikely. This is a very interesting finding, one similar dataset was found in the visual cortex of adult mice (Cheng et al., 2022). We set out to test whether the expression of these marker genes recovers once the song of the animals recovers. To study this, we performed in situ hybridization for the mRNA encoded by these marker genes.

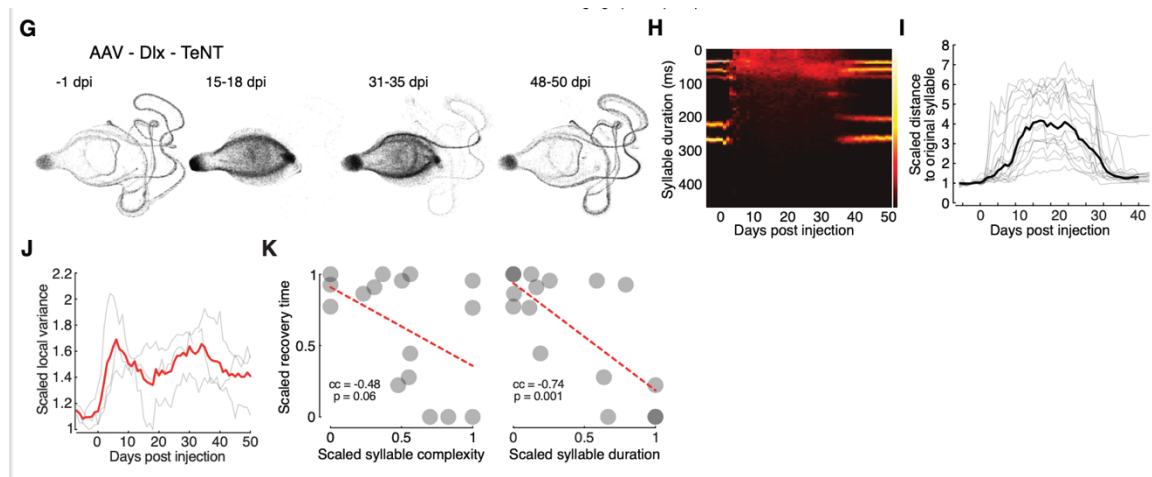
Fourth, we found changes in the neurotransmitter receptors in glutamatergic neurons as well as changes in voltage gated ion channel content of both glutamatergic and GABAergic neurons in HVC. These changes correlate with the hyperactivity that eventually becomes silenced and re-emerges during the recovery period.

This set of transcriptome level experiments allowed us to better understand the molecular mechanisms with which individual cell types in the circuit adapt and attempt to recover network activity.

In summary, we studied how drastic loss of inhibition in a pre-motor nuclei leads to changes in the single neuronal and population characteristics.

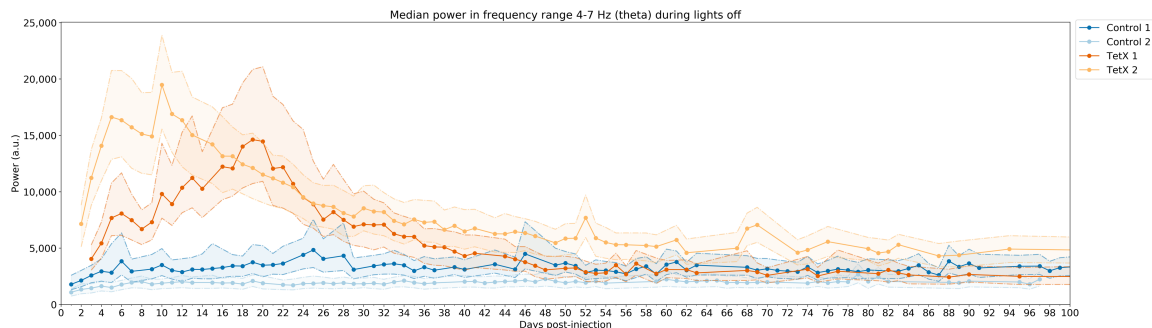
The following figures are recapitulating the findings that were mentioned in the text above, all modified or directly taken from future publications of Torok et al., 2022 which is not currently published.

1. The song degrades and recovers after muting of interneurons in the pre-motor nucleus HVC, from Torok et al., 2022 (in progress):



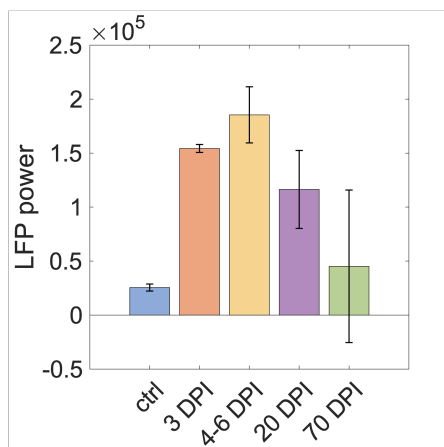
**G-K** Results from birds with perturbation of HVC interneurons after injection of AAV-dlx-TeNT ( $n = 3$ ); **G**, UMAP visualizations of songs from one bird; **H**, Distribution of syllable durations per day; **I**, Plots of distance to original syllables; **J**, Local variance of songs per day; **K**, Scatter plots of recovery time against complexity and duration of each syllable.

- Chronic recordings showing the increase in median LFP power during lights off for the two experimental birds compared to control, during the time period of song degradation and re-establishment between 4-7 Hz:



X-axis showing the time in days after electrode implantation and viral injection. Y-axis is showing the median power values between 4-7Hz (median among all electrodes) that were obtained from the fast Fourier transform of 3 hours of data per night. Tetx1 and Tetx2 are the two animals injected with interneuron muting virus and Control 1 and 2 are the two animals injected with a control virus (same titer and serotype as tetanus toxin carrying virus).

- Bar plots showing the change in LFP power during the snapshots of acute recordings with a high density silicone probe recording neuronal activity from HVC and Ra in control and experimental animals (with interneuron muting virus in HVC the pre-motor nucleus) :

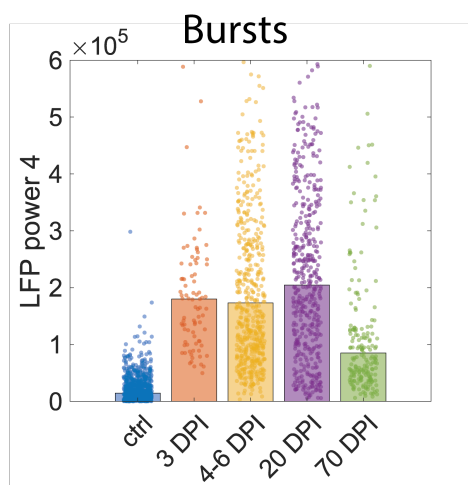


The Y-axis of this bar plot is showing the median LFP power between 4-7 Hz in HVC during lights off acute head fix recordings with high density silicone probes. Ctrl refers to animals ( $n=1$ ) with control virus, 3DPI (3 days post injection of interneuron muting virus) animals ( $n=1$ ) right after the start of song degradation. The 4-6 DPI ( $n=4$ ), 20

DPI (n=3) and 70 DPI (n=4) animals at 4-6, 20 and 70 days post injection of virus.

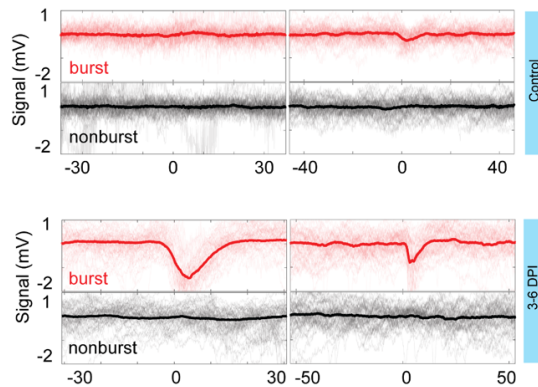
The standard deviation is plotted on each bar. A proportion of animals (n=2) at 70 days did not fully recover their original song therefore that could account for the large standard deviation measure.

- Bar plot showing the increase in LFP power at low frequencies associated with sleep population bursts:



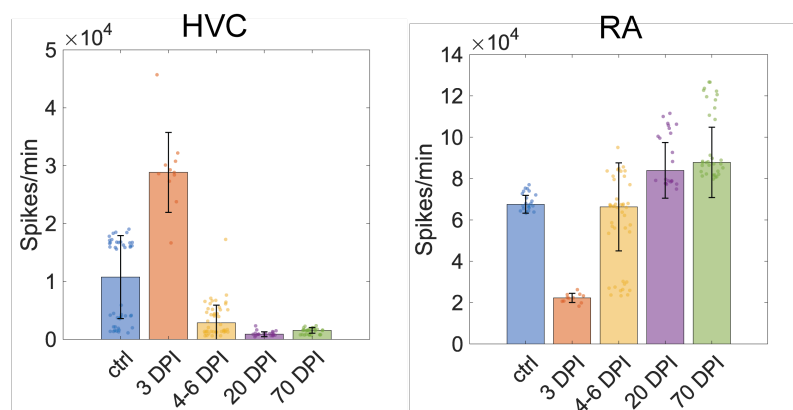
The bar plot represents the median LFP power at low frequencies during bursting events for control (ctrl) and all days (3, 4-6, 20, 70) post injection of interneuron muting virus.

5. Raw traces of averages LFPs in HVC during lights off burst and non-bursts in a control and an experimental animal:



These 4 traces are the raw averages LFP signal during bursting and non-bursting events in HVC in a control and in an experimental animal 3 days post injection of the interneuron muting virus. Red traces indicate instances of burst of neuronal activity while the black traces indicate LFP traces during non-burst periods. X-axis represents time in msec Y-axis represents signal in mV.

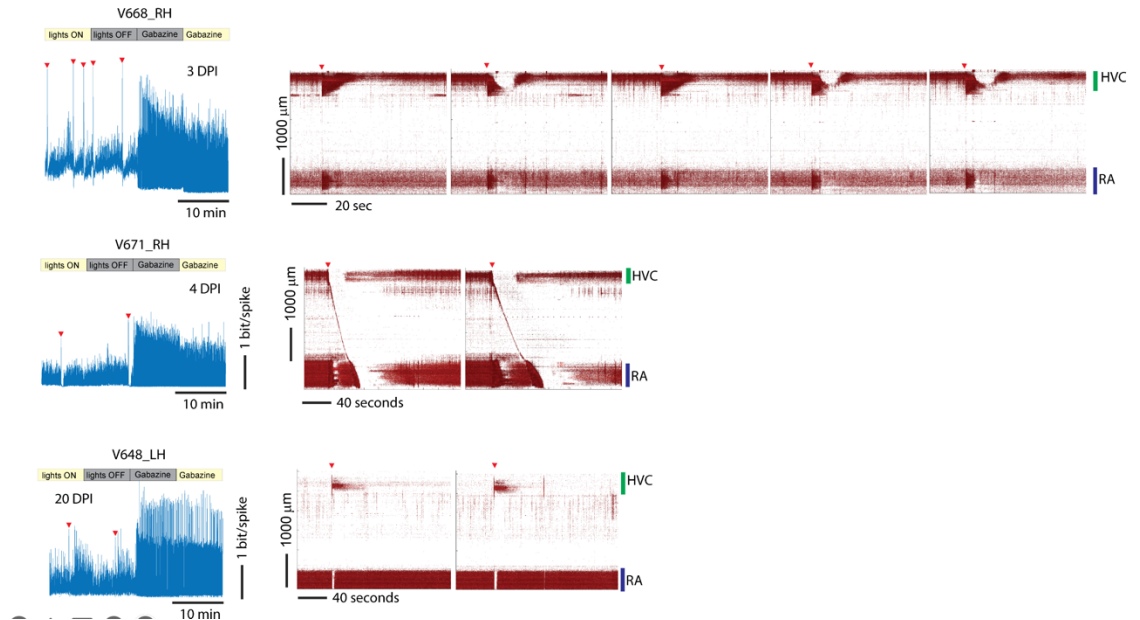
6. Bar plots showing the average spiking in HVC and Ra during the whole length of the lights off recording session (10-20 mins) in control and all stages of manipulation. These plots indicate that when there is elevated activity in HVC the pre-motor are then the motor area Ra decreases overall activity as a compensatory mechanism.



Bar plot shows number of spikes per minute by common average referencing then thresholding spikes that are 3 standard deviation about the median signal in a 2 minute window. Blue bar shows the average spikes per minute in the control animals (n=2 for HVC, n=1 for Ra), 3 days post injection (DPI) of interneuron muting virus (n=1), 4-6

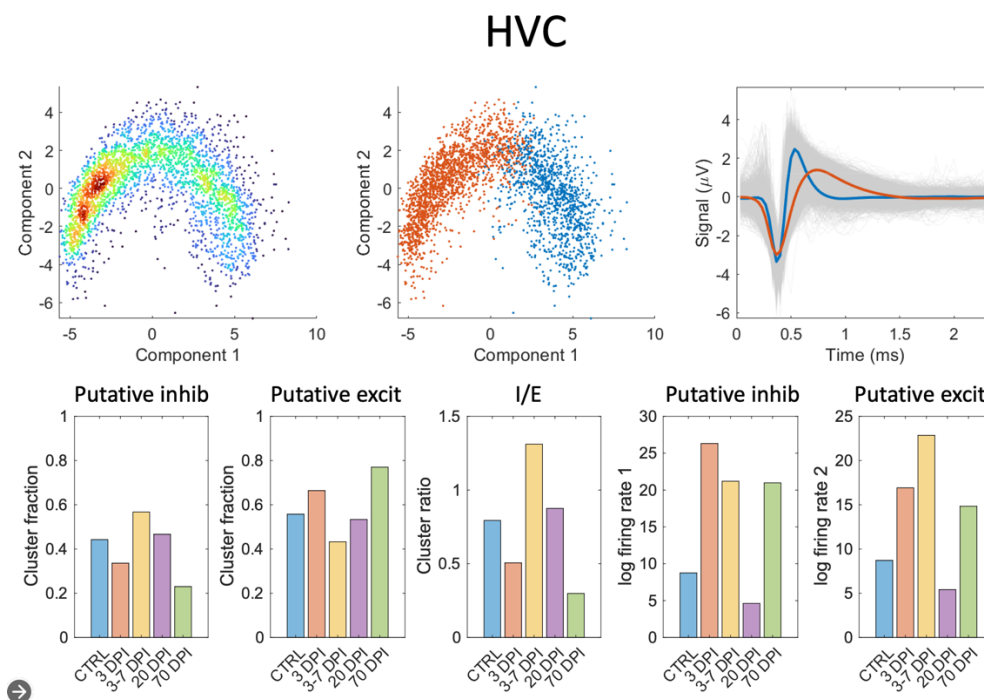
DPI (n=4), 20 DPI (n=3) and 70 DPI (n=3). The standard deviation is plotted for each bar.

- Spike raster showing abnormal large discharges 3-20 days post injection of interneuron muting virus in HVC, that then spreads through the whole brain.



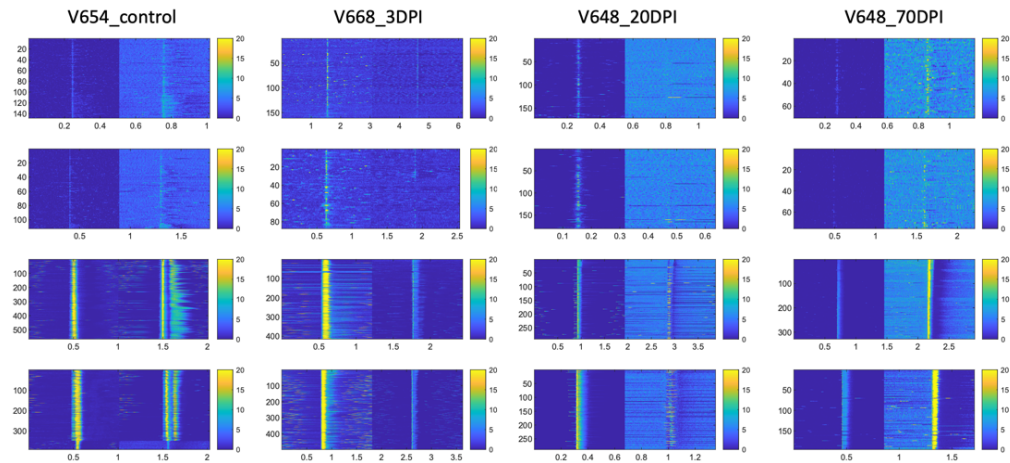
The left panels show the firing rate related information transfer between HVC and Ra for the whole duration of the acute recordings. The red triangles indicate the large abnormal discharge events that occur with low frequency in each animal. The right traces show individual spikes along the shank of the electrode based on the same thresholding as the previous bar plot. The green vertical line shows the location of HVC the blue line shows RA during the discharge events. The X-axes for both is time.

8. Showing the types of single neurons based on their waveform properties in HVC during the whole length of the acute recording session.



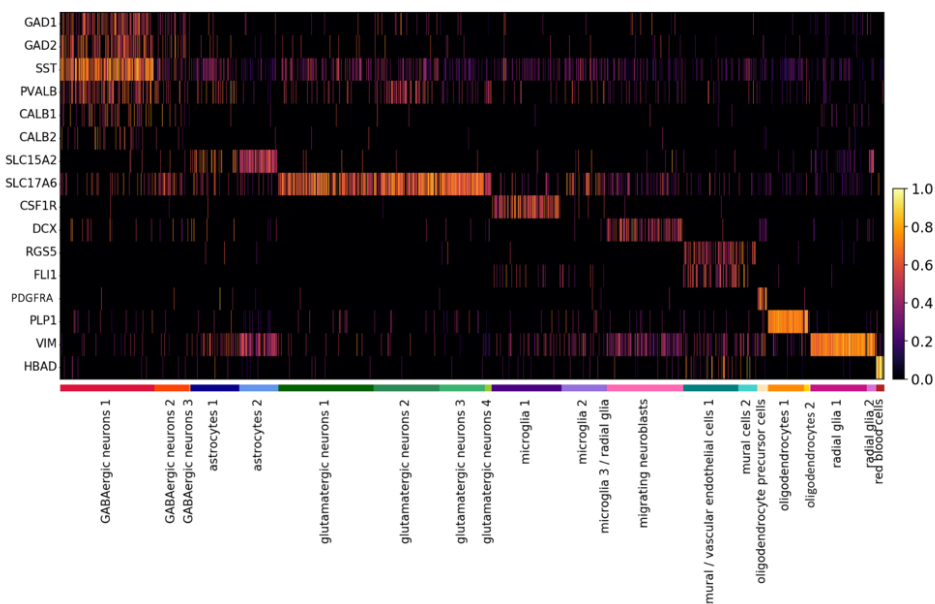
The top panel shows the isolated waveform shapes clustering in high dimensional space projected to a 2D plane after spike sorting with Kilosort and manual sorting of individual waveforms. The first two bar graphs show the fraction of putative inhibitory (blue tighter waveform from the top panel) and putative excitatory neurons (orange broader waveform from the top panel) contribution into the total cluster at each point of the experiment and at the control state. The middle bar graph shows the inhibitory to excitatory ratio. The two right bar graphs show the log of the firing rate of the two sub clusters neurons based on their waveform shape. There is no significant trend so no p-values or standard deviation is included here.

9. All the burst profiles of individual animals during the 4 separate recording sessions:



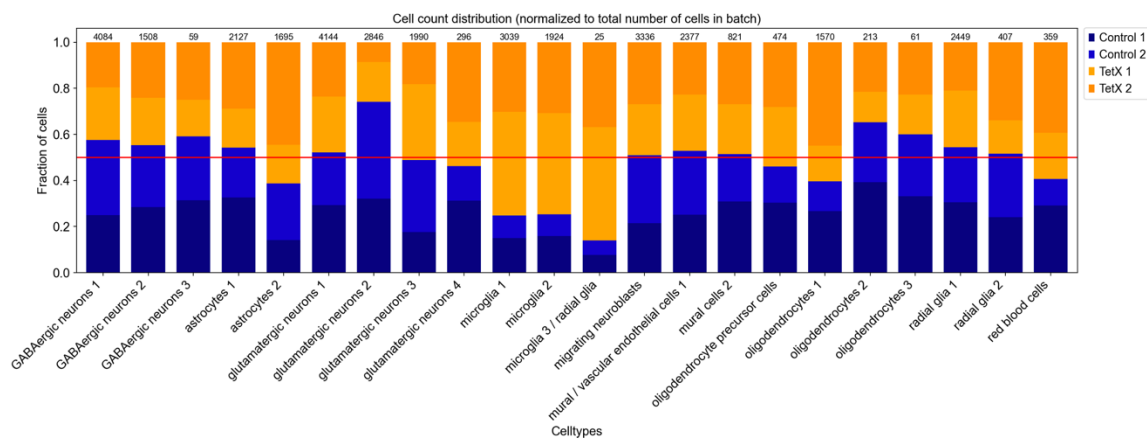
Each 4 by 4 panel show the spiking activity aligned at each burst in HVC and Ra for an individual bird. Each panel is a recording session, the first panel is rec1 which is silence lights on. Then rec2 which is silence lights off; rec3 which is silence lights off and Gabazine administered, rec4 that is with lights on. The scale from blue to yellow is the average firing rate per minute during the burst. The Y-axis is burst number in a temporal order, the X-axis is time in seconds.

10. Cell type assignment with unsupervised and semi-supervised Leiden clustering. Marker genes were collected from previously published and identified marker genes for each cell type.



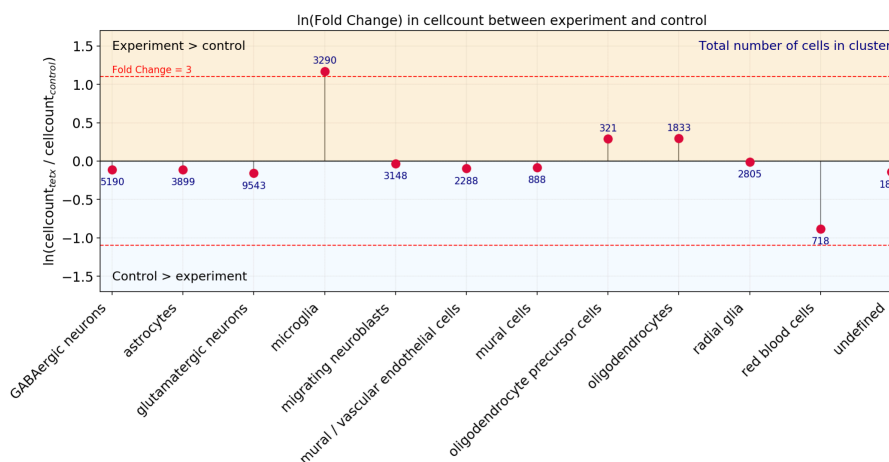
The Y-axis represents several markers genes previously identified for cell-types. Clusters on the X-axis were identified by unsupervised and semi-supervised Leiden clustering. The intensity is the normalized gene expression of each gene on the Y-axis in each cluster.

11. The contribution from each biological replicate into each cluster of cells identified. The main difference is shown in number of microglia between experimental and control samples which is a finding it is not an artifact of the clustering or sampling of cells for sequencing.



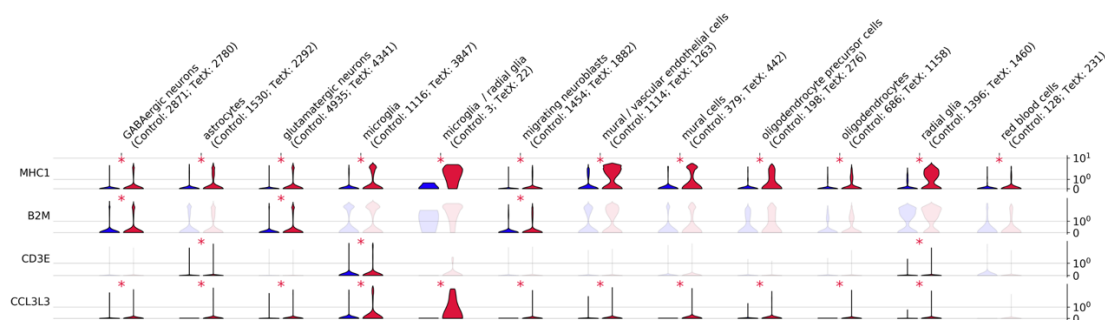
The Y-axis has the normalized (to the total number of cells sequenced per sample) fraction of cells per each Leiden cluster obtained that then was identified by known marker genes when using the clustering algorithm together for both control ( $n=2$ ) and experimental ( $n=2$ ) samples. The X-axis lists the cell types found. Blue color represent the two control biological replicates (shaded slightly different per sample), the orange color represents experimental animals. The red line is the 50% percent indicating that most clusters contain equal amount of fraction of cells from each biological replicate (control or experimental). Except for microglia which we will address in the following figure.

12. Large fold increase in microglia markers in the single cell RNA seq experiments at 20 days post injection of interneuron muting virus in HVC. This indicates that the circuit is using microglia to rewire neuronal connections within HVC, which is a process that has previously been reported during development and motor learning in other organisms.



The Y-axis shows the log<sub>2</sub> normalized cell count between experimental (n=2) and control animals (n=2). The X-axis shows the cell-type clusters that were obtained after semi-supervised clustering and marker gene assignment to each. If the red dot is above the horizontal 0 line it means there was an x fold increase in number of cells in the experimental animals compared to control, if the dot is below the line then the control has an increase compared to experimental birds.

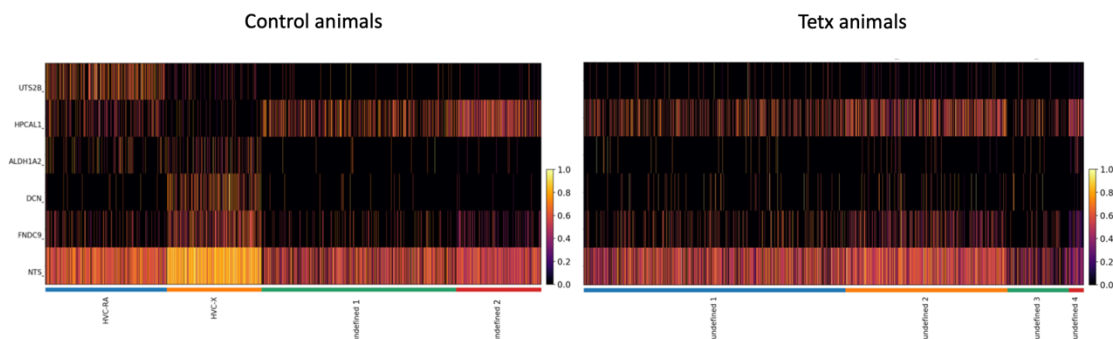
13. Upregulation of MHC1 associated genes in the experimental animals compared to control, that suggests a similar line of evidence as microglia for synaptic reorganization:



The violin plots are showing the normalized median expression of the genes named on the Y-axis along the several different clusters of cells identified in our dataset. The red violin plots represent the two experimental replicates while the blue violin plots show the expression level in the control replicated. A star indicates a significant difference of

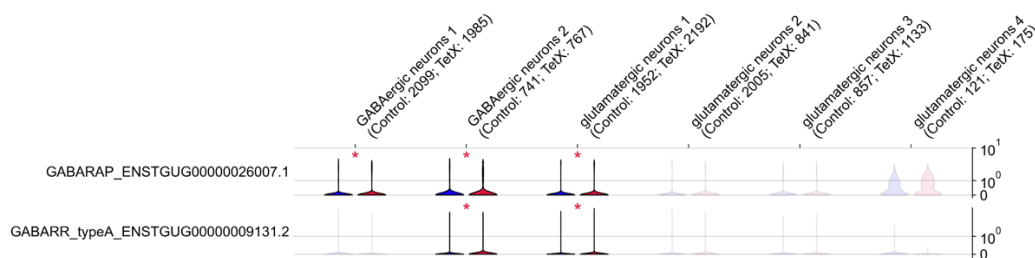
$p < 0.05$  (by Welch's t-test) and a fold change  $> 1.5$ . The star is red if the mean expression of the gene is greater in experiment, and blue if the mean expression is greater in control.

14. Loss of identity of HVC projection neurons upon manipulation.



These heatmaps show the normalized expression of the marker genes for HVC-Ra ( UTS2B and HPCAL1) and for HVC-X ( ALDH1A2, DCN, FNDC9, NTS) in all clusters of the glutamatergic neuronal clusters in the control and experimental dataset. In the control there is a clear population of HVC-Ra and HVC-X neurons based on the expression of these marker genes. However, this seem to be lost in the experimental dataset. This implies that re-organization of the pre-motor neuronal connectivity leads to loss of identity marker genes in these neuronal cell populations.

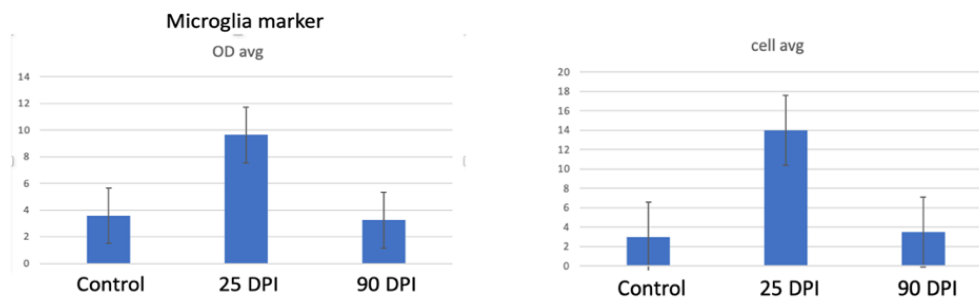
15. Expression of GABA type A receptor changes in the experimental dataset in the glutamatergic and GABAergic neuronal cell clusters:



These violin plots show the normalized median expression of two genes names on the Y-axis that are associated with the GABA type A receptor complex. The red violin plots represent the two experimental replicates while the blue violin plots show the expression level in the control replicated. A star indicates a significant difference of  $p < 0.05$  (by Welch's t-test) and a fold change  $> 1.5$ .

The star is red if the mean expression of the gene is greater in experiment, and blue if the mean expression is greater in control.

16. In situ hybridization experiments showing microglia in control animals, and experimental animals at 25 dpi and 90 dpi.



In situ hybridization results for microglia numbers in experimental and control animals.

Both microglia average numbers (based on the number of puncti in the situ brain slices) and average optical density compared to background shows and increase at day 25 post injection (DPI) of interneuron muting virus compared to control (animals injected with AAV9-CAG-Neongreen) that then goes back to control level at 90 days post interneuron muting virus injection when the song of these animals is recovered.

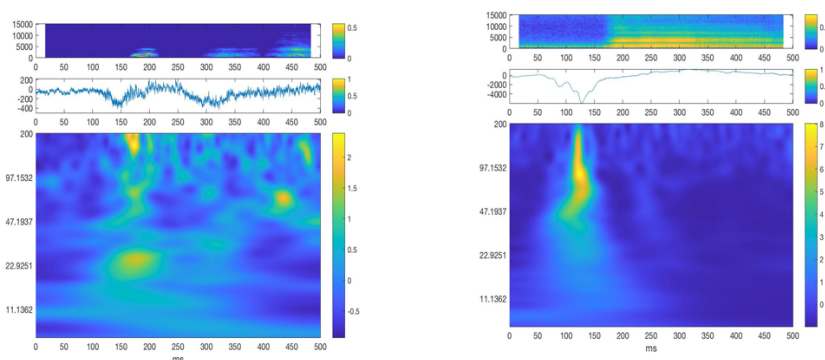
In addition to testing levels of microglia in control adult animals and animals during song degradation and recovery we also tested levels in juveniles during song learning. Our hypothesis is that establishing (as in juveniles) and re-establishing (as in perturbed animals) a circuit might employ similar mechanisms of plasticity. Therefore, microglia that is involved in synaptic pruning during development might be a key factor also in juvenile learning and in song maintenance or injury repair in adult circuits. We see that microglia numbers peak in juvenile males at 25 days post hatch and gradually decreases (day 50 to 70 post hatch) as the song crystallizes (data not shown). This observation could be key to studies that would like to aid motor circuits in injury repair given that microglia could be a good candidate to upregulate during repair.

These collective lines of evidence show detailed information about the single neuronal and circuit level response to loss of inhibition in a pre-motor nucleus. The elevated levels of activity in HVC in the beginning of removal of inhibition looks very similar to the acute removal of inhibition by Gabazine. This observation is hard to quantify given that each HVC micro-circuit is different therefore the level of perturbation and timeline of perturbation could lead to differences between biological replicates rendering significance testing impossible. However, this increase in excitation gets toned down (by possibly homeostatic processes) with time and the circuit falls silent in its offline lights off state. This period is followed by decreased activity in the downstream motor nucleus Ra that then re-establishes to control levels once the HVC circuit is silenced. In addition, we observe elevated power values comparing control to experimental in

the first 30 days at low frequencies during lights off periods. The phenomena behind this could be some sort of change in the sleep population bursting from control to experimental. To further test this we aligned the low (alpha: 1-4 Hz) and high (gamma: 30-90 Hz) oscillations within the sleep bursts with the spiking data extracted during the discharges. From this we hope to see some sort of similarity between sharp wave ripples in other organisms and our experimental paradigm. This could further strengthen our hypothesis that the changes in sleep bursts play a role in memory consolidation, retention and recall. Therefore when we manipulate the circuit and these burst patterns and activity get perturbed and does not ever go back to baseline. Suggesting that the returned motor activity is not identical to pre-perturbation but is sufficient in driving the proper execution of behavior.

### Discussion and Results of sharp wave ripple- like event detection and quantification in the chronic and acute dataset

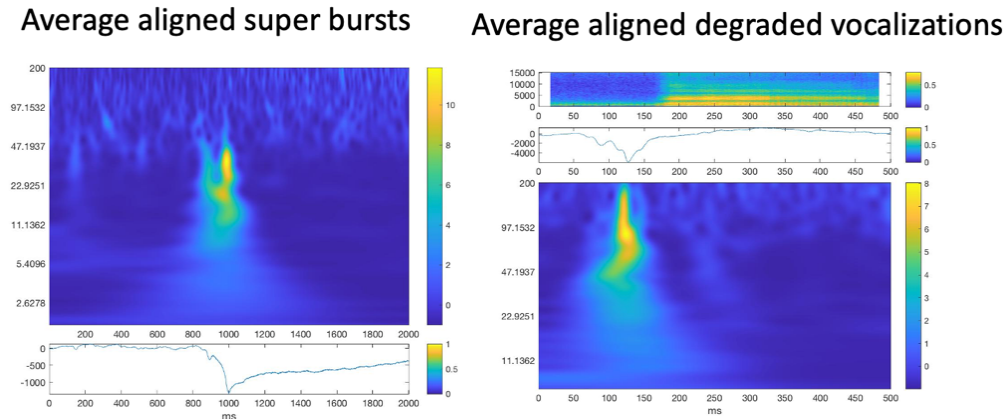
We attempted to quantify and analyze LFP signatures of chronic recordings within control (AAV9-CAG-Neongreen) and experimental (AAV9-DLX-Tetx-GFP) animals during song production according to previous methods (Brown et al., 2020; Markowitz et al., 2015). However, as mentioned above the degraded song of interneuron muted animals is highly variable from rendition to rendition, therefore, making averaging over multiple trials an unreliable metric. We decided to focus on the first few days of song degradation in experimental animals when the is production of vocalization that are very long and acoustically distorted but look similar among renditions. Aligning LFP data to the start of the these vocalizations showed us a completely different pattern of LFP spectral features than aligning the start of bouts in control animals ( $n=5$  vocalizations both in control and experimental animals). Shown in the figure below.



### Perturbed and unperturbed song and brain activity.

The top panels are spectrograms of sound in the control and experimental animals 5 days post implantation of the electrode array (dpi). The traces right below the spectrograms of sound is the raw average trace of extracellular signal and below the raw signal there is the continuous wavelet transform (cwt) of the LFP signal during each vocalization event. As you can observe the pattern and size of deflections is very different between control and experimental animals.

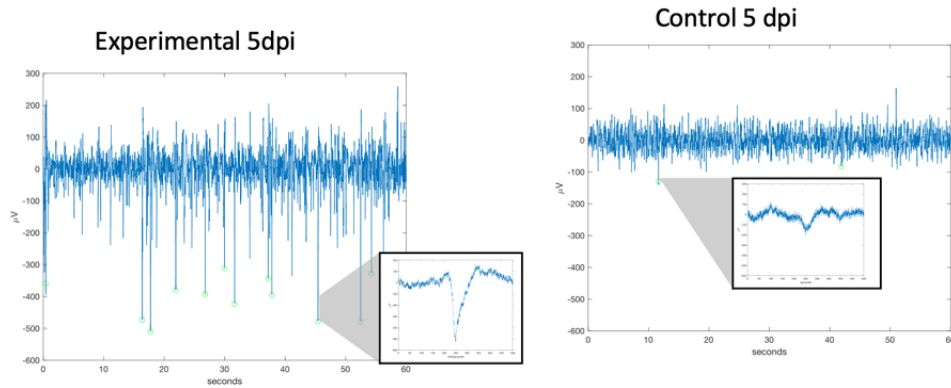
Since experimental animals only produce these vocalizations above very few times and then the degraded song becomes very different we decided this is a non-reliable metric that we will not be able to follow for the whole length of the perturbation. We noticed that these distorted vocalizations in the raw extracellular trace look highly similar to deflections that we detected within experimental animals during sleep. Comparison is shown below.



Similarity of degraded vocalization brain activity and abnormal sleep bursts.

The left panel shows the averaged cwt and raw trace of abnormal deflections ( $n = 5$  events) detected during lights off head fixed acute recordings. The right side is showing the same figure as previously shown of the averaged cwt and raw trace of degraded sounds ( $n = 5$  sounds) produced by an experimental animal at 5 dpi. The amplitude and shape of averaged raw trace deflections for both events are similar.

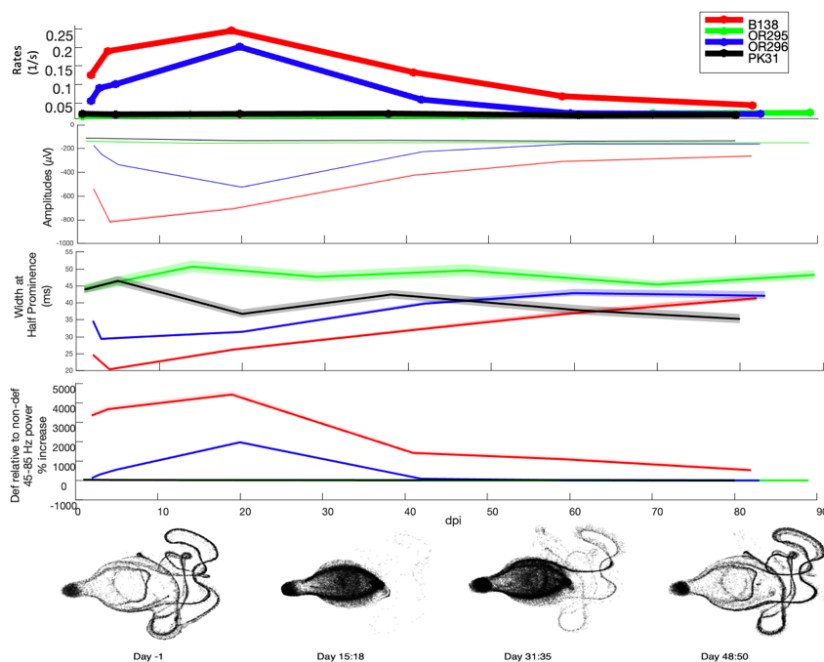
We decided to focus on lights off periods in both chronic and acute recordings given that occurrence of events and noise to signal ratio is much better when the animals is not moving and is not active. In addition, the stereotypy of sleep deflections allows us to collect a large enough sample size for quantification and analysis that would be not possible with the constantly changing degraded song dataset. Moreover, we hypothesize that events occurring from loss of inhibition will be more apparent during sleep when the global level of inhibition lowers and neuronal populations are more likely to fire in synchrony (Zhang et al., 2012). First, we visually observed raw extracellular traces of chronically recorded animals (control and experimental  $n = 2$  each) at 5 days post implantation. We immediately noticed large amplitude deflections that are much higher in amplitude and more frequent in the experimental animals (figure below).



Raw electrophysiology traces of control and experimental animals.

The top panel is the raw extracellular trace with an inset showing an example deflection in an experimental animal at 5 dpi, the bottom panel is showing similar events (less frequent and smaller in amplitude) in a control animal.

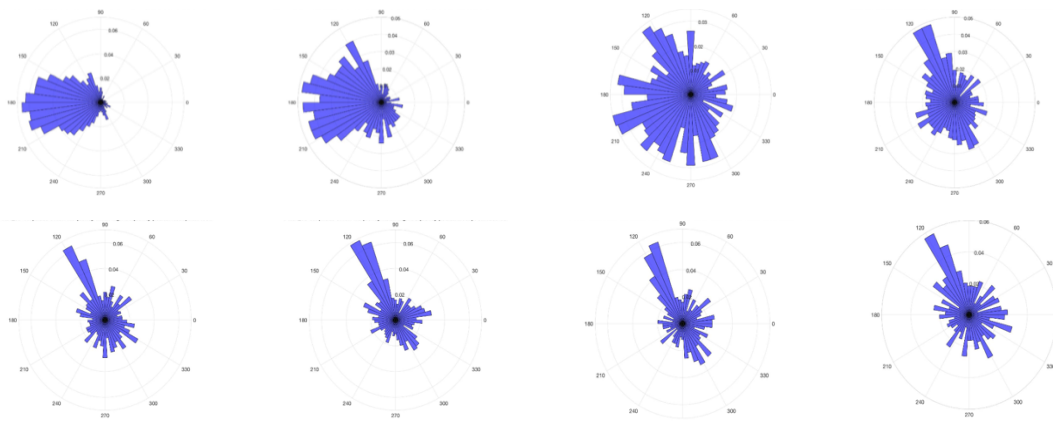
We proceeded to quantify the frequency of these events over the course of the manipulation in both groups in the chronic dataset, as well as, showing the power at specific frequencies during this event (alpha and gamma). Since these deflections look similar to sharp wave ripples we wanted to understand the phase-amplitude coupling of the sharp wave and the ripple within our detected peaks. Figures below show quantification and characterization of these events in experimental and control animals during the experimental timeline.



Abnormal deflection events in the brain coincide with degraded vocalization production.

The top panels show the frequency with which these deflections in control and experimental animals occurred per second. Individual lines represent each animal (red and blue experimental, green and black control). The x-axis on all plots is time in days. Then we show the amplitude (it is a negative scale so in reality shows the same trend), with of the peak of the deflection and the normalized (to non-deflection average power at the same frequency range) average power at 45-85 Hz during the deflections. Lastly, we show an example experimental animal's high dimensional representation (using UMAP from Chapter 2, 4 for methods) of the sounds made at a snapshot day along the timeline. Between days 30 and 45 the song recovers as well as most of the measured metrics of the deflections return to a control animal like state.

The next figure shows that there is a 60 degree shift in angle of the phase-amplitude coupling between control and experimental animals, that eventually disappears by the time the song is recovered.

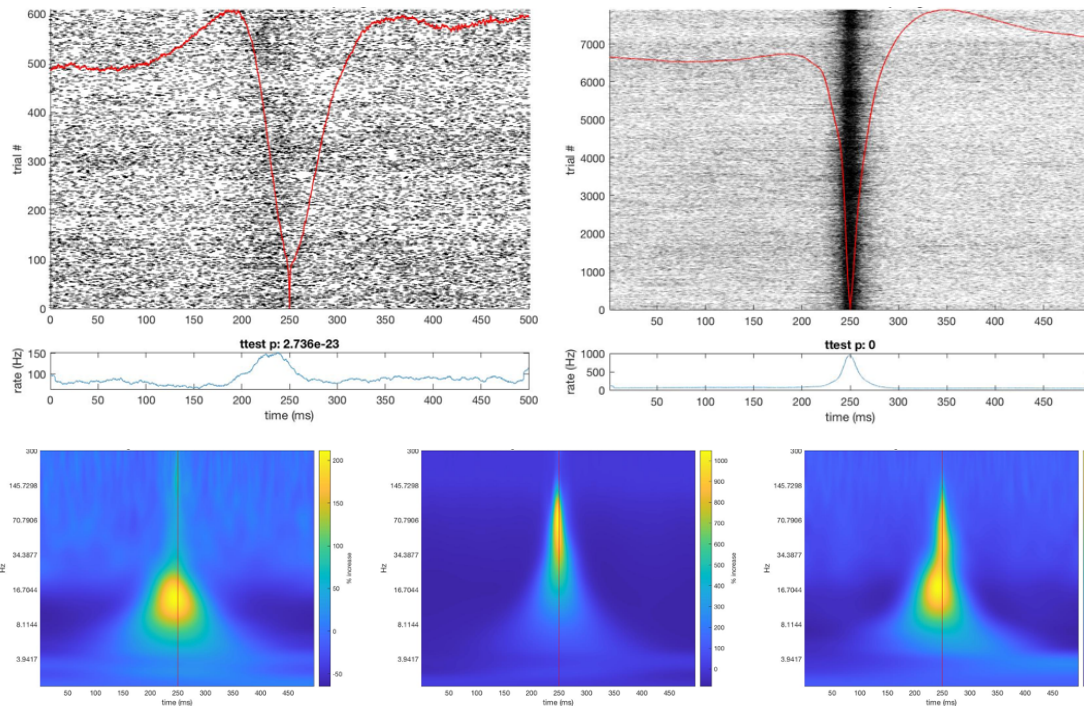


Polar plots showing the relationship between low and high frequency LFP activity during the manipulation time course.

These plots show the histogram of angles with which the high frequency (50-90Hz) phase is coupled with the highest amplitude of the low frequency (1-20 Hz) oscillation. The top panels are the angle distributions in an experimental animal at day 5, 25, 40, and 60 post implantation. The bottom panel shows the angles of a control bird's oscillations at the same time points.

The above figure shows that deflection events are constantly occurring with a phase-amplitude relationship at 120 degree whereas, the experimental animal starts at 180 degree that returns to a control-like 120 degree once the song is recovered. We hypothesize that the relationship between the sharp wave-like and the ripple-like events during these deflections is related to the song degradation and recovery. We see decrease in frequency and amplitude of the SWR-like events, as well as, re-establishment of the correct phase-amplitude coupling within the events as the song of the experimental animals recover. Therefore, it is possible that these deflections relate to the behavioral phenomena we observed.

To further assess the underlying neuronal firing during the detected deflections in non-movement lights off periods we turned to the first day of chronic recordings (multiunit activity can only be obtained in the first 24-48 hours then glial scar formation masks spikes moving forward). Glial scar formation in chronic recordings makes spike detection during song degradation and recovery not possible. Therefore we performed a set of head fixed acute recordings with a high density silicone probe to take "snapshots" of the activity pattern within HVC to further quantify these ripple like events along the song degradation and recovery timeline. The next figure shows the relationship between the sharp wave (low frequency oscillation) and the multiunit activity on the first day of chronic recording at night.



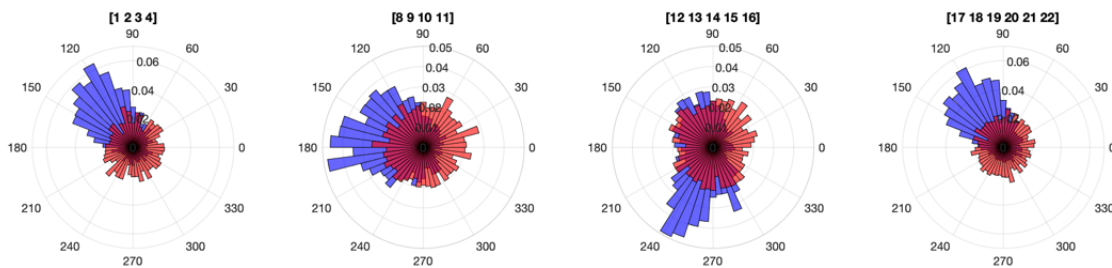
Multi-unit activity and spectral decomposition of deflection events in chronic control and experimental recordings.

The top panel shows the raster of multiunit activity for each detected SWR-like event with the red trace showing the low frequency oscillation during those events. On the bottom of the raster is the averaged (over trials  $n = 600$  for a control and  $7000$  for an experimental animal) distribution of firing rates for the same timescale of the deflections. The left side is control and the right side is an experimental animal at 1dpi. The bottom average cwt plots are showing the power content of LFPs during the deflections and the red line shows the peak of the sharp wave within the deflection. The first cwt is the control animal, the second is the experimental animal at 5 dpi, the third cwt shows the experimental animal at 60 dpi.

From the phase-amplitude coupling of sharp wave-like and ripple-like events during the detected deflections, we see that the relationship in control and experimental differs at day 5 and 25 and 40 but once the song recovers this relationship resembles a control like state. However, even at 60 dpi there is a proportion of events that are not recovered. This supports our previous findings where we show that neither LFP power nor firing rate resets to control level. This suggests that there is sufficient drive to produce the behavior and correct sleep activity patterns in enough trials to re-establish the behavior. The chronic data only enables us to look at the first day of multiunit activity in relations to the SWR-like events. Here we find that the firing of neurons is prior to the peak of the sharp wave in control animals, as opposed to the experimental multiunit activity which coincides with the peak of the negative deflection. We show that both the phase-amplitude coupling and the multiunit activity local within HVC shifts as a result of our perturbation.

The next set of acute experiments will aim to answer whether single and or multi-unit activity coupling with the SWR-like events also recovers to a control like state or there might be just a sufficient proportion of these events that need to have correct locking of neuronal firing during SWRs that accompany the behavioral recovery.

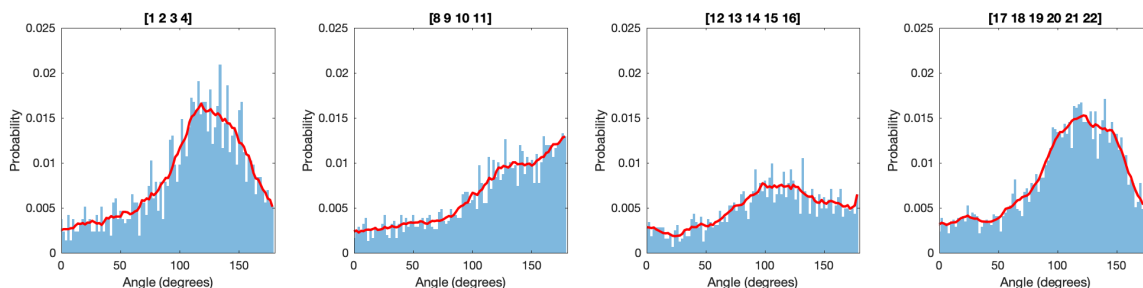
First we demonstrate that the phase amplitude shift that we observed with the chronic recordings between control and experimental SWR-like events also holds true and passes statistical testing in the acute dataset. In the acute high density silicone probe dataset we combined deflections from multiple animals to calculate a highly similar angle plot like shown in the chronic data. Then, we calculated the distribution of phases of the low frequency (1-10Hz) sharp wave at which the amplitude of the ripple (30-40Hz) reaches maximum value.



Polar plots showing the relationship between low and high frequency LFP activity during the manipulation time course in acute recordings in multiple animals.

These angle plots show the distribution of angles of the low frequency oscillation when the maximum amplitude of the ripple occurs. The blue is the true distribution of the data and the red/pink represents a randomly shuffled dataset (if the angle distribution is similar to random chance these the blue and pink would overlap). The plot order from left to right starting on the left most represents  $n=4$  (1,2,3,4) of control animals averaged SWR-like deflections;  $n=4$  (8,9,10,11) is 3-6 days post injection (DPI) of the interneuron muting virus;  $n=5$  (12,13,14,15,16) 20 DPI animals' SWR-like deflections;  $n=6$  (17, 18,19,20,21,22) animals at 70-80 DPI once song is stereotypic.

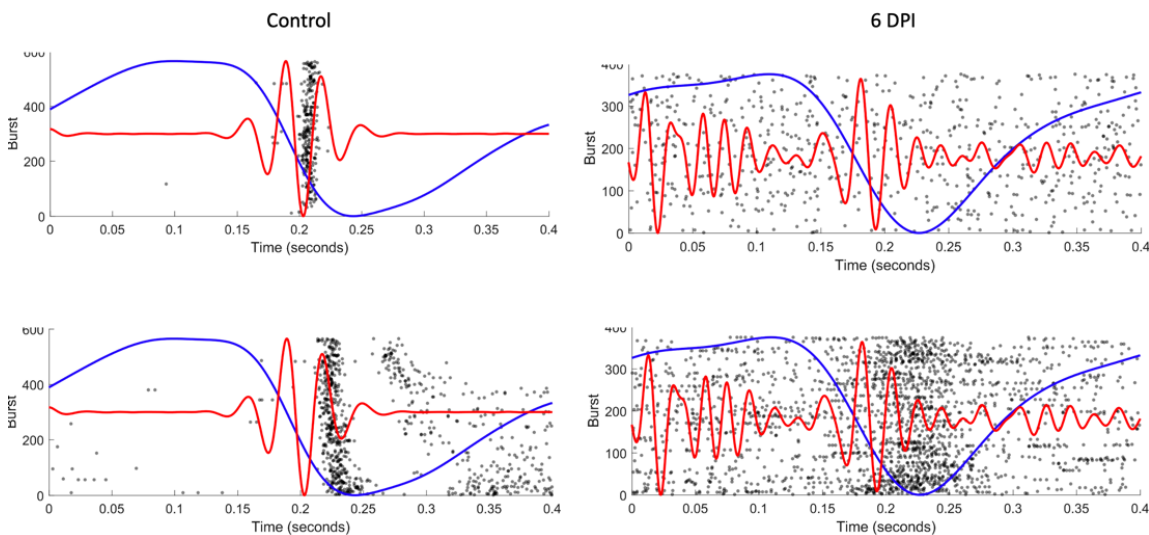
From the plots you can see that the angles are different from the angle measurements obtained from the chronic dataset at day 25 post perturbation. This could be due to the fact that we have a larger population of animals sampled for the acute compared to chronic recordings or that song distortion reached higher levels in the acute animals' behavior. Control animals lock to around 120 degrees, which shifts to 180 degrees at day 3-6 post manipulation, that further shifts for 240 degrees at day 20 and by the end of the manipulation at day 70-80 the events lock back to a similar to control 120 angle. This is further quantified as a distribution of probability of locking at specific angles of the sharp wave when the ripple reaches maximum amplitude below.



Probability distribution of SWR-like events at different time point during the experiment.

These graphs represent the probability distribution of the sharp wave events of locking as a specific angle of the ripple at its maximum amplitude. Red line is the mean distribution. Y axis is probability and X axis is angle in degrees of the sharp wave relative to the maximum amplitude of the ripple. The plot order from left to right starting on the left most represents  $n=4$  (1,2,3,4) of control animals averaged SWR-like deflections;  $n=4$  (8,9,10,11) is 3-6 days post injection (DPI) of the interneuron muting virus;  $n=5$  (12,13,14,15,16) 20 DPI animals' SWR-like deflections;  $n=6$  (17, 18,19,20,21,22) animals at 70-80 DPI once song is stereotypic.

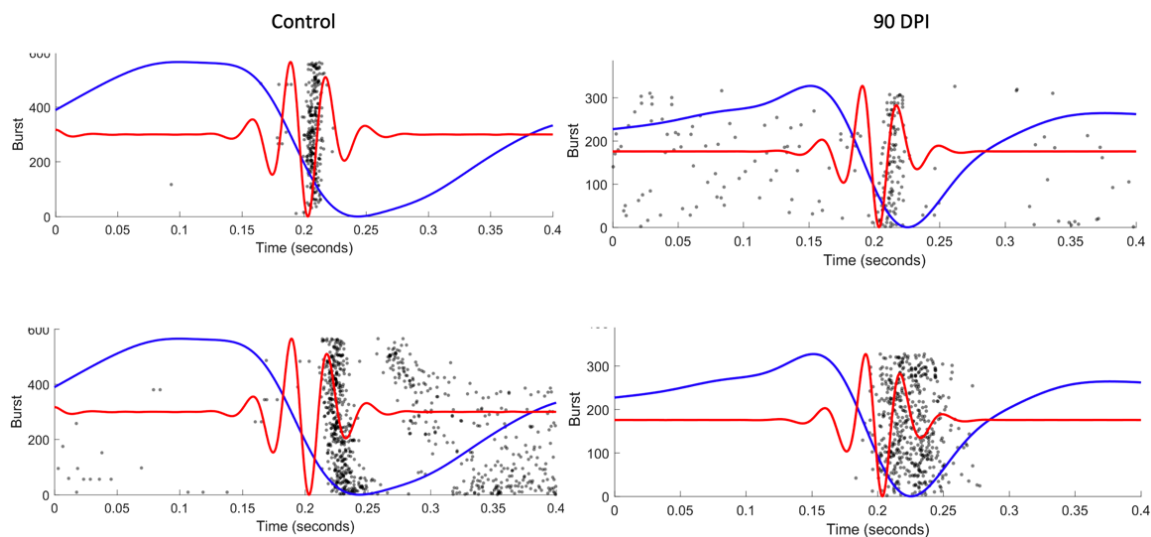
Here below are some figures representing the accuracy of spikes for multiple SWR-like events where the sharp wave (SW) and the ripple are aligned to the trough of the SW and the spike raster of each single unit is superimposed.



Accuracy of spikes for multiple SWR-like events

The left panels are representative single unit (of a control animal) firing during a SWR-like events where the neuron for each Burst (SWR) fires at a specific location relative to the SW and the ripple. The blue trace represents (average over burst) the slow oscillation (1-20 Hz) or sharp

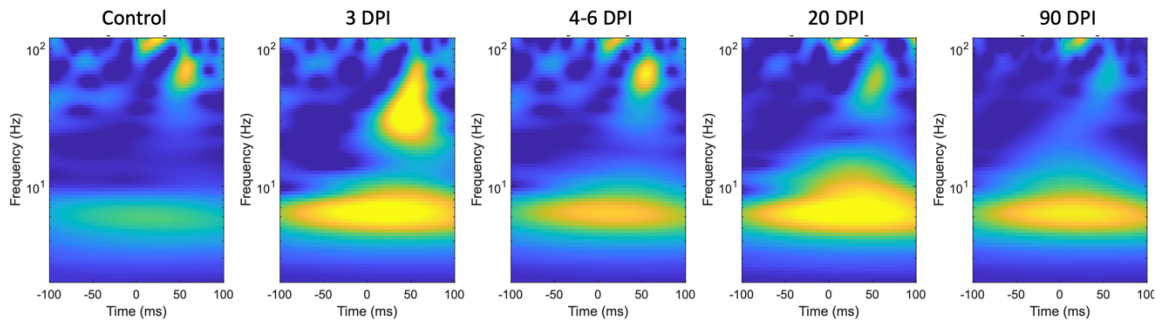
wave and the red trace represent the ripple or fast oscillations (30-70 Hz). The right side contains the firing of single units in an experimental animal 6 days post injection of the interneuron muting virus.



#### Accuracy of spikes for multiple SWR-like events

The left panels are representative single unit (of a control animal) firing during a SWR-like events where the neuron for each Burst (SWR) fires at a specific location relative to the SW and the ripple. The blue trace represents (average over burst) the slow oscillation (1-20 Hz) or sharp wave and the red trace represent the ripple or fast oscillations 30-70 Hz). The right side contains the firing of single units in an experimental animal 90 days post injection of the interneuron muting virus when the song is recovered.

Based on these example plots, we observed that the firing of neurons within HVC gets broader or less locked to specific phases of the SWR-like event oscillations. We hypothesize that this imprecise locking contributes to the broadening frequencies at which we detect high power during the perturbation compared to control events. The figure below illustrates this shift in power to high frequencies and then return to control like state when the song recovers. Moreover, at the point of recovered behavioral output the single neuronal firing “tightens” and locks to similar phases of the SWR-like events as observed in a control animal.



The change in spectral decomposition of the LFP signature during the detected deflections in multiple groups of animals.

Control (n=4); 3 days post injection of interneuron muting virus (DPI) (n=1); 4-6 DPI (n=4); 20 DPI (n=4); 90 DPI (n=4) averaged deflection events' LFP signature spectral decomposition via continuous wavelet transform.

Based on the spectral decomposition, we can observe increase in power around 10 Hz compared to control and the appearance of a new band of frequencies (40-70 Hz) that now carry significantly higher power, putatively due to the imprecision introduced in neuronal firing by our manipulation. This band according to prior studies constitutes interneuron firing frequencies in other animal models. Hence, we propose that the interneurons that are muted therefore lose precision of their firing and get more excitation from the projection neuron population (due to the lack of inhibition from interneurons) and fire even more. This shift gradually settles back to a similar power spectral landscape as a control state as the quality of the behavioral execution improves with the neuronal precision. Nevertheless, some of the increase in power stays unchanged, this we explain by the drastic reduction in putative neurons available in the circuit now have to increase their firing or have larger discharges to achieve an overall similar input to their post-synaptic partners to achieve proper motor production.

In sum, we detected deflection events during no-motion or sound periods in the putative sleep states of control and experimental birds. We observed that events that occur in an animal with a virus that mutes a large portion of interneurons in the pre-motor area are significantly differ from the events detected in animals that receive a control virus that does not alter motor production. Importantly, we do not postulate whether these detected deflections are the same but distorted upon manipulation in the experimental animals or they are completely different in nature. Either hypotheses mentioned prior could potentially occur, but neither takes away from the observation that the experimental animal specific event type and rate coincides with the behavioral degradation and recovery. However, this does not mean that we can argue whether these detected SWR-like events in the interneuron muted animals give rise to the behavior phenomena or they are the side product of significant removal of inhibition. We hypothesize that the SWR-like events described in the experimental animals suggestive of the state of behavioral deterioration or repair. This finding provides us a great tool to indirectly study the state of a pre-motor network without having to observe neuronal firing during behavioral

execution. Detection of SWR-like events during offline states (sleep or quiescent awake) of the network will serve us in the future as a reliable measure to give a broad indication to the quality of execution. This is important because LFP signatures of adult song require lots of renditions of singing that are hard to detect and the signal to noise ratio is so low that detection period for events during song production is limited. As opposed to detection of SWR-like events during offline periods is reliably quantifiable with large enough sample size per sleep period that it will provide a clearer view into the current state of the network.

## Chapter 4

### METHODOLOGY FROM CHAPTER 2 & 3.

#### **Methodology from Chapter 2: Wang et al., 2022.**

##### **Animals**

All procedures involving zebra finches are approved by the Institutional Animal Care and Use Committee of the California Institute of Technology. All birds used in the current study were bred in our own colony and housed with multiple conspecific cage mates of mixed genders and ages until use for experiments. Before any experiments, adult male birds (>120 days post hatch (dph)) were singly-housed in sound isolation cages with a 14/10 hour light/dark cycle for >5 days until they habituated the new environment and started singing. Thereafter, birds were kept in isolation until the end of the experiment.

##### **Viral vectors**

Lentiviral vectors were cloned using standard procedures, and were produced and titrated and described in (33). All LVs contained the internal Rous sarcoma virus (RSV) promoter driving expression of different transgenes. LV-TeNT encoded the light chain of tetanus toxin fused to EGFP with a PEST domain in its C-terminus. LV-NaChBac encoded the open reading frame of NaChBac fused to EGFP. AAV-TeNT contained the promoter from the human *dlx5* gene driving expression of the light chain of tetanus toxin fused to EGFP with a PEST domain (16). AAV-*dlx*-TeNT was produced by the Duke viral core facility.

##### **Stereotaxic injection**

Birds were anesthetized with isoflurane (0.5% for initial induction, 0.2% for maintenance) and head-fixed on a stereotaxic apparatus. Firstly, to inject a retrograde tracer in area X or RA, craniotomies were made bilaterally and fluorescent tracers (cholera toxin b 555 0.2% or fluoro-ruby 10%, 100-300 nL) were injected through a glass capillary (tip size ~25  $\mu\text{m}$ ) into the corresponding nuclei (coordinates from dorsal sinus in mm - area X: Anteroposterior (AP) 3.3-4.2, Mediolateral (ML) 1.5-1.6, Deep (D): 3.5-3.8; RA: AP 1.5, ML 2.4, D 1.8-2.1). To deliver virus (LV or AAV) into HVC, a second surgery was performed 7-10 days after retrograde tracer injection, by then HVC was strongly labeled by fluorescence and visible through a fluorescent stereoscope. Because LVs only diffuse a short distance from the injection site (~100-200  $\mu\text{m}$ ), LVs were injected into multiple locations (up to 16 sites per hemisphere, ~100 nL each) to deliver the transgenes into as many cells as possible throughout HVC. AAVs diffuse extensively (~500  $\mu\text{m}$ ), and single injection (~100 nL) in the center of HVC was sufficient to label enough cells. All injections in HVC were performed ~20 nL/min to minimize physical damage. At the end of every surgery, craniotomies were covered with Kwik-Sil and the skin incision was closed with Glutur.

##### **Song analysis**

Song analysis was performed using Matlab (Mathworks).

##### **Song feature parameterization**

Continuous audio recordings (44.1 kHz) were segmented into individual bouts manually and filtered to remove low frequency noise (cutoff frequency = 500 Hz). We used the open source Matlab software

package, Sound Analysis Pro 2011 (34) to generate spectrograms and derive non-linear, time-varying song parameterizations. The time-varying features were: pitch, goodness of pitch, Wiener entropy, frequency modulation (FM), amplitude modulation (AM), amplitude, aperiodicity, mean frequency, and the maximum power in each quadrant of the frequency range 0-11 kHz (labeled power 1, power 2, power 3 and power 4). These features were computed across the entire bout every 1 ms. These time-varying features were the base from which various portions of the song were further characterized.

### **Syllable parameterization**

A high-dimensional, acoustic parameterization of individual syllables was generated by then sampling a moving average (over 10 ms) of song features (pitch, goodness of pitch, mean frequency and entropy) at 10 points across the first 50 ms of each syllable. This resulted in a 40-dimensional song feature parameterization of each syllable. If a syllable was shorter than 50 ms, the feature vectors were padded at the end with zeros. This method allowed syllables to be compared in the same parametric acoustic space despite differences in duration.

### **Syllable segmentation**

We identified syllables and silences within each bout by imposing local thresholds on the time-varying log-power of the spectrogram, summed over all frequencies. To address variations in background noise during recordings across days, thresholds were defined individually for each bout. We first defined a conservatively high syllable threshold, below which the sound segment was defined as silence. The mean ( $\mu$ ) and standard deviation ( $\sigma$ ) of the silent regions for that bout were computed from the distribution of summed log-power values in the middle 50% of the conservative silent windows. A new threshold was defined as:  $\text{threshold} = \mu + a * \sigma$  within that bout. The multiple,  $a$ , was selected upon manual inspection of the stereotyped song structure for each bird and then applied across all recorded bouts across all days. We then performed a smoothing step wherein periods of silence less than 15 ms were converted to syllables. Syllables less than 20 ms were excluded from analysis.

### **Syllable timing distributions**

Syllable durations were extracted from the syllable segmentation process. Distributions of syllable durations were computed by normalizing each distribution of all syllable durations within individual days such that the sum of each daily distribution was one. Distributions for individual days were then assembled into a matrix wherein the columns represented distributions for individual days. This matrix was plotted as a heat map (Fig. 1C,G; 2H; 3D; S3B,E; S8B).

### **Syllable recovery trajectories**

To quantify fluctuations in song quality, we computed the average k-neighbor distances of individual syllables from original, stereotyped syllables in the undistorted song (35). This was calculated in the high-dimensional, acoustic space described in the Syllable Feature Parameterization section. In stereotyped, normal adult songs, most individual syllables form distinct clusters in a variety of parameterized acoustic spaces. We defined a normative set of syllables from 1-3 days of recording pre-viral injection when the bird was singing undisrupted, stereotyped songs. This syllable set was labeled according to syllable identity. Syllable identity was defined in an unsupervised manner using the Matlab clustering algorithm, dbSCAN. The dbSCAN clustering was performed on a reduced 2-dimensional acoustic space generated using the dimensionality reduction algorithm, Uniform Manifold Approximation and Projection (UMAP) (36, 37). The syllable assignments were cross checked by visual examination of a randomly selected subset of bouts and found to be in strong alignment with hand-marked syllable assignments. Syllables that did not cluster

into distinct groups were excluded from this analysis. Each individual syllable was then assigned a k-nearest neighbor distance ( $k = 25$ ) from the syllables in each normative syllable cluster. This is the average distance to the 25 closest syllables within the defined cluster. In normal, stereotyped songs, syllables have small k-neighbor distances to the syllable cluster to which they belong and larger k-neighbor distances to the other syllable clusters.

### **Song quality**

As a measure of local song quality, we tracked the quality of the syllables which most closely resemble our original syllable set, defined within a local window of singing. We quantified the k-neighbor distance of the closest syllables to each original syllable cluster in a local window of consecutively sung syllables ( $N = 400$  syllables; the .025 quantile of local k-neighbor distances to each syllable cluster) (Fig 1D,H; 2I; 3E,F; S3C,F; S8C). When the song is highly distorted, syllables do not cluster into clearly defined groups, nor do they resemble original syllable types. This method allows us to track syllable distances even when syllables are highly distorted.

### **Speed of recovery**

We use these syllable recovery trajectories to measure the speed with which the song recovers. We measure the point of half recovery by tracking how much time and practice respectively are required post-perturbation to achieve a 50% recovery to the pre-perturbation baseline. 50% recovery is calculated relative to the point of maximum syllable distortion for each syllable individually. This measurement is shown for the speed of recovery as a function of practice in Fig 3F,G.

### **Feature-dependent recovery**

We measured how different syllables in the song recovered at different rates by computing the correlation between syllable features and speed of recovery (Fig 2E,F,K). The two syllable features we considered were (1) the average maximum entropy for each syllable as a measure of syllable complexity and (2) the average duration of the original, undistorted syllable. Within each bird we normalized syllable features and speeds of recovery to be between 0 and 1, so that we could compare relative speeds of recovery within individual songs, across different birds. After normalizing, we computed Pearson correlation coefficients between the relative recovery time and the syllable features and assessed the significance of the correlation by computing the p-value testing the null hypothesis that there is no correlation between syllable features and recovery speed.

### **Song variability**

As a measure of song variability, we track the local variability of syllables to other syllables that have been sung within a consecutive 400 syllable window (Fig 2C,D,J). We quantify local variability as the average k-neighbor distance of each syllable to the closest 5 syllables within the local 400 syllable window. This measure of variability quantifies how different renditions are from one another, not how similar they are to the original song.

### **Continuous representation of bout trajectory**

We generated continuous representations of bouts across the entire perturbation trajectory as shown in Fig 2A,B,G, Fig 3C, and Fig S4 (38, 39). We randomly sampled 100 bouts from each day of recording to build a representative sample of the song over the course of the experiment. For each bout, we slid a 150 ms window in 3 ms steps along the bout length. We then generated a high-dimensional, acoustic parameterization of each 150 ms song window by taking the moving average in 20 ms segments every 5

ms of seven song features (mean frequency, pitch, goodness of pitch, power 4, power 2 and summed log power of the spectrogram). We performed principal component analysis on this high-dimensional set across all bouts to reduce the feature set to 30 dimensions and applied the UMAP algorithm to project this high-dimensional representation into two dimensions.

### **Song prevention**

Adult zebra finches 120-150 dph ( $n = 3$ ) were fitted with custom made fabric vests and a 20-40 gram weight attached to their vest pulling them towards the ground to prevent them from acquiring singing posture. All birds received LV-TeNT injection bilaterally into HVC. Before we prevented the birds from singing we allowed them to sing a few renditions to confirm that their songs were degraded. Afterward, the birds were restricted from singing for ~10 days, during which they were monitored with a video camera to make sure they did not sing but make calls. We confirmed that all the birds were able to move, perch, drink and eat freely and even allowed them to sing several renditions occasionally (1-3 every 2-3 days, which allowed us to track the degradation/recovery of songs). The size of the bullet weight on the birds had to be adjusted since they got accustomed to the weight in 2-3 days and attempted to sing more frequently. The weights and vest were removed daily, 1 hour prior to the light-off period while the experimenter stood next to the chamber to closely monitor that the birds were not singing. The vest and weights were put on the birds again as soon as lights were turned back on the next day. After the prevention period, the birds were free to sing in their respective isolation chambers.

### **Electrophysiology**

Birds were first overdosed by an intramuscular injection of ketamine/xylazine (120/12 mg/kg) and after they became unresponsive to toe pinching, they were decapitated. The forebrain was quickly removed and kept in ice-cold slicing solution (in mM: sucrose 213, KCl 2.5,  $\text{NaH}_2\text{PO}_4$  1.2,  $\text{NaHCO}_3$  25, Glucose 10,  $\text{MgSO}_4$  2,  $\text{CaCl}_2$  2, pH 7.4). Sagittal slices (300  $\mu\text{m}$ ) were cut using a vibratome (Leica VT1200S) and then incubated in HEPES holding solution (in mM: NaCl 102, KCl 2.5,  $\text{NaH}_2\text{PO}_4$  1.2,  $\text{NaHCO}_3$  30, HEPES 20, Glucose 25,  $\text{MgSO}_4$  2,  $\text{CaCl}_2$  2, pH 7.35) at 34.5 °C for 30 minutes. Afterwards, slices were kept at room temperature (~ 22 °C) between 30 minutes to 5 hours before being moved to the recording chamber. Bath ACSF (in mM: NaCl 124, KCl 2.5,  $\text{NaH}_2\text{PO}_4$  1.2,  $\text{NaHCO}_3$  26, Glucose 25,  $\text{MgSO}_4$  1,  $\text{CaCl}_2$  2, pH 7.35, 33-34°C) was continuously perfused (~2 mL/min) during recording. For current clamp whole-cell recordings, glass pipettes were filled with an intracellular solution (in mM): K-gluconate 135,  $\text{MgCl}_2$  3, HEPES 10, EGTA 0.2,  $\text{Na}_2\text{-ATP}$  2, phosphocreatine 14, pH 7.25. HVC(RA) cells were identified by the presence of the retrograde fluorescent tracers injected into RA. We used voltage clamp to record miniature EPSCs with the following chemicals added to the bath (in  $\mu\text{M}$ ): TTX 0.5, nimodipine 5 and picrotoxin 50, and glass pipettes were filled with (in mM)  $\text{Cs}(\text{CH}_3\text{SO}_3)$  135,  $\text{MgCl}_2$  2, HEPES 10, EGTA 0.2, QX-314.Cl 5,  $\text{Na}_2\text{-ATP}$  2, phosphocreatine 14, pH 7.25. To record mIPSCs the following chemicals were added to the bath (in  $\mu\text{M}$ ): TTX 0.5, nimodipine 5, CNQX 10 and APV 25, and pipettes were filled with (in mM) CsCl 120, K-Gluconate 12,  $\text{MgCl}_2$  2, HEPES 10, EGTA 0.2, QX-314.Cl 5,  $\text{Na}_2\text{-ATP}$  2, phosphocreatine 14. For whole-cell NaChBac current recording, the bath solution did not contain any  $\text{CaCl}_2$  to eliminate  $\text{Ca}^{++}$  currents, and TTX and 4-AP were added to block currents from the endogenous  $\text{Na}^+/\text{K}^+$  channels, and glass pipettes were filled with (in mM) CsCl 135,  $\text{MgCl}_2$  3, HEPES 10, EGTA 0.2, TEA-Cl 2,  $\text{Na}_2\text{-ATP}$  2, phosphocreatine 14. We only analyzed recordings in which access resistance was always smaller than 10 percent of the membrane resistance of the cell and no compensation was applied. Membrane potential was held at -70 mV to measure mEPSCs and -60 mV for mIPSCs. Liquid junction potential was not corrected. Electric signals were amplified and sampled at 20 kHz by an EPC-10 system (HEKA). Data analysis was performed off-line using Fitmaster (HEKA), Mini-Analysis

(Synaptosoft) and Matlab (Mathworks). Data were presented as mean  $\pm$  s.e.m. Statistical difference was tested using one-way ANOVA followed by student's t-test.

### **Histology**

After the experiments concluded, animals were sacrificed and their brains were processed for histological analysis. Animals were first deep anesthetized by intramuscular injection of ketamine/xylazine (100/10 mg/kg) and perfused intracardially with room temperature 3.2% PFA in 1xPBS. Brains were then extracted and incubated in the same fixative for 2-4 hours at room temperature. Each brain hemisphere was cut sagittally with a vibratome into 70-100  $\mu$ m thick sections. The brain slices containing HVC were collected and incubated overnight with a rabbit anti-GFP antibody (1/1000, AB3080P, EMD Milipore) in 1xPBS containing 10% donkey serum and 0.2% Triton at 4 °C. Sections were washed in 1xPBS with 0.05% Triton and incubated for 2 hours at room temperature with a secondary antibody (goat anti rabbit IgG Alexa 488, ab150077 Abcam). Brain slices were washed and mounted in Fluoromount (Sigma). Confocal images were taken with a LSM800 microscope.

### **Methodology from Chapter 3: Torok et al., 2022 (in progress).**

#### **Chronic electrophysiology recording**

Animals (n=4, 300-700dph) were implanted in the right hemisphere HVC with 4 by 4 electrode arrays (Neuronexus A4x4-3mm-50/100-125-703-CM16LP) based on retrograde fluorescent labeling of HVC (just as for viral injections). Electrode implantation occurred within the same surgery as the viral injection.

This procedure follows the same surgical steps as the viral delivery protocol, until the point of electrode implantation. A small opening was cut on the dura (just big enough to fit the electrode array) to lower the electrodes manually. The reference and ground was a gold screw pin placed into the cerebellum. The skin was removed from the surface of the skull for the majority of the surface, in order to secure the implant. Before implantation the skull and the craniotomies were cleaned with saline and dried and the skull was prepared according to the protocol of the C&B Metabond cement system. Post implantation we covered the craniotomies with kwik-sil, once that hardened we covered the whole skull and the part of the electrode still exposed with metabond. The headstage (Intan RHD Part # C3335) was connected to the probe before implantation and securely metabonded to the connection between probe and headstage in order to prevent detachment when the bird is moving. SPI interface cables (Intan Part #C3203, #C3213) connected to the acquisition board (Open ephys). Data was recorded at 30000 Hz with the open ephys software system. Animals were freely moving with a passive counter-weight based committor system.

#### **Analysis of the chronic electrophysiology recording**

Data was collected with the open ephys software at 30KHz for 24 hours of the day most days. Custom matlab code was written to pre-process and calculate the power per hour per channel per day for each bird for the length of the 100 day recording epoch. Data pre-processing involved: downsampling (1KHz) and de-meaning after excluding electrodes that based on histology or singing related activity seemed to be outside of HVC. Then we used the built in matlab function pwelch to calculate the power per channel at each frequency per hour for a 3 hour window during the lights off (1-3 am) and lights on (8-10 am) period. The hamming window size used was 700 (samples) and the overlap was 50%, we specified 'power'

not power spectral density to retain an averaged value of power. After obtaining these power values per channel per frequency we calculated the median for all hours and channels per frequency bin. Our binned frequencies are 1-3Hz (delta), 4-7Hz (theta), 8-12Hz (alpha), 18-25Hz (beta), 30-70Hz (gamma) and 71-200Hz.

### **Acute electrophysical recording**

Animals (n=10, 140-250 dph) went through the same surgical procedure as described for a stereotaxic viral injection. However, at the end of the surgery the skin was removed from the skull and the whole skull was pre-treated and covered in metabond except for the craniotomies over HVC that were covered with kwik-cast until the day of the acute recording session. Shortly before the recording session a head-bar was glued on top of the frontal surface of the metabonded skull to allow head-fixation of the bird for the recording session. Then the kwik-cast was removed from the craniotomy over HVC (left or right hemisphere or both depending on the animal) and a small incision was made in the dura over HVC, which was identified by the retrograde tracer previously injected. The ground was placed into the cerebellum. Then the high-density silicone probe (Neuropixel) was lowered with a motorized arm over hours for 2.6-3 mm deep into the brain. The headstage and acquisition board was connected to the computer and data was recorded with the open ephys software. Once the probe settled in the brain we had 4 distinct recording sessions. Recording sessions: lights on silence (10 mins) then playback of the BOS (bird's own song) (3-10 mins); lights off silence (10 mins) then playback of the BOS (bird's own song) (3-10 mins); microinjection of 100nL 250microM Gabazine (Hellobio, HB0901) then repetition of the same protocol of lights off and on as without Gabazine.

### **Analysis of the acute electrophysiology recording**

The low frequency electrophysiology data was recorded at 2500Hz while the high frequency data was recorded at 30000 Hz. Custom matlab script was written to analyze the low and high frequency oscillations. All low frequency data was high pass filtered (1-300Hz) and median subtracted. All high frequency data was common average referenced and low-pass filtered (300-7000Hz). For spike detection we used two separate methods, one to threshold the high frequency data to only consider spikes that are 9 standard deviations above the average signal in a 2 minute window. The second method used for spike detection was using the Kilosort software v2.5 to extract spikes from the raw data.

To calculate the power at low frequencies we used the exact same script developed for the chronic recordings. Detection of large discharges were done in a semi-automated way with thresholding that then we manually sorted.

### **Dissociation and cDNA generation protocol**

Animals were anesthetized with a mix of ketamine-xylazine (0.02 mL / 1 gram) and quickly decapitated, then the brain was placed into a carbogenated (95% O<sub>2</sub>, 5% CO<sub>2</sub>) NMDG-ACSF petri dish on ice. The brains were dissected on a petri dish with NMDG-ACSF surrounded by ice under an epifluorescent microscope guided by the fluoro-ruby retrograde tracing from Area X to HVC.

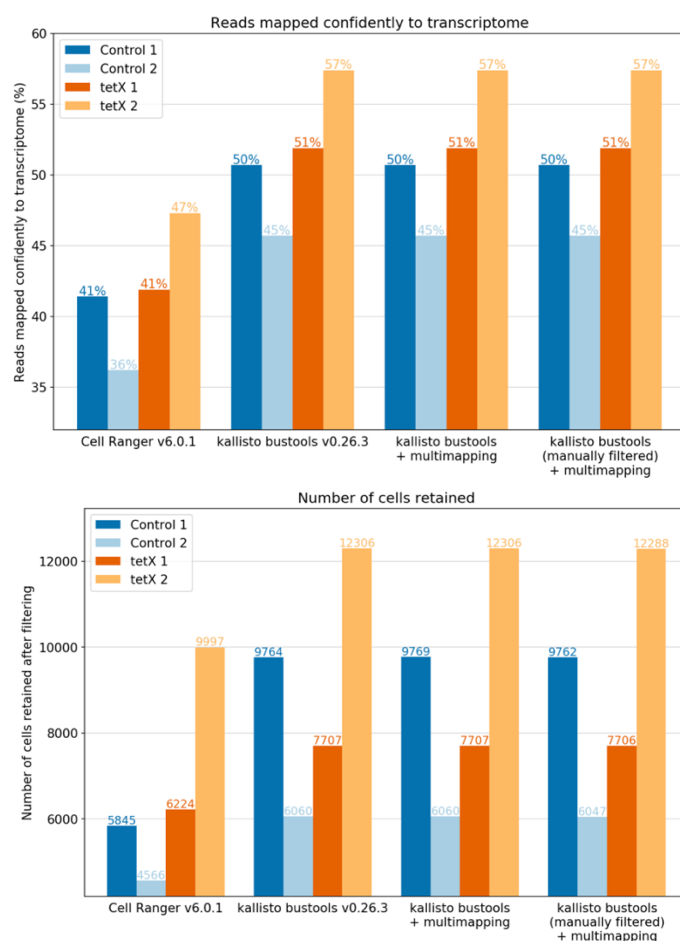
We used the commercially available Worthington Papain Dissociation system with some minor changes and add on steps. We followed all the steps included in the Worthington protocol with a final concentration of 50 U/mL of papain. To match the intrinsic osmolarity of neurons in zebra finches we used NMDG-ACSF (~310 mOsm) instead of the EBSS for post dissection and STOP solution. Another addition was to add 20µL of 1mg/mL Actinomycin D (advanced from Allan-Hermann Pool) into 1mL

of the post dissection medium and the STOP solution in which trituration occurred. Papain digestion occurred for an hour on a rocking surface with constant carbogenation in a secondary container above the sample viral on RT. We performed trituration with increasing smaller diameter glass pasteur pipettes. Trituration was performed inside the papain solution then when the tissue was fully dissociated we centrifuged the samples at 300 g RT for 5 minutes and resuspended in STOP solution. Then, we used a 40µm Falcon cell strainer pre-wet with the STOP solution and centrifuged again at 300 g RT for 5 mins. Finally, we resuspended the cell pellet in 60µl of STOP solution and proceeded to barcoding and cDNA synthesis. The cell barcoding, cDNA synthesis and library generation protocol was performed according to the chromium next GEM single cell 3' reagent kits v3.1. Sequencing was performed on a Illumina Novaseq S4 sequencer with 2x150 bp reads.

### **Single-cell RNAseq analysis by Laura Luebbert**

#### **Generation of count matrices**

The reference genome GCA\_003957565.2 (Black17, no W) was fetched from Ensembl on March 20, 2021 ([http://ftp.ensembl.org/pub/release-104/gtf/taeniopygia\\_guttata/](http://ftp.ensembl.org/pub/release-104/gtf/taeniopygia_guttata/)). We quantified the gene expression in each of the four datasets using the kallisto-bustools workflow (Melsted et al., 2021). The reference index was built using kallisto-bustools (v0.26.3) and the above-mentioned reference genome. Subsequently, the WRE sequence was manually added to the cDNA and t2g files generated by kallisto-bustools to allow the identification of transgenic cells. The count matrix was generated for each dataset using the kallisto-bustools count function. The resulting count matrices were compared to those generated by the 10X Cell Ranger pipeline (v6.0.1) and kallisto-bustools count with multimapping function. For all four datasets, kallisto-bustools mapped approximately 10% more reads than Cell Ranger (shown in the figures attached below). No increase in reads mapped confidently was observed when using the multimapping function, indicating that reads align confidently to one gene in the reference genome as indicated by the figures below.



## Quality control and filtering

The datasets were filtered separately based on the expected number of cells and their corresponding minimum number of UMI counts. Following quality control based on apoptosis markers and library saturation plots and the count matrices were concatenated and normalized using  $\log(\text{CP10k} + 1)$  for downstream dimensionality reduction and visualization (e.g., PCA) using Scanpy's *normalize\_total* with target sum 10,000 and *log1p*.

## Dimensionality reduction and normalization

The concatenated data was mapped to a lower dimensional space by PCA to the expression data filtered for highly variable genes using Scanpy's *highly\_variable\_genes* on the log-normalized data. Next, we computed nearest neighbours and conducted Leiden clustering (Traag et al., 2019) using Scanpy.

Initially this approach was performed on the control and tetX datasets separately. This resulted in the identification of 19 clusters in the control data and 22 clusters in the tetX data. For both conditions, equal contribution from both datasets confirmed that there was minimal batch effect, as expected since the data was sequenced in a pooled sequencing run. We also performed batch correction using scVI (Lopez et al., 2018) which did not change the

contribution of each dataset per cluster. As a result, we continued the analysis using the data that was not batch-corrected with scVI.

Next, we concatenated all four datasets and followed the approach described above. This resulted in the identification of 21 Leiden clusters (shown in Chapter 3 in the cell-type assignment heatmap Figure 10), which we also refer to as cell types. Each cluster was manually annotated with a cell type based on the expression of previously established marker genes (Chapter 3 cell type assignment heatmap, Figure 10). The cell type annotation was validated by the top 20 markers extracted from each cluster using Scanpy's `rank_genes_groups` (P values were computed using t-test and adjusted with the Bonferroni method for multiple testing). Clusters identified as glutamatergic neurons were further broken down into HVC-X- and HVC-RA-projecting glutamatergic neurons using previously established marker genes. We found that re-clustering all cells labeled as glutamatergic neurons using the Leiden algorithm did not yield different results and hence continued with the initial clusters.

### **Comparative analysis of clusters and conditions**

Differentially expressed genes between clusters were identified using Scanpy's `rank_genes_groups` (P values were computed using t-test and adjusted with the Bonferroni method for multiple testing, and confirmed by comparison to P values generated with wilcoxon test with Bonferroni correction). In the violin plots, a star indicates a P value  $< 0.05$  and a fold change  $> 1.5$  difference in mean gene expression between the indicated conditions (P value computed with stats' `ttest_ind` and adjusted with the Bonferroni method for multiple testing) (unless otherwise indicated).

### **In situ hybridization protocol by Alex Nevue**

Brains were coronally blocked anterior to the tectum and flash frozen in Tissue-Tek (Sakura) prior to being sectioned at 10um on a cryostat and mounted onto charged slides (Superfrost Plus, Fisher). *In situ* hybridization was performed as previously described (Carleton et al., 2014; Nevue et al., 2020[MOU1]). Briefly, DIG-labeled riboprobes were synthesized from cDNA clones for RGS10 (CK312091) and LOC100231469 (class I histocompatibility antigen, F10 alpha chain; DV951963)[MOU2]. Slides containing the core of HVC were hybridized overnight at 65°C. Following high stringency washes, sections were blocked for 30 min and then incubated in an alkaline phosphatase conjugated anti-DIG antibody (1:600, Roche). Slides were then washed and developed overnight in BCIP/NBT chromogen (Perkin Elmer). To minimize experimental confounds between animals, sections for each gene were fixed together in 3% paraformaldehyde, hybridized with the same batch of probe, and incubate in chromogen for the same duration.

Sections were imaged under consistent conditions on a Nikon E600 microscope with a Lumina HR camera and imported into ImageJ for analysis. We quantified the expression level of the gene as measured by optical density and the number of cells expressing the gene per unit area, as previously described (Zemel et al., 2021[MOU3]). Optical density was measured by taking the average pixel intensity of a 300x300 pixel square placed over the center of HVC. This value was normalized to the average background level of the tissue. To quantify number of labeled cells, we established a threshold of expression that was 2.5x the background level. Binary filter (Close-, Open) were applied and the number of particles in the same 300x300 pixel square were quantified.

## *Chapter 5*

### PILOT EXPERIMENTS AND RESEARCH PROPOSALS

This chapter will summarize a handful of pilot experiments that I have conducted to improve existing methodology or to reproduce previously published results. As well as a handful of research proposals that I formulated based on some preliminary data.

I will not include figures. This serves as information for future experiments to build upon.

#### **Tracheosyringeal nerve (ts nerve) resection in zebra finches**

The ts nerve is the final executor of the motor circuit that innervates the syrinx. Previous studies have shown that severing this nerve on one side of the syrinx causes acoustic degradation of the song (Williams & McKibben, 1992). Bilateral lesion of this nerve would lead to insufficient breathing in the animals, therefore that is not possible. My experimental paradigm was interested in looking at the fine scale level of how syllable composition changes upon unilateral resection of this nerve.

My findings showed that for male zebra finches between (90-300 days post hatch) there is not only change in the acoustic structure of the syllables but also the syllable content that makes up a bout of song. Animals can drop or increase the number of syllables produced after lesion and naturally the acoustic parameters of all changes. However, if you lesion this nerve in older animals (2 years or older) then only the acoustic features of the sound produce change, there is not addition or deletion on the syllable content. This was a finding that to my knowledge was novel to the field but did not stand on its own as an observation to be publishable.

#### **Song playback of altered bird song at night for adult male zebra finches**

Previously (Leonardo & Konishi, 1999) has shown that if you play back an altered auditory feedback of the bird's own song (BOS) when the bird sings then eventually the crystallized adult bird song shifts and changes. This change can recover if the experimenter stops the playback paradigm. This line of evidence together with the finding that there is replay of the BOS during sleep, I set out to test what happens to full adult animals if you playback and altered version of its song at night. This experimental paradigm had multiple challenges, one of it being that the playback has to be loud enough so the bird can register it but not too loud so the sleep of the bird is unperturbed. I had 4 control (playback unaltered BOS) and 3 experimental animals (leaving out or switching one of the middle or last syllables of the BOS) that I played their song or an altered version back to for 4-6 weeks. There was no obvious change in the song of these animals after the experiment was finished. I believe this is due to some uncontrolled parameters in the experimental design and that maybe if a revised protocol was performed there would be changes.

First, the animals were housed with a female which makes them sing more female directed songs that could help in stabilizing the song that is about to shift. Second, the animals were older than 1 year, it is possible that animals between 90-300 days post hatch have a more plastic motor circuit (based on my previous observations) therefore I would choose animals

in the young adult age group. Third, the Leonardo paper played back online distorted song for almost 4 months, and some animals never shifted their song. Hence, it is possible that if I extended the length of the experiment and increased the n numbers we would have seen differences.

### **Ablation of LMAN in adult male zebra finches**

In many previous studies researchers have attempted to lesion brain nuclei in zebra finches (Hampton et al., 2009; Kao & Brainard, 2006; C. Scharff & Nottebohm, 1991; J. A. Thompson et al., 2007; Wilbrecht et al., 2002). Most use electrolytical lesion which have certain problems, such as lesioning axonal pathways that pass by the area of target. In my experimental paradigm, I aimed to ablate LMAN a nucleus important for song learning (as an injector of noise into the circuit to allow for vocal exploration and plasticity) after injection of interneuron muting virus into HVC. The idea behind this is the following: if the reason why the animal produces degraded songs after perturbation of HVC is because LMAN drives activity of Ra (like in a juvenile bird) the motor nucleus then if lesioned there will be no degraded song production.

I used ibotenic acid dissolved in NaOH to chemically ablate LMAN, this compound binds to the ligand binding site of glutamatergic receptors on neurons and hyperactivates them until they die. This type of ablation is much more precise to the site of injection so many surrounding important areas such as Area X. In most previously published papers the percentage of LMAN ablated is around 30-50% ( this is confirmed by CGRP antibody staining, it is a protein that is specifically expressed in this area). In my experimental design in most animals I achieved ablation of 80-100% of LMAN bilaterally confirmed by CGRP staining. After lesion of LMAN many animals do not sing for 1-3 days, but after this initial period of no singing the song is the same as before lesion. In addition, the acoustic variability within each syllable decreases (which agrees with previous findings).

In terms of the outcome of the full experimental paradigm, meaning LMAN lesion then muting of interneurons in HVC. I found that the song of these animals does degraded and that it takes longer for the song to recover. However, this is hard to measure because some animals post interneuron muting do not recover their song completely. Even though this result does not seem straight forward there is indication that without LMAN the song does degraded so degraded vocalization is not due to LMAN drive to Ra and that recovery might take longer without LMAN induced vocal plasticity even in adults. This finding would suggest that LMAN that was believed to have no role in adult song production might be needed to maintain some level of vocal plasticity to be able to maintain the song of adult birds in case of injury or damage.

### **Viral vectors to target specific motor nuclei and cell types**

In collaboration with Viviana Gradinaru's lab I have tested many variants of the AAV9 capsid that was randomly mutated to see whether these enhance the viral expression in certain brain areas or if it will allow us to develop a system delivery method in which the virus could cross the blood brain barrier and get highly expressed within the brain. In order to test whether the blood brain barrier (bb) can be crossed I performed retro-orbital injections in adult zebra finches. This is a very difficult procedure because birds have double eyelids so correctly targeting the retro-orbital vessels is challenging. However, I observed

very inefficient bb barrier crossing with high expression of some AAV9 variants in the liver and the heart tissue.

After this preliminary test of bb barrier crossing, I decided to do direct injection of several of these variants of AAV9 directly ( by stereotaxic injection) into the motor nuclei of birds. A main source of problem in the song bird field is to target Ra by viral injection. Possibly the lack of infectivity in this area can be due to very high levels of myelination or some sort of lack of cell surface receptors to be able to take up viruses. Since AAV9 has the highest level of infectivity based on our observations in zebra finches, we set out to test variants of it.

After a long period of testing variants, I have identified ZF5 and ZF3 ( code names for the mutant variant capsids of these AAV9s) as promising candidates to target Ra.

In HVC only interneurons and HVC-X projecting neurons are labelled with the commercially available AAV9 viruses, however, it is possible these new variants could also infect the HVC-Ra population. This is a potential avenue for follow up experiments in our laboratory.

In another set of experiments, we asked whether this general resistance to viral infections is limited to zebra finches. For this purpose, we used Bengalese finches (inbred and cannot be found in the wild) with the hypothesis that these animals since always in captivity have a weaker immune system, hence, can be more susceptible for viral infection in their brains.

To our surprise, the tested AAVDJ virus did not seem to have a higher rate of infectivity in the Bengalese finch brain compared to zebra finches. On the other hand, it is possible that this is specific to this AAV capsid DJ that we tested. Further testing of different capsids of AAVs and other viral vectors will be needed to decide the outcome of this study.

In another attempt to increase infectivity of AAV viruses in birds, we developed an in vitro paradigm to test if we can introduce AAV receptors (previously published) onto the cell surface of finch cells. This would hypothetically increase the uptake of the virus by the target neurons. However, in vitro in zebra finch cultured cells there was no difference between level of infectivity with or without the AAV cell surface receptors.

### **Summary and Discussion of the thesis work**

The aim of my doctoral study was to investigate the resilience of a highly specialized motor circuit in the adult zebra finch brain. This was established by several different lines of experimental paradigms. First, I investigated the changes in behavior after directed muting of either interneurons or projection neurons in the pre motor area. This experiment is fundamentally different from other song manipulation studies in the field due to the specificity of targeting different neuronal subtypes reliably. However, there is a publication that perturbed HVC-Ra or HVC-X neurons by selective lesion with a light sensitive toxin (Constance Scharff et al., 2000). This resulted in widely different results from our perturbation studies both in length and nature of song degradation and reliability of the perturbation (only 4 birds out of 13 has song degradation). Studies causing electrolytical micro lesions within HVC lacked precision and cell type specific targeting in the area. In addition, the length and severity of song degradation was much less pronounced. There has been no publication to date that genetically manipulated interneurons in the pre-motor circuit. In the previously mentioned cell-type specific neuronal death induced changes the authors argue that only manipulation of neuronal types that have adult neurogenesis leads to degradation and full recovery of the behavior. However, in my experiments with muting interneurons I showed that manipulating interneurons also leads to behavioral changes that are recoverable. This suggests an important idea, that the HVC microcircuit needs to function as a whole in order to produce the stereotypic adult song. In addition, that since there is no new interneuron addition in adult finches this shows that there are other mechanisms at play to induce the recovery of the circuit that does not solely rely on adult neurogenesis (Scotto-Lomassese et al., 2007). Furthermore, in the single cell RNA sequencing dataset at 25 days post injection of interneuron muting we did not detect an increase in neurogenesis marker genes, further proving that this is not the main mechanism of song recovery on the neuronal level within HVC.

Second, I focused on the bulk changes in neuronal dynamics after removal of interneurons from the HVC microcircuit. There has not been any published finding that compared neuronal activity in unmanipulated and manipulated HVC patterns of activity. This study followed the progression of song degradation and recovery in HVC interneuron muted animals and control animals. Since the HVC anatomical organization is not well understood we were unsure of the quality of signal we could detect for an experimental timeline of this length. Unlike the hippocampus, HVC does not have a columnar organization, therefore LFP (low frequency 1-200 Hz, extracellular oscillations) signals are very weak (given that the dipoles do not align). The weakness of the signal and the nature of song degradation (the bird's song loses all stereotypy) did not allow us to reliably assess the LFP signature during singing for the length of the experiment. In previous publications (Gardner, Brown) researchers have shown that if you extract the LFP content of HVC while the bird is singing, you can obtain a very reliable and stereotypic LFP signature. Unfortunately, even for the control birds that I injected with a virus that does not perturb the behavior this LFP signature was not clearly detectable. The main reason for this could be that actually just the presence of the virus does affect the stability of the LFP pattern, which does not lead to changes in song but makes quantification impossible.

To be able to study the dynamics in HVC for this chronic electrophysiology recordings we decided to focus on sleep related activity. Previous studies have shown the importance of sleep during song learning and the presence of replay of the birds' own song during sleep within HVC and Ra. In addition to previous studies, my findings about song prevention (if you prevent animals from singing

after muting projection neurons in HVC, the song can recover significantly without practice) also point to the need for some offline unsupervised process that aids in song recovery.

To gain a better understanding on larger trends in the dataset, I decided to look at the median power at all LFP frequencies at night over the length of the experiment and compare that to the control animals. Surprisingly, I found that in the lower frequencies 1-20 Hz there is a large increase in the LFP power in the interneuron muted HVCs compared to control. One hypothesis to explain why drastic changes in activity would be easier to detect in sleep comes from the observation that during sleep the overall tone of inhibition in a circuit decreases and synchrony within the same brain area increases. This is an essential tool used in seizure studies, because most seizures in human and mammalian subjects occur in slow wave or deep sleep in the beginning hours of sleep. This made us think that it is possible that we can better detect discharges due to muting interneurons that lead to overexcitation of excitatory neurons in sleep.

However, detecting single neuronal signal is not feasible with the chronic electrode implants for the length of the song degradation and recovery period. In order to overcome this technical hurdle we decided to do acute recordings with high density probes in head fixed sleeping animals at multiple snap shots of song degradation and recovery. Another advantage of this method is that we can simultaneously record from both the pre-motor (HVC) and the motor (Ra) nucleus and we can observe the direct affects HVC activity has on Ra in real time. The findings show short term hyperactivation of HVC that is paired with decrease in Ra activity. In the mid and long term experimental animals HVC gets silenced and its sleep related activity does not return to baseline even when the song of the animal is recovered. This suggests that there is a need for sufficient level of activity to produce the song but that does not mean that it has to be reset to baseline. Activity in Ra in the mid and long term song degraded and recovered animals returns to control levels.

In addition to studying how does lights off / sleep activity is in the experimental and control animals behave we administered a GABA type A receptor blocker (Gabazine 250 $\mu$ M) to assess the effect sudden loss of inhibitory tone. This is important because in the experimental animals the interneurons slowly start expressing the muting agent which means there could be constant homeostatic processes shifting circuit level activity in order to avoid pathological discharges. This is a hypothesis that was reinforced by the difficulty we encountered to detect large discharges at 3-5 days post muting of interneurons in experimental animals. Additionally, experimental animals produced longer abnormal discharges from time to time than the control animals after administering Gabazine. This also shows that the state of the HVC circuit is completely different from control animals, and that homeostatic mechanisms are probably in the works to balance for the disruption. In existing literature, scientists have applied drugs that achieved sudden loss of inhibition that effected song production and lead to degradation of song. The discharges detected during lights off periods are a good tool to measure whether the relationship between single neuronal activity and LFP signature changes due to the manipulation. Historically sharp wave ripples in the hippocampus serve for memory formation and maintenance which is a phenomena of single neurons reliable firing at certain phases of slow wave components of the LFP signature. Although, zebra finch HVC is not the hippocampus the post perturbation discharges are a form of sharp wave ripples and this phase locking phenomena could be essential for maintaining the information about the song. We found a broadening of single neuronal firing relative to certain phases of alpha (1-30) and gamma (60-90Hz) oscillations that could indicate the imprecision and loss of information when the song is degraded. This broadening recovers to sharper phase locking to the ripples as the song quality improves during recovery similar to controls. To add, we detected and characterized the frequency, amplitude and power content of negative deflections during sleep in control and experimental chronically implanted animals. We

concluded that the rate, amplitude and power of events in the experimental decreases to a similar level of the event characteristics in control animals (that stay constant from day 1-60 of the recordings, indicating that glial scar formation does not prevent the detection accuracy of these events). This is the first publication describing sharp wave ripple like events that become distorted and recover on the same time scale as those same animals song behavior does. This study drew an important correlation between observing offline activity to assess the state of the pre-motor circuit and to infer the quality of behavioral execution.

Third, after in depth analysis of the changes in neuronal firing during the gradual muting of interneurons in the pre motor circuit I decided to look at the genetic changes that accompany this drift and re-establishing of the behavior. In order to study this, we used single cell RNA sequencing of experimental and control animals' HVCs to assess gene expression changes in each cell type within HVC at 25 days post manipulation (to give time for homeostatic processes to work on the circuit recovery. One previous publication performed single nuclei RNA sequencing in the zebra finch HVC, where their findings were focused on the origins of cells types and comparison to mammalian neurons of similar regions. Even though this study captured the nucleus of cells ( gives much more immature transcripts that might not represent the true state of the cellular transcriptome) the major cell types found in our control animals and the previously reported ones are similar. However, our preparation was different in that we used retrograde tracing to fluorescently guide us to achieve complete resection of both HVCs for each birds, whereas, they used myelination as a guide. The goal of this experiment was to compare the transcriptomic profile of birds with viral injection but with or without interneuron muting within HVC. This type of analysis is unique and has not been done in zebra finches before. Our main findings indicated two major pathways of homeostatic regulation. First is the increased number of microglia in experimental animals, microglia as the resident immune cell of the central nervous system plays a role in immune response and also in synaptic reorganization during learning in several brain areas like the visual cortex (Ma et al., 2019). Since our control animals also go through a viral infection, we believe that the microglia upregulation is more related to synaptic reorganization then to immune response. Second is the increase in major histocompatibility complex 1 (MHC1) associated gene expression in all cell types in the experimental animals. MHC1 is a receptor used for presenting antigens to cytotoxic T cells for immune response. Moreover, MHC1 also plays are role in synaptic reorganization during development (Turrigiano, 2011). These findings need to be confirmed by in situ hybridization to make sure that the differential gene expression patterns are not a side effect of the random sampling of cellular population from HVC or of the RNA capturing and amplification methods.

In situ hybridization studies we conducted showed that the increase in number of microglia between control and experimental animals at 24 days post injection is supported. Furthermore, we also looked at levels of microglia after song recovery and during juvenile song learning. We showed that after the song is repaired the levels of microglia are similar to control levels where there was no behavioral change only viral injection. In addition, the levels of microglia in juvenile male birds are the highest at 25 days when the bird starts sensorimotor learning of the song, as the song becomes stereotypic and crystallizes the levels of microglia taper off. These lines of evidence support our hypothesis that mechanisms of circuit establishment during development and injury repair or adult memory maintenance could be shared. We suggest microglia to have a key role in synaptic plasticity and proper circuit maintenance. This finding can serve as a candidate pathway for putative induction of injury repair in other motor circuits.

Together, the series of experiments I have conducted over the years aid in a better understanding of the nature of the motor circuit in zebra finches. Several new lines of hypothesis could be tested based

on the findings I obtained in very diverse experimental paradigms. I show that singing behavior can degrade and recover via muting of specific types of neuronal populations within HVC and that this recovery is somewhat independent on practice. I demonstrated the importance of interneurons in the HVC microcircuit and the putative role of sleep in recovering motor function. As well as, I was able to identify mechanisms with which the brain is coping with injury.

In the future I aim to further my studies and investigate the relationship between single neuronal activity locked to SWR-like events during song learning or recovery from a diverse pool of manipulations. Detection of offline events that can predict or indicate the state of the pre-motor circuit will be an important tool that I will take for further studies to prove this hypothesis. I aim to characterize the phase amplitude coupling between sharp waves and ripples as well as, phase locking of single neuronal firing to SWR events that is correlated with a pool of manipulations or natural behavioral events (like learning or aging). This set of experiments would further prove the importance of offline dynamics in shaping motor execution.

In addition, I would like to test whether MHC1 is also upregulated during song learning in juvenile zebra finches. If this would be true one could hypothesize that directed injury of the motor circuit can re-open the critical period for learning and identify the key factors needed to achieve this. The broader scientific field of neurodegenerative disease would benefit from finding ways in which neuronal plasticity can be precisely and controllably induced.

## Bibliography

- Brown, D. E., Chavez, J. I., Nguyen, D. H., Kadwory, A., Voytek, B., Arneodo, E., Gentner, T. Q., & Gilja, V. (2020). Local field potentials in a pre-motor region predict learned vocal sequences. *BioRxiv*, 1–49. <https://doi.org/10.1101/2020.06.30.179861>
- Brown, D. E., Chavez, J. I., Nguyen, D. H., Kadwory, A., Voytek, B., Arneodo, E. M., Gentner, T. Q., & Gilja, V. (2021). Local field potentials in a pre-motor region predict learned vocal sequences. In *PLoS Computational Biology* (Vol. 17, Issue 9). <https://doi.org/10.1371/journal.pcbi.1008100>
- Buzsáki, G. (2015). Hippocampal sharp wave-ripple: A cognitive biomarker for episodic memory and planning. *Hippocampus*, 25(10), 1073–1188. <https://doi.org/10.1002/hipo.22488>
- Cheadle, L., Rivera, S. A., Phelps, J. S., Ennis, K. A., Stevens, B., Burkly, L. C., Lee, W. C. A., & Greenberg, M. E. (2020). Sensory experience engages microglia to shape neural connectivity through a non-phagocytic mechanism. *Neuron*, 108(3), 451-468.e9. <https://doi.org/10.1016/j.neuron.2020.08.002>
- Cheng, S., Butrus, S., Tan, L., Xu, R., Sagireddy, S., Trachtenberg, J. T., Shekhar, K., & Zipursky, S. L. (2022). Vision-dependent specification of cell types and function in the developing cortex. *Cell*, 185(2), 311-327.e24. <https://doi.org/10.1016/j.cell.2021.12.022>
- Colquitt, B. M., Merullo, D. P., Konopka, G., Roberts, T. F., Brainard, M. S., & Chase, C. (2021). *Cellular transcriptomics reveals evolutionary identities of songbird vocal circuits*. 371(6530), 1–23. <https://doi.org/10.1126/science.abd9704>. Cellular
- Crandall, S. R., Adam, M., Kinnischtzke, A. K., & Nick, T. A. (2007). HVC neural sleep activity increases with development and parallels nightly changes in song behavior. *Journal of Neurophysiology*, 98(1), 232–240. <https://doi.org/10.1152/jn.00128.2007>
- Dave, A. S., & Margoliash, D. (2000). Song replay during sleep and computational rules for sensorimotor vocal learning. *Science*, 290(5492), 812–816. <https://doi.org/10.1126/science.290.5492.812>
- Dayton, R. D., Wang, D. B., & Klein, R. L. (2012). The advent of AAV9 expands applications for brain and spinal cord gene delivery. *Expert Opinion on Biological Therapy*, 12(6), 757–766. <https://doi.org/10.1517/14712598.2012.681463>
- Dehghani, N., Peyrache, A., Telenczuk, B., Le Van Quyen, M., Halgren, E., Cash, S. S., Hatsopoulos, N. G., & Destexhe, A. (2016). Dynamic balance of excitation and inhibition in human and monkey neocortex. *Scientific Reports*, 6, 1–12. <https://doi.org/10.1038/srep23176>
- Durand, S., & Cimorelli, A. (2011). The inside out of lentiviral vectors. *Viruses*, 3(2), 132–159. <https://doi.org/10.3390/v3020132>
- Elmaleh, M., Kranz, D., Asensio, A. C., Moll, F. W., & Long, M. A. (2021). Sleep replay reveals premotor circuit structure for a skilled behavior. *Neuron*, 109(23), 3851-3861.e4. <https://doi.org/10.1016/j.neuron.2021.09.021>
- Gunner, G., Cheadle, L., Johnson, K. M., Ayata, P., Badimon, A., Mondo, E., Nagy, M. A., Liu, L., Bemiller, S. M., Kim, K. W., Lira, S. A., Lamb, B. T., Tapper, A. R., Ransohoff, R. M., Greenberg, M. E., Schaefer, A., & Schaefer, D. P. (2019). Sensory lesioning

- induces microglial synapse elimination via ADAM10 and fractalkine signaling. *Nature Neuroscience*, 22(7), 1075–1088. <https://doi.org/10.1038/s41593-019-0419-y>
- Hahnloser, R. H. R., Kozhevnikov, A. A., & Fee, M. S. (2006). Sleep-related neural activity in a premotor and a basal-ganglia pathway of the songbird. *Journal of Neurophysiology*, 96(2), 794–812. <https://doi.org/10.1152/jn.01064.2005>
- Hampton, C. M., Sakata, J. T., & Brainard, M. S. (2009). An avian basal ganglia-forebrain circuit contributes differentially to syllable versus sequence variability of adult Bengalese finch song. *Journal of Neurophysiology*, 101(6), 3235–3245. <https://doi.org/10.1152/jn.91089.2008>
- Hong, S., Dissing-Olesen, L., & Stevens, B. (2016). New insights on the role of microglia in synaptic pruning in health and disease. In *Current Opinion in Neurobiology* (Vol. 36, pp. 128–134). Elsevier Ltd. <https://doi.org/10.1016/j.conb.2015.12.004>
- Hulse, B. K., Lubenov, E. V., & Siapas, A. G. (2017). Brain state dependence of hippocampal subthreshold activity in awake mice. *Cell Reports*, 18(1), 136–147. <https://doi.org/10.1016/j.celrep.2016.11.084>
- Joo, H. R., & Frank, L. M. (2018). The hippocampal sharp wave–ripple in memory retrieval for immediate use and consolidation. *Nature Reviews Neuroscience*, 19(12), 744–757. <https://doi.org/10.1038/s41583-018-0077-1>
- Jun, J. J., Steinmetz, N. A., Siegle, J. H., Denman, D. J., Bauza, M., Barbarits, B., Lee, A. K., Anastassiou, C. A., Andrei, A., Aydin, Ç., Barbic, M., Blanche, T. J., Bonin, V., Couto, J., Dutta, B., Gratiy, S. L., Gutnisky, D. A., Häusser, M., Karsh, B., ... Harris, T. D. (2017). Fully integrated silicon probes for high-density recording of neural activity. *Nature*, 551(7679), 232–236. <https://doi.org/10.1038/nature24636>
- Kao, M. H., & Brainard, M. S. (2006). Lesions of an avian basal ganglia circuit prevent context-dependent changes to song variability. *Journal of Neurophysiology*, 96(3), 1441–1455. <https://doi.org/10.1152/jn.01138.2005>
- Kosche, G., Vallentin, D., & Long, M. A. (2015). Interplay of inhibition and excitation shapes a premotor neural sequence. *Journal of Neuroscience*, 35(3), 1217–1227. <https://doi.org/10.1523/JNEUROSCI.4346-14.2015>
- Kozhevnikov, A. A., & Fee, M. S. (2007). Singing-related activity of identified HVC neurons in the zebra finch. *Journal of Neurophysiology*, 97(6), 4271–4283. <https://doi.org/10.1152/jn.00952.2006>
- Leonardo, A., & Konishi, M. (1999). Decrystallization of adult birdsong by perturbation of auditory feedback. *Nature*, 399(6735), 466–470. <https://doi.org/10.1038/20933>
- Long, M. A., & Fee, M. S. (2009). *Motor Pathway*. 456(7219), 189–194. <https://doi.org/10.1038/nature07448>. Using
- Lopez, R., Regier, J., Cole, M. B., Jordan, M. I., & Yosef, N. (2018). Deep generative modeling for single-cell transcriptomics. *Nature Methods*, 15(12), 1053–1058. <https://doi.org/10.1038/s41592-018-0229-2>
- Lubenov, E. V., & Siapas, A. G. (2009). Hippocampal theta oscillations are travelling waves. *Nature*, 459(7246), 534–539. <https://doi.org/10.1038/nature08010>
- Ma, Z., Turrigiano, G. G., Wessel, R., & Hengen, K. B. (2019). Cortical circuit dynamics are homeostatically tuned to criticality in vivo. *Neuron*, 104(4), 655–664.e4. <https://doi.org/10.1016/j.neuron.2019.08.031>
- Markowitz, J. E., Liberti, W. A., Guitchounts, G., Velho, T., Lois, C., & Gardner, T. J. (2015). Mesoscopic patterns of neural activity support songbird cortical sequences.

- PLoS Biology*, 13(6), 1–20. <https://doi.org/10.1371/journal.pbio.1002158>
- Melsted, P., Boeshaghi, A. S., Liu, L., Gao, F., Lu, L., Min, K. H. (Joseph), da Veiga Beltrame, E., Hjörleifsson, K. E., Gehring, J., & Pachter, L. (2021). Modular, efficient and constant-memory single-cell RNA-seq preprocessing. *Nature Biotechnology*, 39(7), 813–818. <https://doi.org/10.1038/s41587-021-00870-2>
- Nick, T. A., & Konishi, M. (2001). Dynamic control of auditory activity during sleep: Correlation between song response and EEG. *Proceedings of the National Academy of Sciences of the United States of America*, 98(24), 14012–14016. <https://doi.org/10.1073/pnas.251525298>
- Reiner, A., Perkel, D. J., Mello, C. V., & Jarvis, E. D. (2004). Songbirds and the revised avian brain nomenclature. *Annals of the New York Academy of Sciences*, 1016, 77–108. <https://doi.org/10.1196/annals.1298.013>
- Scharff, C., & Nottebohm, F. (1991). A comparative study of the behavioral deficits following lesions of various parts of the zebra finch song system: Implications for vocal learning. *Journal of Neuroscience*, 11(9), 2896–2913. <https://doi.org/10.1523/jneurosci.11-09-02896.1991>
- Scharff, Constance, Kirn, J. R., Grossman, M., Macklis, J. D., & Nottebohm, F. (2000). Targeted neuronal death affects neuronal replacement and vocal behavior in adult songbirds. *Neuron*, 25(2), 481–492. [https://doi.org/10.1016/S0896-6273\(00\)80910-1](https://doi.org/10.1016/S0896-6273(00)80910-1)
- Scotto-Lomassese, S., Rochefort, C., Nshdejan, A., & Scharff, C. (2007). HVC interneurons are not renewed in adult male zebra finches. *European Journal of Neuroscience*, 25(6), 1663–1668. <https://doi.org/10.1111/j.1460-9568.2007.05418.x>
- Shank, S. S., & Margoliash, D. (2009). Sleep and sensorimotor integration during early vocal learning in a songbird. *Nature*, 458(7234), 73–77. <https://doi.org/10.1038/nature07615>
- Steinmetz, N. A., Koch, C., Harris, K. D., & Carandini, M. (2018). Challenges and opportunities for large-scale electrophysiology with Neuropixels probes. *Current Opinion in Neurobiology*, 50, 92–100. <https://doi.org/10.1016/j.conb.2018.01.009>
- Sweeney, S. T., Broadie, K., Keane, J., Niemann, H., & O’Kane, C. J. (1995). Targeted expression of tetanus toxin light chain in *Drosophila* specifically eliminates synaptic transmission and causes behavioral defects. *Neuron*, 14(2), 341–351. [https://doi.org/10.1016/0896-6273\(95\)90290-2](https://doi.org/10.1016/0896-6273(95)90290-2)
- Thompson, J. A. . F. J. (2005). HVC Microlesions Do Not Destabilize the Vocal Patterns of Adult Male Zebra Finches with Prior Ablation of LMAN. *Developmental Neurobiology*, n/a-n/a. <https://doi.org/10.1002/dneu>
- Thompson, J. A., Wu, W., Bertram, R., & Johnson, F. (2007). Auditory-dependent vocal recovery in adult male zebra finches is facilitated by lesion of a forebrain pathway that includes the basal ganglia. *Journal of Neuroscience*, 27(45), 12308–12320. <https://doi.org/10.1523/JNEUROSCI.2853-07.2007>
- Traag, V. A., Waltman, L., & van Eck, N. J. (2019). From Louvain to Leiden: guaranteeing well-connected communities. *Scientific Reports*, 9(1), 1–12. <https://doi.org/10.1038/s41598-019-41695-z>
- Turrigiano, G. (2011). Too many cooks? Intrinsic and dynaptic homeostatic mechanisms in cortical circuit refinement. *Annual Review of Neuroscience*, 34(1), 89–103. <https://doi.org/10.1146/annurev-neuro-060909-153238>
- Vallentin, D., Kosche, G., Lipkind, D., & Long, M. A. (2016). Neural circuits: Inhibition

- protects acquired song segments during vocal learning in zebra finches. *Science*, 351(6270), 267–271. <https://doi.org/10.1126/science.aad3023>
- Verhaltensphysiologie, L., Biologie, F., Bielefeld, U., & Germany, W. (1983). *Song Learning in the Zebra Finch (Taeniopygia Guttata)*: 369–374.
- Wilbrecht, L., Petersen, T., & Nottebohm, F. (2002). Bilateral LMAN lesions cancel differences in HVC neuronal recruitment induced by unilateral syringeal denervation. *Journal of Comparative Physiology A: Neuroethology, Sensory, Neural, and Behavioral Physiology*, 188(11–12), 909–915. <https://doi.org/10.1007/s00359-002-0355-1>
- Williams, H., & McKibben, J. R. (1992). Changes in stereotyped central motor patterns controlling vocalization are induced by peripheral nerve injury. *Behavioral and Neural Biology*, 57(1), 67–78. [https://doi.org/10.1016/0163-1047\(92\)90768-Y](https://doi.org/10.1016/0163-1047(92)90768-Y)
- Zhang, Z. J., Koifman, J., Shin, D. S., Ye, H., Florez, C. M., Zhang, L., Valiante, T. A., & Carlen, P. L. (2012). Transition to seizure: Ictal discharge is preceded by exhausted presynaptic GABA release in the hippocampal CA3 region. *Journal of Neuroscience*, 32(7), 2499–2512. <https://doi.org/10.1523/JNEUROSCI.4247-11.2012>

*Appendix A*

## PROPOSAL TO INDUCE REDUCTION OF NEURONAL PLASTICITY IN THE ADULT MOTOR CIRCUIT BY MANIPULATION OF SEX HORMONE RECEPTORS

*This is a proposal I designed experiments for that served as my candidacy examination. This writing contains original ideas and preliminary results from me and Carlos Lois.*

**The role of synaptic plasticity and resilience in acquiring and storing information**

Vertebrate brains have the ability to acquire and retain new information throughout life. A deep understanding of the synapse at a molecular level holds the key to this fascinating phenomenon. The developing brain, is characterized by constant changes to neural circuits – either genetically or environmentally driven – in order to give rise to behaviors essential for survival. This is driven by synaptic plasticity, a foundational mechanism for encoding new information.

When information is learned, the brain has to implement some operation that stores the acquired knowledge. In the 1950s, Hebb postulated the most foundational rule about how connections between neurons are strengthened or weakened to achieve the storage of information. Summarized by Carla Schatz as “neurons that fire together, wire together”. Later on, this hypothesis would be supported by experimental results. The molecular mechanisms of memory formation is an active area of research to this day. Studies in this field implicated the role of long term activity dependent potentiation (LTP) between pre- and post-synaptic partners as a primary process for memory encoding and maintenance (1). The signaling cascade involved in LTP leads to transcriptional changes, a crucial step in how neurons store information.

We understand the need for plasticity to learn new information and that hard-wired neuronal connections serve to retain information (2,3). This implies a fine balance between plastic and resilient synaptic connections underlying the proper execution of learned behavior, especially as organisms adapt to a new environment. A songbirds’ singing is a well-established system to study innate learning and memory. The process of song learning is time-sensitive. After hatching, a male bird has 90 days to learn, store and produce a highly stereotyped song almost identical to its father’s. A specific species of songbird, the zebra finch, produces the same song from sexual maturation at around 90 days until death. For a motor circuit to be able to output such stereotyped behavior for so long, there has to be a balance between the conflicting phenomena of plasticity and robustness to learn and maintain song information (4).

With age, there is a reduced capacity to change the song circuit (5), which we believe is connected to sexual maturation. Testosterone has been linked to reduced neuronal plasticity (6), but the molecular mechanisms underlying this phenomenon are unknown. The aim of this proposal is to investigate the changes in plasticity of the different projection neuron populations in the song circuit. I believe, following these changes as a function of sexual maturity and age will help uncover the underlying processes governing long term storage and retrieval of procedural memories. In other words: How does the brain establish the appropriate balance between plasticity, which is required to acquire information, and resilience, which is required to store information?

**Aims to explore:**

1. Age, neuronal plasticity and resilience.
2. Sexual maturation and song degradation upon song circuit perturbations.
3. Sexual maturation and synaptic plasticity.

**Introduction**

Learned motor behaviors play a key role in the survival and reproduction of animals. Thus, acquiring a particular motor skill and preserving it for an extended period of time is a fundamental process in the life of an animal. While an extensive body of work has been devoted to study learning, much less is known about the mechanisms by which the brain maintains the information.

Adult males of the zebra finch species *Taeniopygia guttata* consistently produce a highly stereotypical song, following a time-restricted learning period. From the day a male bird hatches there are three major stages of song production to reach a successful adult song. The three stages are subsong (30-60 days post-hatching), a plastic song (60-90 dph) and a crystallized song (90 to death). Once crystallized, each rendition of the song will remain identical throughout the animal's life. This raises the question of whether their adult song is maintained by active or passive processes. Initial works by Lombardino & Nottebohm (5) demonstrated that deafening an adult finch caused the song to degrade over time, indicating that adult song requires auditory feedback to maintain its stereotypy. This observation illustrates that song maintenance is an active process. Interestingly, these experiments showed that deafening led to more severe song degradation in young adults (90-120 dph) compared to older animals (>1 year dph). At approximately 120 dph the song should be hard-wired and fully crystallized. This observation indicates that younger animals might be more prone to neuronal plasticity, compared to older animals. This loss of plasticity might give rise to extreme levels of resilience allowing older animals to retain their song stereotypy in the face of perturbation.

Attention was focused on the role of nuclei giving sensorimotor feedback to the cortical motor nuclei HVC (proper name), which itself gives rise to the song through the premotor output nuclei, the robust nucleus of archistriatum (Ra). Brainard et al. (7) observed that even adult males can perform adjustments to the pitch of their song based on negative conditioning. Researchers started to investigate whether temporary perturbations of HVC could fully recover. Thompson (8) and colleagues showed that electrolytic lesions of both the left- and right-hemisphere HVC leads to song degradation that recovers within 2-3 weeks after perturbation.

Based on these findings, we set out to study whether manipulating the neuronal activity in HVC perturbs the precision of stereotypic singing behavior. We genetically perturbed the projections neurons in HVC by introducing a voltage-gated bacterial sodium channel, NachBac, that hyperpolarizes neurons. By bilateral stereotaxic injection into HVC, we delivered a replication-deficient lentiviral vector (LV) containing NachBac. Our observation,

similar to Thompson's, was that the song of adult male zebra finches degraded and fully recovered to within 2-3 weeks post perturbation. We set out to study the underlying behavioral phenomena of losing and recovering the song at the neuronal level in HVC. For this, we will investigate the projection neurons involved in song learning and execution. There are two major types of excitatory neurons in HVC that project to two downstream nuclei: HVC-Ra and HVC-X, projecting to nucleus Ra and Area X, respectively. Studies have shown that Ra is essential for adult song production (9), whereas ablating Area X (10) does not alter song production or song quality in adults. However, Area X plays an important role in the song-learning of juveniles.

The plasticity and resilience of HVC projection neurons with age and sexual maturation is a representative simplified model system to study acquiring and maintenance information. One hypothesis is that elevated levels of testosterone decrease the synaptic plasticity in adult males. In canaries, Gardner (11) and colleagues found that the administration of testosterone to juveniles that are in the sensorimotor phase of song learning prematurely crystallize their song. Moreover, Williams et al. (12) showed that permanent perturbations in adult males, such as severing the tracheo-syringeal (Ts) nerve which leads to song alteration and degradation, are affected by the administration of testosterone or testosterone antagonists. Males (120-350 dph) altered their songs to a lesser degree when testosterone was administered into their circulation two weeks before nerve resection. In contrast, in males that received testosterone antagonists, their songs were altered to a higher degree after Ts nerve lesion. Our goal is two-fold: one, to investigate plasticity and resilience of HVC neurons with age; two, to observe whether androgens play a role in altering the balance between mechanisms needed to acquire and retain information.

## **Research Plan**

### **Aim 1: The relationship between age, neuronal plasticity and resilience**

#### **Aim 1.a: Investigation of NachBac induced adult age-dependent synaptic plasticity**

We observed that NachBac induced changes in synaptic plasticity in Ra projection neurons but not X projectors in more than 1-year-old adult males by electrophysiological recordings. This supports the observation that once a song is crystallized the plasticity of neurons essential for learning is lost. However, in a scenario where neurons are perturbed in young adults there could be an extended period of plasticity to re-adjust the recently formed stable song.

Our hypothesis is that HVC-X neurons play an essential role in learning and engraving the memory of the song. Hence, we propose that HVC-Ra and HVC-X projectors of younger males both possess synaptic plasticity as opposed to > 1-year-olds. This HVC-X plasticity could enable a final checkpoint to hard-wire the crystallized song. To assess the nature of this change we will inject NachBac bilaterally into old (1 year or older), young (90-120 dph) and juvenile (70 dph) animals. We will then investigate the changes in the plasticity of projection neurons by slice recordings. We will measure the input properties characterized by mEPSCs and mIPSCs. This experiment will investigate the window of plasticity in HVC-Ra and HVC-X projectors in HVC at different ages that have never been shown before.

#### **Limitations/Alternatives**

Potential faulty conclusions might emerge from synaptic differences due to the loss of NachBac channels overtime or the death of infected cells. We have performed pilot experiments to assess the effect of NachBac infection. Our preliminary data show that neurons

infected with NachBac survive and continuously express NachBac even after the recovery from song distortion (also see surgical limitations and alternatives in Aim 1.b).

### **Aim 1.b: Effects of perturbation on HVC projector synaptic plasticity**

Since NachBac hyperpolarizes neurons, we plan to deliver Kir (voltage-gated potassium channel) to silence neurons in a similar fashion as NachBac should. Both NachBac and Kir are genetic manipulations directly targeted to HVC projection neurons. We aim to perform circuit-level perturbations to assess if synaptic changes are different when HVC is directly or indirectly affected. The first circuit-level manipulation will be to permanently damage one HVC. Based on existing literature, we expect the bird to recover its song within 5 days to 2 weeks after unilateral lesions. The second circuit-level manipulation will be the unilateral lesion of the Tracheo-syringeal (Ts) nerve. The Ts nerve originating in the nucleus nXII is the final output from where HVC-RA signals lead to song production.

We hypothesize that circuit-level perturbations (Ts nerve, unilateral lesion) could differ in the synaptic plasticity responses of HVC-Ra and HVC-X neurons. If only NachBac and Kir evoke synaptic plasticity in HVC-Ra and HVC-X of young adults that potentially could be due local changes in HVC not at the circuit level. Whereas, altering input and output pathways to HVC leads to similar observations that could be interpreted as a circuit-level response achieved by synaptic plasticity. We will observe young (90-120 dph) , old (>1 year dph) and juvenile males.

#### **Limitations/Alternatives**

Stereotaxic injection of LVs based on retrograde labeling proposed some challenges in the past, many birds did not show behavioral change due to insufficient amount of positive cells and injection locations missing HVC. We have developed LVs that have higher expression levels by changing the resuspension buffer and promoters used. In addition, we are perfecting the retrograde labeling agent and coordinates for injection of tracer. However, the anatomy of the brain slightly differs in certain age groups and birds from different vendors, so we decided to breed in house and track the families that have good anatomical brain structures for reproducibility. In addition, birds will have to go through two independent brain surgeries (more challenging for older and juveniles) that increases chances of infections. We are very careful with our surgical hygiene and limit the amount of brain surgeries to two per occasion to avoid infections.

#### **What do we gain from Aim 1?**

We will observe whether induced plasticity during song recovery following perturbation depends on age or perturbation type used. In addition, we could better understand whether plasticity changes are specific to motor- (HVC-Ra) or sensorimotor (HVC-X) projection neurons in a given age and perturbation.

### **Aim 2: Testosterone levels and song degradation after song circuit perturbations**

#### **Aim 2.a: Expression of androgen receptors in HVC with age**

This aim will determine whether we can proceed with studying the role of androgens in decreasing synaptic plasticity of HVC projectors. Several publications have indicated that neurons in HVC possess androgen (AR) receptors (4,6,13,14,15). However, there has not been a study that showed the localization of these receptors in different projection neuron populations. We will identify androgen receptors at different ages of male birds by fluorescent

in situ hybridization (FISH) or immunohistochemistry (IHC). First, we will inject a retrograde tracer into Ra or X one week before FISH / IHC in 70 dph, 90-120 dph and 1 year or older adult males. We will assess the results by confocal imaging brain slices containing song nuclei at all ages. Then we will quantify cell labeling from retrograde and FISH / IHC signals.

#### **Limitations/Alternatives**

The survival of surgery and success of retrograde labeling has been established in limitations in Aim 1.a and b. We have two different approaches FISH and IHC because we might be unsuccessful with the commercial antibodies available for androgen receptors. If that is the case we will make probes for AR and perform FISH that will give us a more quantitative analysis of receptor numbers.

#### **Aim 2.b: Pattern of song degradation and Testosterone level manipulations**

While NachBac causes hyperactivation of neurons expressing the channel there are different more naturalistic manipulations that we can perform such as Tracheo-syringeal nerve resection. It is important to show the effects of age and sexual maturation in manipulations performed on HVC directly or indirectly. We will study whether age and sexual maturation change the way the song degrades in young adults (90-120 ) and old (>1 year) animals in these two types of perturbation. Williams and colleagues (12) showed that implantation of Testosterone or an antagonist effects song degradation upon T's nerve resection. However, this paper lacks important observations regarding the age-dependent effects of testosterone on song degradation. In addition, there is no emphasis on studying how the song disruption patterns change in response to sexual maturation and age. We hypothesize that trends in vocalization changes upon perturbation will correlate with Testosterone (T) levels. The purpose of this experiment is to gain a better understanding of whether sexual maturation and age influence the way the song is perturbed by Nachbac or T's nerve resection.

Zebra finches possess a highly stereotypical song, which is relatively straightforward to analyze. However, when the song of the birds is disrupted by NachBac or T's nerve resection it degrades to an extent that analysis other than hand selection is challenging. We aim to develop a method to properly analyze thousands of songs per day in a reliable way even when song structure is highly disrupted and find major trends in which the song degrades. To quantify this we will use Sound Analysis Pro (SAP2011, developed and used in our field) to segment the songs into units that are recurrently seen by looking at individual songs (not units generally used for song analysis). The experiment will involve a subcutaneous T implant or antagonist two weeks before either perturbation study. Then a bilateral injection of NachBac into HVC or T's nerve lesion of young adults (90-120 dph) and older animals (>1 year dph). We will record their song and observe any major trends in song alteration. We will measure bird's T levels before, during and after perturbation.

#### **Limitations/Alternatives**

If computational approaches lead us no closer to a bulk analysis observing trends in song degradation then we will stick to the traditional manual analysis and build foundational observations about song degradation with age and sexual maturation. We will look at whether the length and song content, as well as, ordering of song syllables are altered during the perturbation periods. The surgical procedures will be carefully executed and birds with complications will be excluded from the analysis. If T or DHT implants cause no change in behavior compared to non-implanted perturbed birds we will still hold an important age-

related observation. To add, we can also study whether there is only one way the song falls apart or if it is perturbation specific ( NachBac, T's nerve resection).

### **Aim 2.b alternative: Changes in directed and undirected song upon perturbation with age and sexual maturation**

Previous studies have shown that when adult males sing directly towards a female (directed song) those songs are more stereotypic from rendition to rendition than undirected songs. This is due to the fact that Area X is not involved in directed singing, only Ra produces the song (16). We will repeat Aim 2.a (without the DHT/T implantations experiments) and record the birds' song before, during and after NachBac/T's nerve resection perturbation when the bird is singing directed or undirected songs. Our hypothesis is that directed songs will be intact (do not fall apart) even when the highest degree of perturbation is observed in undirected singing. Whether this differs in young (90-120 dph) and older adults (>1 year dph) is an open question. We expect that the singing of directed unperturbed songs will speed up the recovery of undirected distorted songs in NachBac injected birds. In the case of the T's nerve resection, we expect that the song will not be altered to the extent that only undirected singing would lead to. We will have two groups: one with bilateral NachBac injection/ T's nerve resection exposed to a female for 2 hours a day and the control group with no female exposure. After recording the songs of all the males in this experiment we will attempt the same song analysis proposed in Aim 2.b. We will measure whether the increased amount of directed singing increases endogenous T levels in the manipulated birds. We will measure blood T before/during and after perturbation experiments to observe any changes. We hypothesize that birds singing more directed songs in the young adult category will have a higher surge of T than older males used to breeding conditions. If this observation holds then we can postulate that increased T levels and directed singing could induce recovery/ less alteration to song post manipulation. The mechanism for this could be lowering the window of synaptic plasticity of HVC projection neurons. However, the androgen surge might take effect slower than the natural recovery time of 14 days in the NachBac perturbation.

### **Limitations/Alternatives**

There could be individual differences between the response of males to female exposure, to limit that we will use brothers from the same clutch as controls for no directed singing. Even if our hypothesis fails we will learn something new about the long-standing dilemma of the field, whether directed and undirected songs are perturbed in the same manner in different age groups.

### **What do we gain from Aim 2?**

We establish the expression patterns of AR throughout the sexual maturation of males in HVC projection neurons. We learn about the song degradation pattern after NachBac injection or T's nerve resection in different age groups with different levels of T. Even if T is not effective in changing the plasticity of projection neurons in HVC it could pose a broader effect on the motor circuit shown by this experiment.

If only NachBac triggers differential plasticity in young adult animals, we will proceed with Aim 3 only looking at NachBac.

### **Aim 3: The connection between Testosterone and synaptic plasticity**

#### **Aim 3.a: Role of androgens in increasing resilience upon perturbations in HVC**

After assessing which HVC perturbation experiments - NachBac, Kir, T's nerve resection, unilateral HVC lesion - lead to differential projection neuron plasticity corresponding to age groups we can assess whether T/ dihydrotestosterone (DHT) alters this synaptic plasticity. We will implant birds as young juveniles (70 dph), adults (90-120 dph), old adults (>1 year dph) two weeks before perturbation of the song system. The T blocker and subcutaneous implants without any hormone or blocker will serve as controls. It is essential to make sure blood T levels before and after implants are recorded for comparison since that could vary and influence the results of our experiments. We will perform patch clamp slice recordings to assess the synaptic plasticity based on changes in mEPSCs and mIPSCs.

#### **Limitations/Alternatives**

In these experiments, the birds will have to go through a subcutaneous hormone administrator implant as well as two major brain surgeries. This could result in severe complications leading to longer timescale and fewer animals with successful experimental outcomes. We found that increasing the nutritional intake (kale, high protein mesh) and injection of intraperitoneal saline post-surgery (compensative for fluid volume loss) increases the chances for a healthy and speedy recovery. An additional problem can be if we see no change in plasticity based on the amount of androgen administered. This could be due to the birds having an already too high T level or the implant is not sufficient in increasing T levels. In which case we will castrate animals 2 weeks before T implantation or change the T hormone implant used.

#### **Aim 3.b: Extended learning period in juveniles reared in social isolation and synaptic plasticity**

Juveniles reared in social isolation (not exposed to tutor or siblings) can extend their plastic learning period (17). This observation could suggest that the HVC-X projector population of these birds is more plastic since Area X is important for learning. We will raise juveniles in a sound isolated environment post-hatching. We will impose synaptic plasticity by either bilateral NachBac injection into HVC or T's nerve resection. We will collect control and socially isolated males in between 120-400 dph for slice recording. All animals will have retrograde tracers stereotaxically injected into Ra or Area X one week before slice recording. After assessing the plasticity of HVC-X and -RA projectors in adults raised in social isolation we will investigate the effect of high T level on projection neuron plasticity. We will implant T/DHT ( 2 weeks before perturbation) into the birds raised in social isolation and controls. We will study if social isolation BUT high levels of testosterone changes the plasticity of projectors back to a less or non-plastic state. Given only if social isolation has any effect on plasticity. The synaptic plasticity of HVC-X and -Ra projectors will be assessed by measuring the changes in mEPSCs and mIPSCs in the different experimental groups.

#### **Limitations/Alternatives**

This aim also encounters the challenges of multiple surgeries during a long time span of the life of the birds, these will be counteracted by the aforementioned technical improvements. If this experiment yields no change apart from the one observed in the younger (90-120dph) and

older adults that is intriguing. This could mean that this differential plasticity in HVC-X and -Ra projectors are independent of song learning or sexual maturity.

### **What do we gain from Aim 3?**

Observations whether sex steroid hormones affect the plasticity of HVC projection neurons differently at a young or old adult stage of song production. Understanding whether social isolation has any effect on projection neuron plasticity and whether this effect can be reversed by the administration of T as a process of maturation related loss of HVC-X projector plasticity.

### **Summary**

We are interested in the balance between plasticity and resilience of X and Ra projectors in HVC in relation to acquiring and retaining the song. The field believes that after 120 dph a zebra finch male is a full adult and has lost the capacity to change some aspects of its song motor circuit to maintain its song. This is contrasted by the evidence that deafening of 3-4-year-old males will not lead to song degradation, whereas deafening of younger <1-year-old males leads to subtle but major song degradation over time (5). We propose that there is an actively changing fine-tuned balance between plasticity and resilience of HVC projectors with age and sexual maturity of the bird. The 3 aims serve as independent observations that could lead us closer to understanding the role of synaptic plasticity and resilience at different stages of life. We would like to find out if neurons that transmit sensorimotor (X) or solely motor (Ra) information could possess different windows of plasticity correlated with age or hormonal state in order to give rise to an ideal combination of learning and retaining information.

The observations from these experiments would provide us with deeper insights into the nature of synaptic plasticity and resilience in a motor circuit that is successful in maintaining information throughout the life of an organism. To sum up, we attempt to find an answer to the question: How does the brain establish the appropriate balance between plasticity, which is required to acquire information, and resilience, which is required to store information?

## Preliminary results

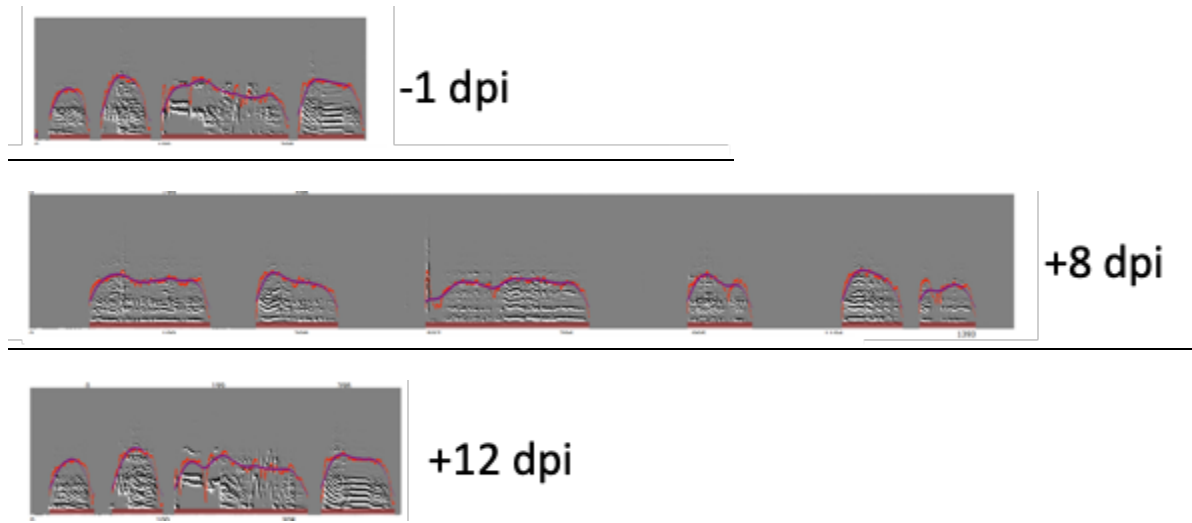


**Figure 1:** Bilateral NachBac perturbation and song recovery of an old adult male (>1 year old). In these sonograms, the Y-axis represents the Frequency (Hz) and X-axis Time (msec) over dpi = day post-injection. Unpublished data, Lois lab.

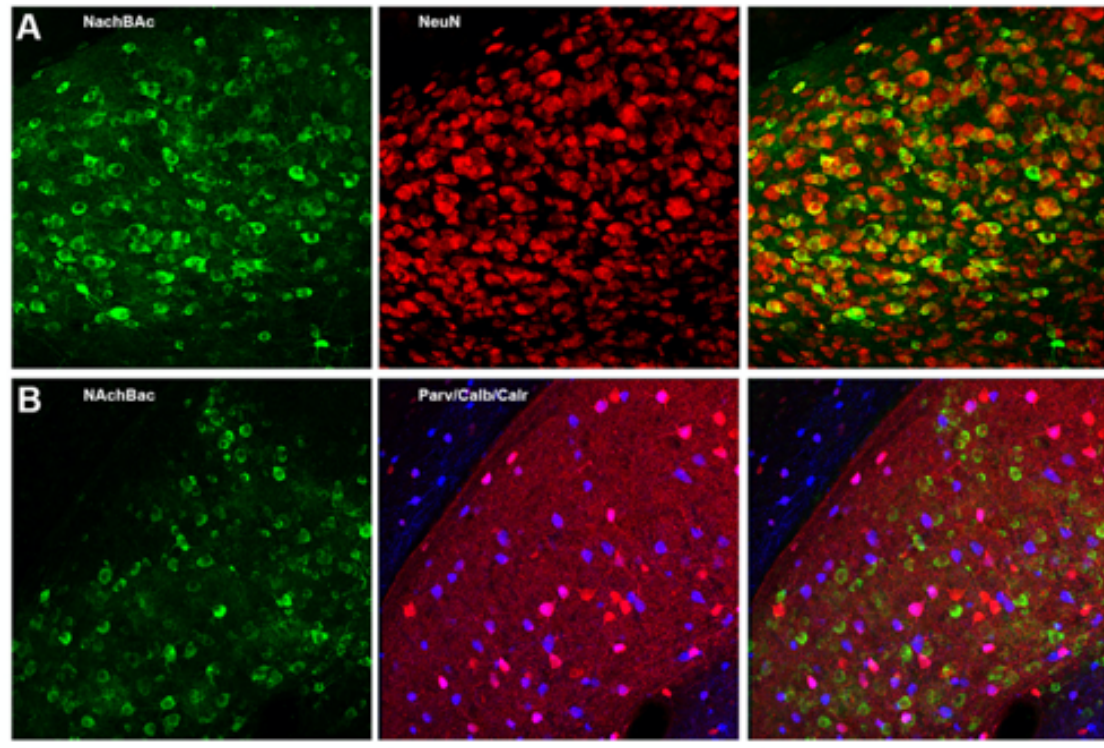


**Figure 2:** NachBac expression in HVC of a >1-year-old adult male with distorted song, NeuN for neurons and Parv/Calb for interneurons. No interneurons are labeled in the NachBac positive neuronal population. Lois lab, unpublished data.

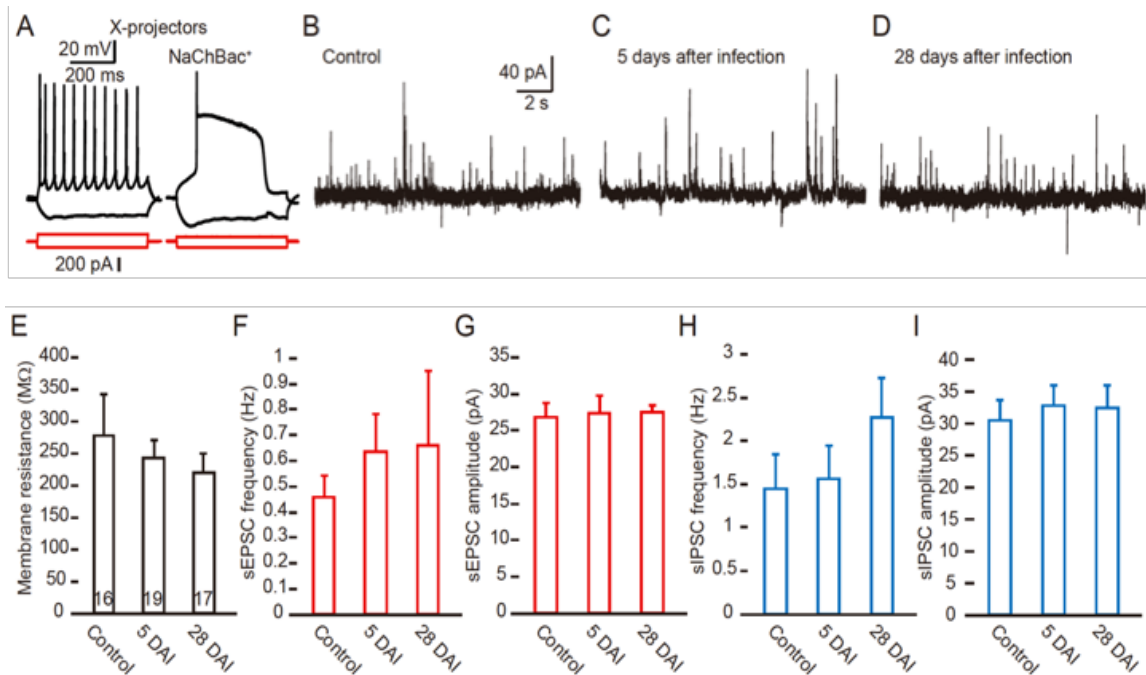


**Figure 3(A-I):** Non-plastic HVC-X projectors upon NachBac perturbation in >1 year adult males (spontaneous EPSC and spontaneous IPSC traces in slice recordings). Figure 3.A showing example membrane potential traces in response to depolarizing and hyperpolarizing current steps of control and NachBac-expressing HVC-X neurons, B, C and D shows raw spontaneous synaptic current traces of control (B), 5 days post (C) and 28 days post manipulation (D). Figure 3.E: the membrane resistance of HVC-X projectors. Figure 3.F-I: sEPSC and sIPSC frequency and amplitude changes 5 and 28 days post bilateral NachBac injection, no significant change compared to control. Note: spontaneous (no Tetrodotoxin (TTX), action potential (AP) occurs) and miniature EPSCs and IPSCs showed the same trend. Unpublished data from Bo Wang, Lois lab.

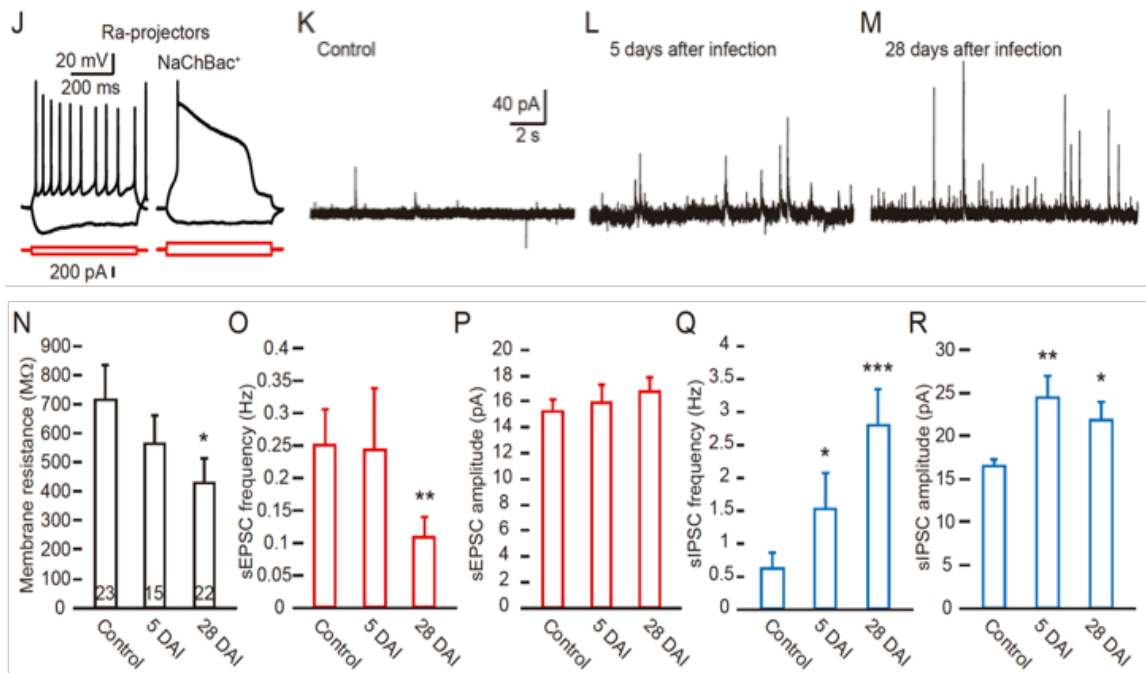


**Figure 3(J-R):** Plastic HVC-Ra projectors upon NachBac perturbation in > 1 year adult males (spontaneous EPSC and spontaneous IPSC traces in slice recordings). Figure 3.J showing example membrane potential trace in response to current steps of control and NachBac-expressing HVC-Ra neuron, K, L and M show raw recordings of control (K), 5 days post (L) and 28 days post manipulation (M). Figure 3.N: changes in the membrane resistance of HVC-Ra projectors. Figure 3.O-R: sEPSC and sIPSC frequency and amplitude changes 5 and 28 days post bilateral NachBac injection. We observed a significant change in sEPSC frequency and sIPSC frequency and amplitude compared to control. Note: \*,  $p < 0.05$ ; \*\*,  $p < 0.01$ ; \*\*\*,  $p < 0.001$ . Spontaneous (no TTX, AP occurs) and miniature EPSCs and IPSCs showed the same trend. Unpublished data from Bo Wang, Lois lab.

*Bibliography*

- Bliss, T. V. P., Gardner-Medwin, A. R. Long-lasting potentiation of synaptic transmission in the dentate area of the unanaesthetized rabbit following stimulation of the perforant path. *J. Physiol.* 232, 357–374 (1973).
- Moser, E. I., Krobot, K. A., Moser, M. B. & Morris, R. G. M. Impaired spatial learning after saturation of long-term potentiation. *Science*. 281, 2038–2042 (1998).
- Nabavi, S. *et al.* Engineering a memory with LTD and LTP. *Nature* 511, 348–352 (2014).
- Mooney, R. Synaptic Basis for Developmental Plasticity in a Birdsong Nucleus. *J. Neurosci.* 12, (1992).
- Lombardino, A. J. & Nottebohm, F. Age at deafening affects the stability of learned song in adult male zebra finches. *J. Neurosci.* 20, 5054–5064 (2000).
- White, S. A., Livingston, F. S. & Mooney, R. Androgens modulate NMDA receptor-mediated EPSCs in the zebra finch song system. *J. Neurophysiol.* 82, 2221–2234 (1999).
- Sober, S. J. & Brainard, M. S. Adult birdsong is actively maintained by error correction. *Nat. Neurosci.* 12, 927–931 (2009).
- Thompson, J. A., Wu, W., Bertram, R. & Johnson, F. Auditory-dependent vocal recovery in adult male zebra finches is facilitated by lesion of a forebrain pathway that includes the basal ganglia. *J. Neurosci.* 27, 12308–12320 (2007).
- Ashmore, R. C., Bourjaily, M. & Schmidt, M. F. Hemispheric coordination is necessary for song production in adult birds: Implications for a dual role for forebrain nuclei in vocal motor control. *J. Neurophysiol.* 99, 373–385 (2008).
- Scharff, C. & Nottebohm, F. A comparative study of the behavioral deficits following lesions of various parts of the zebra finch song system: Implications for vocal learning. *J. Neurosci.* 11, 2896–2913 (1991).
- Gardner, T. J., Naef, F. & Nottebohm, F. Freedom and rules: The acquisition and reprogramming of a bird's learned song. *Science* (80-.). 308, 1046–1049 (2005).
- Williams, H., Connor, D. M. & Hill, J. W. Testosterone decreases the potential for song plasticity in adult male zebra finches. *Horm. Behav.* 44, 402–412 (2003).
- Frankl-Vilches, C. & Gahr, M. Androgen and estrogen sensitivity of bird song: a comparative view on gene regulatory levels. *J. Comp. Physiol. A Neuroethol. Sensory, Neural, Behav. Physiol.* 204, 113–126 (2018).
- Sohrabji, F., Nordeen, K. W. & Nordeen, E. J. Projections of androgen-accumulating neurons in a nucleus controlling avian song. *Brain Res.* 488, 253–259 (1989).

Kim Y-H., Perlman WR., Arnold AP. Expression of androgen receptor mRNA in the zebra finch song system: Developmental regulation by estrogen. *Journal of Comparative Neurology* 469:535-547 (2004).

Jarvis, E. D., Scharff, C., Grossman, M. R., Ramos, J. A. & Nottebohm, F. For Whom The Bird Sings. *Neuron* 21, 775–788 (1998).

Morrison RG. , Nottebohm F. Role of a telencephalic nucleus in the delayed song learning of socially isolated zebra finches. *J Neurobiol* 24:1045–64 (1993).

## Appendix B

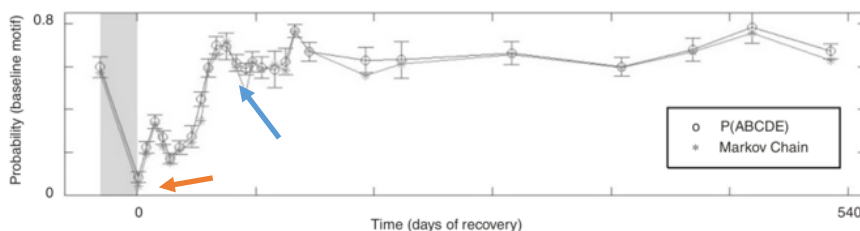
### PROPOSAL FOR THE ROLE OF SLEEP IN ADULT SONG MAINTENANCE

*I was awarded the Chen Innovator Grant for this work.*

#### The role of sleep in birdsong maintenance

The song of birds is used for courtship purposes, where only the male sings and juvenile males learn this behavior from an adult tutor. The motor pathway consists of several connected brain nuclei that participate in the production of the bird's song. HVC is considered to be an equivalent of the motor cortex, whereas the robust nucleus of archistriatum or RA transforms HVC firing patterns into a premotor output for singing. Zebra finches are one of avian species that can learn how to vocalize in a period of plasticity in which juvenile birds perfect their memorized song learned from the tutor. After the song is learned, adult zebra finches produce an extremely stereotypical song that remains virtually unchanged for the rest of their lives. In a pioneering work, Margoliash and Dave (2000) showed that during sleep there is 'replay' of the song in HVC. Deregnacourt et al. (2005) proposed that sleep has a fundamental role during the period of song learning in juvenile finches, supporting the hypothesis that sleep is necessary for consolidating the learning of the song that occurs during the day in juveniles. However, the role of sleep in adult song maintenance is not understood. Leonardo and Konishi (1999) demonstrated that perturbing auditory feedback while a bird sings impairs song maintenance.

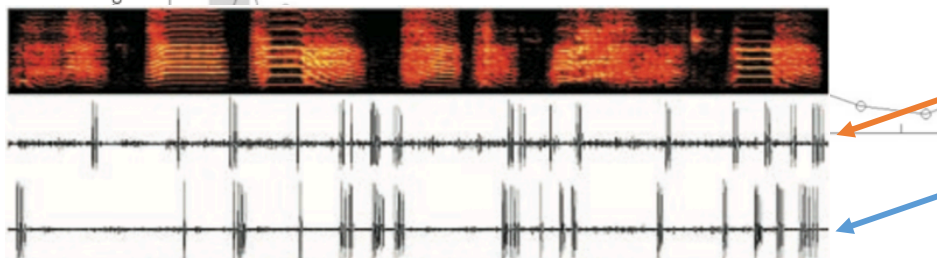
In sum, I would like to integrate three separate lines of evidence regarding the potential role of sleep for the long-term stability of song in adult birds: (i) song is spontaneously replayed during sleep in nucleus HVC in adult and juvenile birds, (ii) sleep plays a role in song learning in juvenile birds, and (iii) song maintenance in adult animals is an active process that requires proper practice.



after the end of the perturbation the highly stereotypical structure of the song re-emerges (blue arrow).

**Figure 1.:** Leonardo and Konishi in 1999 showed that upon perturbation of auditory feedback the song of adult male zebra finches falls apart (orange arrow) but several weeks

**Figure 2.:** Dave and Margoliash in 2000 demonstrated how the neuronal activity - specific to each syllable of the song - in RA during singing matches the neuronal activity observed during sleep replay. Top panel shows the spectrogram of the song sung during the day. Orange arrow points to extracellular recording of activity in RA during singing. Blue arrow points to recording of RA activity during sleep. Notice that activity in RA is highly similar during active singing and sleep replay.



This proposal aims to explore the putative role of sleep and replay in adult zebra finches for the maintenance of a stereotypical behavioral output. The Lois lab studies this motor circuit in song production but nobody else in the lab has ever studied any topics related to sleep.

The main objective of the project is to manipulate the electrical activity in HVC to investigate the role that sleep and replay play in song maintenance in adult animals. Towards this goal I plan to perform two types of experiments, which complement each other. First, I will locally silence HVC during sleep using a chemogenetic approach (with the use of inhibitory DREADDs). Second, I will introduce noise locally into HVC with a stimulation electrode. Both methods have advantages and disadvantages that will be discussed below.

The goal of both approaches is to perturb normal functioning of HVC selectively during sleep and use the song analysis as a behavioral readout of both perturbation approaches. The overall design of the experiments is to record birds' song ( $n=6$  animals) before any manipulation is performed, and then perturb HVC activity during the night when the animal: (i) is asleep (ii) is asleep and replaying the song (in the electrophysiological perturbation experiments only). Sleep states will be assessed by EEG.

The role of sleep on song maintenance will be measured by comparing pre-perturbation song structure to post-perturbation songs as well as comparisons of negative and positive controls.

### Using chemogenetics to silence HVC overnight

The most widely used inhibitor DREADDs (designer receptor exclusively activated by designer drugs) in rodents is hM4Di. The wt muscarinic Acetylcholine receptor uses the  $G_i$  mediated pathway to silence neuronal activity by activating inward rectifying potassium channels. hM4Di is a variant of the muscarinic Acetylcholine receptor that has been modified to selectively bind Clozapine-N-oxide (CNO) and not acetylcholine, its endogenous ligand. Thus, administration of CNO can be used to silence the electrical activity of neurons expressing hM4Di. I will deliver hM4Di locally into neurons in HVC by stereotaxic injection of lentiviruses, which the Lois lab has demonstrated can be used to selectively deliver genes into projection neurons in HVC. To confirm that we can silence HVC with this method, we will first inject CNO in awake animals, where we anticipate that animals will cease singing around 30 minutes after CNO injection. Once we confirm that we can silence HVC with CNO in awake animals, we will proceed to silence HVC during sleep. Previous works have demonstrated that a single intraperitoneal injection of CNO (0.3-3 mg/kg) is sufficient to silence

neurons for 10 hours in rodents. Thus, we anticipate that injecting CNO 30 minutes before the animals go to sleep (at 9 PM) will allow us to silence HVC activity during the whole night (birds sleep between 9 PM and 7 AM) and thus block the song replay that usually occurs at night. Based on the work by Leonardo and Konishi (1999), where they showed that it took approximately one month of auditory feedback perturbation to degrade the song, for initial experiments, we will administer CNO for a month and examine whether silencing HVC during sleep for this period affects song maintenance.

### **Difficulties and alternatives**

(i) side effects of CNO: recent works have indicated that CNO is metabolized into clozapine, a potent psychoactive drug that can severely perturb neuronal function. However, I have performed initial experiments in which I injected CNO into wt animals (that did not carry any hm4di) and have observed that neither the general behavior of the birds, nor their songs are affected by CNO injection.

(ii) blocking the “metabolic effects” of sleep could be problematic: recent works suggested that sleep is necessary for the removal of metabolic waste that accumulates in brain circuits during the day. A potential caveat of this approach is that it will silence HVC for several hours every night (regardless of whether the song is being replayed or not) and thus, interfere with the putative metabolic function of sleep.

To be able to manipulate the activity of HVC selectively during replay we need a method with higher temporal resolution where the manipulation can be time locked to specific sleep states. For this goal we will use an electrophysiological approach as described next

### **Using stimulating electrode to perturb HVC in specific sleep states**

We will use a strategy in which we will record EEG to identify whether sleeping animals are in REM or non-REM phases, and will use this information to trigger the injection of electrical noise into HVC selectively during those phases. Towards this goal we will implant electrodes in frontal, parietal and occipital locations of the brain to record EEG, and the stimulating electrode into HVC. MATLAB script will be used to automatically trigger current injection into HVC upon identification of sleep stages. We will use stainless steel electrodes to inject current locally into HVC by biphasic train of stimulations of 0.4 ms /phase with 10-100 $\mu$ A. This manipulation has several advantages in terms of the temporal resolution of its readout.

### **Difficulties and alternatives**

(i) glial scar -- Long term implantation of the electrodes could lead to glial scar formation that could be reduced by reducing effective electrode tip size and specific coating of the tips.

(ii) not capable of cell-type specificity -- Unable to observe any cell type specific effect by current injection locally into HVC.

(iii) stimulation electrode can move over consecutive days -- Might be stimulating different population of neurons long term.

The analysis of both experimental procedures will provide us with an initial test about whether sleep and in particular replay play a role in song maintenance. This is an exploratory project, and I could encounter several difficulties. For example, it is possible that we may not see any change in behavior. This could be due to the motor circuit not being perturbed efficiently (for example, an insufficient number of neurons), or for long enough, or because the circuit is equipped to overcome noise

injection. My hypothesis is that the long term perturbation of the motor circuit will have subtle but cumulative effects on singing.

*Bibliography*

Dave AS, Margoliash D (2000) Song replay during sleep and computational rules for sensorimotor vocal learning. *Science* 290:812– 816.

Deregnaucourt S, Mitra PP, Feher O, Pytte C, Tchernichovski O (2005) How sleep affects the developmental learning of bird song. *Nature* 433:710 –716.

Anthony Leonardo, Masakazu Konishi (1999) Decrystallization of adult birdsong by perturbation of auditory feedback. *Nature* Vol 399.

Claude Z. H Wang, Joshua A Herbst, Georg B Keller, Richard H. R Hahnloser (2008) Rapid Interhemispheric Switching during Vocal Production in a Songbird. *PLOS Biology* 6(10): e250.

Teresa A. Nick, Masakazu Konishi (2001) Dynamic control of auditory activity during sleep: Correlation between song response and EEG. *PNAS* 14012–14016.

*Appendix C*

## UNSUPERVISED RESTORATION OF A COMPLEX LEARNED BEHAVIOR AFTER LARGE-SCALE NEURONAL PERTURBATION

Bo Wang\*, Zsafia Torok\*, Alison Duffy\*, David Bell, Shelyn Wongso, Tarciso Velho, Adrienne Fairhall, Carlos Lois

Reliable execution of behaviors requires that brain circuits correct for variations in neuronal dynamics. Genetic perturbation of the majority of excitatory neurons in a brain region involved in song production in adult songbirds with stereotypical songs triggered severe degradation of their songs. The song fully recovered within two weeks, and substantial recovery occurred even when animals were prevented from singing during the recovery period, indicating that offline mechanisms enable recovery in an unsupervised manner. Song restoration was accompanied by increased excitatory synaptic inputs to unmanipulated neurons in the same region. A model inspired by the behavioral and electrophysiological findings suggests that a combination of unsupervised single-cell and population-level homeostatic plasticity rules can support the observed functional restoration after large-scale disruption of networks implementing sequential dynamics. In the model the sequence is restored through a parallel homeostatic process, rather than regrown serially, and predicts that sequences should recover in a saltatory fashion. Correspondingly, we observed such recovery in the songs of manipulated animals, with syllables that rapidly alternate between abnormal and normal durations from rendition to rendition until eventually they permanently settled into their original length. These observations indicate the existence of cellular and systems-level restorative mechanisms that ensure behavioral resilience.

Animal survival and reproduction requires reliable execution of behaviors. However, neuronal representations change over time, as a consequence of natural drift, or due to neuronal perturbations caused by trauma, disease, or aging<sup>1,2</sup>. What are the mechanisms that allow brains to maintain reliable behaviors over long periods of time or after neuronal loss? To investigate this question, we studied the zebra finch, a songbird that after learning a song as juveniles, produces stereotypical renditions of the song with minimal variability over several years. Songbirds have a series of brain nuclei dedicated for song learning and production called the song system<sup>3</sup>. HVC is the premotor nucleus in the song system that projects to the motor nucleus RA (robust nucleus of the arcopallium)<sup>4</sup>, involved in song production<sup>3</sup>. Previous experiments have shown that complete ablation of HVC abolishes song production<sup>3</sup>, but localized, partial lesions of HVC cause song degradation followed by recovery after different amounts of time<sup>5-7</sup>, suggesting that the song circuit is somewhat resilient. However, the precise behavioral, circuit and cellular level dynamics responsible for this resilience remain unknown. To investigate this question, we used genetic methods to selectively manipulate the activity of projection neurons in the HVC of adult finches, and quantified the changes in the song as it degraded and recovered. In addition, we investigated the electrophysiological changes that occurred in this brain circuit after the genetic perturbation, and created a data-inspired model to investigate the cellular mechanisms underlying the observed behavioral and electrophysiological findings.

HVC projection neurons fire in an extremely sparse and precise manner when birds sing<sup>8,9</sup>. To explore how singing may be affected by disrupting the precise firing of these neurons, we expressed an ion channel to alter their electrical properties. Towards this goal, we bilaterally injected into both HVCs lentiviral vectors

(LVs. **Fig. 1a**), which have been shown to selectively infect HVC projection neurons<sup>10,11</sup> (**Extended Data Fig. 1**). To alter the electrical properties of HVC neurons, the LVs carried NaChBac, a bacterial voltage gated Na<sup>+</sup> channel<sup>12</sup>. NaChBac expression in neurons perturbs their activity due to two features<sup>13–15</sup>: first, NaChBac is activated at membrane potentials in which the vertebrate Na<sup>+</sup> channels are inactive; second, whereas the vertebrate Na<sup>+</sup> channel depolarizations are 5-ms long, those of NaChBac expressing neurons last up to 1 s. The NaChBac transgene carried by the LVs contains the sequence of NaChBac fused in frame to GFP, which allows for visual identification of the infected neurons (**Extended Data Fig. 1**). Whole-cell patch clamp recording of HVC neurons in brain slices confirmed that GFP<sup>+</sup> neurons displayed the characteristic NaChBac currents (**Fig. 1c and Extended Data 2a-c**).

For the first four days after viral injection there were no changes in the songs. Normal songs consist of repetitions of a so-called motif, which is made up of 3 to 7 syllables, depending on the individual. In unperturbed zebra finches, the acoustical structure of the syllables, the number of syllables per motif, and the duration of each motif are highly stereotypical, with minimal variations between renditions, even across months. In contrast, by 5 day after NaChBac injection the songs became highly irregular and bore no resemblance to their original songs.

To visualize the dynamics of the changes in these perturbed songs, we used Uniform Manifold Approximation and Projection (UMAP), a non-linear dimensionality reduction algorithm, to project the high-dimensional acoustic representation of hundreds of songs onto a 2D plane (see Methods and **Fig. 1b**)<sup>16–18</sup>. NaChBac delivery caused strong acoustic and temporal degradation across all syllables and greatly increased the variance between song renditions, which made it difficult to identify motifs (**Fig. 1d and Supplementary Audio 1-3**). However, at approximately 7 days post-injection (dpi) the song started to recover, and gradually regained structure. By 14 dpi, the songs of NaChBac animals were highly similar to their original songs, and remained so for several months. To investigate how NaChBac expression caused song degradation, we performed whole-cell patch clamp recordings. As early as 48 hours after injection, NaChBac<sup>+</sup> RA-projecting (HVC(RA)) neurons displayed the characteristic NaChBac current and abnormal long depolarizations. However, starting at 4 dpi, at the onset of song degradation, NaChBac<sup>+</sup> HVC(RA) neurons had a substantial increase in inhibitory synaptic inputs leading to their silencing (**Extended Data Fig. 3**), as observed before in the mammalian brain<sup>13,15,19</sup>. These synaptic changes were also present at >25 dpi after the song had recovered. Thus, we hypothesize that the degradation of the song after NaChBac injection is primarily due to the eventual silencing of a large fraction of HVC projection neurons.

To investigate whether directly silencing HVC projection neurons would be sufficient to degrade the song, we delivered a LV carrying the light chain of tetanus toxin (TeNT). TeNT is an enzyme that cleaves synaptobrevin, a protein essential for the release of neurotransmitters. Thus, expression of TeNT in a neuron does not alter its electrical activity, but it abolishes its ability to communicate with its postsynaptic targets<sup>20</sup>. Paired whole-cell patch clamp recordings in brain slices showed that expression of TeNT in HVC(RA) projection neurons abolished their excitatory drive onto inhibitory neurons in HVC at all times, both during song degradation, and after recovery, indicating the TeNT permanently muted the projection neurons (**Fig. 1e and Extended Data Fig. 2d-f**).

Injection of LV-TeNT into HVC caused song deterioration and recovery with an overall similar pattern to that described for LV-NaChBac (**Fig. 1f and Supplementary Audio 1-3**), although songs started to degrade faster with TeNT (as early as 1 dpi). Lentiviral expression starts at ~ 24 hours, TeNT is a powerful toxin, and a handful of TeNT molecules is sufficient to mute a neuron, thus this likely accounts for its rapid action.

To investigate the dynamics of song changes caused by these genetic perturbations, we quantified multiple acoustic features of syllables of birds receiving either LV-TeNT or LV-NaChBac<sup>21</sup>. In both types of perturbation, degraded songs consist of shorter (**Fig. 2a**), weaker (**Fig. 2b**), and noisier (**Fig. 2c**) syllables than those of the original songs. Note, we use the term ‘syllable’ to refer to any continuous song segment in the degraded song, even if they are not stereotypical, and they bear little or no resemblance to the original syllables. We measured the acoustic distortion of songs by calculating the distance of disordered syllables to the original (pre-perturbation) syllables, normalized to the maxima, in a high dimensional acoustic space derived from the spectrograms (**Fig. 2d and Extended Data Fig. 4**, see also Methods), and plotted trajectories of each syllable to show the timeline of dynamics of song degradation and recovery (**Fig. 2e**). We found that, both for LV-TeNT and LV-NaChBac animals, the acoustic distance to all original syllables increased drastically after the virus injection, but the onset and peak distortion occur earlier for LV-TeNT ( $3.53 \pm 0.39$  dpi) than for LV-NaChBac animals ( $6.25 \pm 0.66$  dpi, **Fig. 2e**). Although the peak distortion happens later for NaChBac the time to recovery was comparable for the two types of manipulations ( $13.71 \pm 0.72$  vs  $14.80 \pm 1.90$  dpi, **Fig. 2e**). The recovered song was very close to the original, but some localized aspects of the song changed permanently, including fine-scale acoustical structure, and loss of some syllables (**Fig. 1d,f**).

We also measured the rendition-to- rendition syllable variability across days (See Methods). For both NaChBac and TeNT, the peak of variability in syllable renditions occurred at around 10 dpi (**Fig. 2f**), approximately 4-6 days after the acoustic features of the songs were maximally degraded (**Fig. 2e**). By 20-25 dpi, the acoustic features were fully recovered and the syllable variability returned to the pre-perturbation level (**Fig. 2f**). Importantly, the degradation of song was not due to toxicity or mechanical lesion, because no behavioral change was observed when the same amount of viral vector expressing either GFP or a dead-pore NaChBac was injected (**Extended Data Fig. 5**,  $N = 4$ ). Finally, song recovery was not due to the restoration of normal firing activity in the NaChBac+ HVC(RA)neurons, because they still had the same amount of NaChBac current (**Extended Data Fig. 2a-c**) and highly increased inhibitory synaptic input at >25 dpi, 10 days after the song had recovered (**Extended Data Fig. 3**). Similarly, the muting of HVC(RA) neurons by LV-TeNT also persisted at >25 dpi, even after the song had recovered (**Extended Data Fig. 2a-c**). The similar behavioral outcomes after NaChBac and TeNT delivery suggests that the mechanisms by which these different genetic manipulations caused song degradation were due to the functional loss of a large percentage of HVC projection neurons, by direct muting caused by TeNT, and by homeostatic silencing in response to NaChBac.

Is the process of song recovery after HVC perturbation similar to the way young animals learn the song? Juvenile finches listen to the song of their fathers, memorize it, and attempt to copy it by continuous trial and error over 2-3 months and tens of thousands of practice renditions. The juvenile song is initially unstructured, until it eventually becomes a faithful copy of the father’s song, and it “crystallizes” into a stable motif with minimal variability<sup>22</sup>. To investigate if song recovery after HVC perturbations also required practice, we prevented LV-TeNT animals from singing during the two week period when the recovery usually occurs, and after this time, they were allowed to sing freely (**Fig. 3a and Extended Data Fig. 6**). Surprisingly, the very first song renditions sung on the first day after prevention were already highly similar to the original pre-perturbation song (**Fig. 3b-g**). After singing a few dozens of renditions within the same day, the songs recovered to the same degree as in animals that had sung thousands of renditions for two weeks after viral injections. These observations indicate that much of the song restoration after perturbation could occur without practice, and suggest that offline mechanisms could enable recovery in an unsupervised manner.

What are the cellular mechanisms by which the brain restores the precise execution of the song after such drastic perturbations? Both LV manipulations (NaChBac and TeNT) reduced the number of functioning HVC projection neurons. We hypothesized that the recovery may depend on changes among other neurons that were not genetically perturbed (“unmanipulated neurons”) within the same HVC. We performed whole-cell recordings to measure the synaptic and intrinsic properties of unmanipulated HVC(RA) neurons. These neurons showed no change in their intrinsic excitability or inhibitory synaptic inputs (**Extended Data Fig. 7**). However, they recruited a substantially higher level of excitatory synaptic inputs than neurons in unperturbed animals, as revealed by a much higher frequency of mEPSC ( $193.0 \pm 31.5$  %). **Fig. 4a-c**), suggesting that presynaptic mechanisms, such as formation of new synapses, activation of silent synapses, or strengthening of preexisting synapses might be responsible for these changes. To investigate whether these synaptic changes are caused by local perturbation of neuronal activity within the same region, we injected the virus unilaterally just in one HVC. We detected synaptic changes in unmanipulated neurons in the injected hemisphere, but not in the contralateral (unmanipulated) hemisphere (**Extended Data Fig. 8a,b**). This suggests that the observed synaptic changes are induced by local phenomena restricted to the HVC that was perturbed.

The excitatory inputs received by HVC inhibitory neurons in LV-TeNT animals were initially greatly reduced, consistent with a reduction of the synaptic output from the projection cells expressing TeNT. Dual whole-cell recordings between HVC(RA) projection neurons and interneurons indicated that expression of TeNT leads to permanent muting of the infected cells (**Extended Data Fig. 2**). However, these excitatory inputs to inhibitory neurons eventually recovered to a level that was indistinguishable from control animals (**Extended Data Fig. 8c,d**), suggesting that the recovery of the inhibitory tone was due to changes in unmanipulated neurons. Thus, our findings show that alongside song degradation and following recovery, the HVC network is dramatically restructured.

We used modeling to explore how synaptic plasticity mechanisms could contribute to unsupervised recovery of network activity after perturbation and to account for the observed synaptic changes. Song recovery in animals that were prevented from singing suggests that plasticity mechanisms are initially largely driven locally within HVC rather than by behavioral feedback from practice. We sought to determine which mechanisms are consistent with restoration of the sequence as well as recapitulation of our physiological findings on synaptic strength changes. We modeled HVC as an excitatory-inhibitory (E-I) network, with HVC(RA) neurons connected to each other in a feedforward, polysynchronous chain and recurrently connected to HVC(INT) neurons (**Fig. 4d**)<sup>23,24</sup>. We then inactivated varying fractions of the HVC(RA) population (**Fig. 4d**, supp fig) to mimic the silencing of neurons caused by TeNT expression. To explore mechanisms that may enable recovery, we first implemented spike-timing dependent plasticity (STDP) between excitatory neurons (E→E), which is integral to many models of sequence self-organization<sup>23,25–27</sup>. In addition, implementing STDP between excitatory and inhibitory neurons (E→I) enabled the rebound of input to inhibitory neurons observed in our experiments. However, we found that STDP alone did not reliably restore sequential activity (supp fig ref), as the perturbed chain lacks activity in both pre- and postsynaptic neurons required to strengthen synapses, and further did not produce the overshoot in excitatory connectivity into HVC(RA) neurons observed by our electrophysiological measurements.

As STDP alone was insufficient to restore the sequential dynamics in our model of HVC, we next considered whether cell-autonomous homeostatic mechanisms based on changes on either intrinsic excitability or synaptic inputs may enable recovery of the network. Our recordings revealed that unmanipulated HVC(RA)

neurons did not change their intrinsic excitability post-perturbation (**Extended Data Fig. 7**), but they displayed changes in their synaptic inputs. Thus, we added into the model a cell-autonomous homeostatic rule based on scaling the excitatory synaptic inputs to individual excitatory neurons to maintain their firing rates (**Fig. 4e**). The implementation of this rule is consistent with reports that found activity-dependent synaptic homeostasis in other circuits with sequential dynamics<sup>28</sup>. We found that adding this form of cell-autonomous synaptic homeostasis in excitatory neurons reliably restored sequential network activity (**Fig. 4f,g**); however, in models employing STDP alone or both STDP and cell-autonomous synaptic homeostasis, the recovered HVC outputs were reduced in proportion to the percentage of neurons inactivated, thereby drastically weakening the drive to downstream regions (**Fig. 4h**). [Additionally, these models did not reproduce the overshoot in excitatory synaptic input to unmanipulated excitatory neurons as revealed by our experiments (**Fig. 4c,g**).

One potential mechanism by which HVC might restore its output to downstream targets is the recruitment of neurons that initially do not participate in the sequential dynamics, defined here as “silent” neurons (**Fig. 4i**). Multiple experiments have indicated that a large fraction of HVC(RA) neurons do not fire during song, suggesting a possible redundant role<sup>8,29,30</sup>. We hypothesized that the presence of such silent neurons--assumed to be HVC(RA) neurons connected within the network, but whose inputs are subthreshold--might provide additional resilience by allowing the sequential dynamics to be partially carried by newly recruited HVC neurons when active constituents of the network fail. While such shifts in representation could be due to the loss of inhibition onto silent cells following the loss of excitatory neurons, this picture of recovery is inconsistent with our experiments in that it does not require the large increase in the excitatory inputs onto HVC(RA) neurons that we observed in our recordings. We therefore hypothesized that silent neurons may be recruited into the sequence through a form of population homeostasis, for which there is an emerging body of support<sup>31-34</sup>. In our model, we implemented one potential mechanism by which such population homeostasis can be achieved: synaptic scaling based on the activity-dependent release of secreted factors (**Fig. 4j**), such as BDNF and TNF $\alpha$ , which have been shown to regulate local network activity in a non-cell-autonomous manner<sup>35-38</sup>. While local population homeostasis alone enabled reliable recovery of sequences the recruitment of previously inactive neurons enabled the most complete recovery consistent with our experiments in that the total output of the network was restored and E $\rightarrow$ E synaptic inputs increased by  $\sim$ 100% (**Fig. 4k-m**). Furthermore, the dynamics of the sequence in terms of numbers of participating neurons and their temporal resolution most closely resembles the pre-perturbation state.

The core of our model is that the sequence is restored through a parallel homeostatic process, rather than regrown serially through a timing-dependent process (**Fig. 5a**). A prediction of the model is that the sequence should recover in an abrupt fashion: all links are repaired simultaneously, so that by the time any broken link is restored, all other links tend to have recovered (**Fig. 5b-d**). Correspondingly, we found many examples of such saltatory recovery in the song, whereby syllables show a bimodal temporal distribution (**Fig. 5e-h**), with syllables rapidly alternating between two durations from rendition to rendition until eventually they permanently recover their original duration. Syllables with these bimodal temporal distributions are only present in renditions that include song segments that bear acoustic resemblance to the original syllables. This suggests the existence of a remaining chain “skeleton” that supports production of the correct syllable on occasional renditions until the sequence’s strength fully recovers. A further implication of these observations and the recovery set out by the model is that the skeleton can act as a scaffold upon which the homeostatic plasticity can rebuild the dynamics in an unsupervised manner. As this redundancy can exist very 'locally' in the chain (i.e. only between adjacent links) it is still consistent with an extremely sparse network, and may be a key contributor to resilience in HVC.

The precise recovery of a complex, learned behavior from extensive perturbations to a brain region essential for its production indicates the presence of cellular and systems-level restorative mechanisms that operate locally and in an “offline”, partially unsupervised manner. Song restoration occurred even when animals were prevented from singing during the recovery period, which indicates that the restoration mechanisms were guided by measuring neuronal activity, without any information regarding how these cellular changes may improve behavior. Song recovery was accompanied by increased excitatory synaptic inputs to unmanipulated neurons within the same brain region. Based on these findings we modeled sequential dynamics to test how plasticity mechanisms can support this restoration. The inclusion of population-level homeostasis in the model confers a unique form of resilience as it enables the recruitment of HVC(RA) neurons that did not initially participate in song dynamics, providing a potential role for these inactive cells; neither STDP nor single-cell homeostasis can recruit these silent neurons into the active dynamics. The model predicts that the set of HVC(RA) projection neurons active in song would shift substantially following perturbation. Such population-level activity regulation could support naturally occurring “representational drift”, which has been observed in several brain regions wherein the qualitative nature of the sequential dynamics is preserved but the neurons that participate in the dynamics change<sup>39-43</sup>, potentially increasing circuit robustness<sup>44,45</sup>. Population-level homeostasis accounts for the experimentally observed increase in excitatory synaptic inputs to unmanipulated excitatory neurons as the song recovers. The observed upregulation of synaptic strength may have occurred through a random global process that could be later refined through activity-dependent plasticity. Instead we find that the excitatory weight changes remain after the song has fully recovered in the experiment, suggesting, consistent with our modeling, that these changes represent a persistent network reorganization critical to the recovery process. Finally, the model recapitulated the experimental finding that restoration of sequential firing can happen offline (without feedback from practice) to result in song recovery, pointing to a largely unsupervised, local, circuit-level reorganization. We hypothesize that the potential for self-organized restoration of sequential dynamics may be key to enable such circuit mechanisms to support resilient behavior.

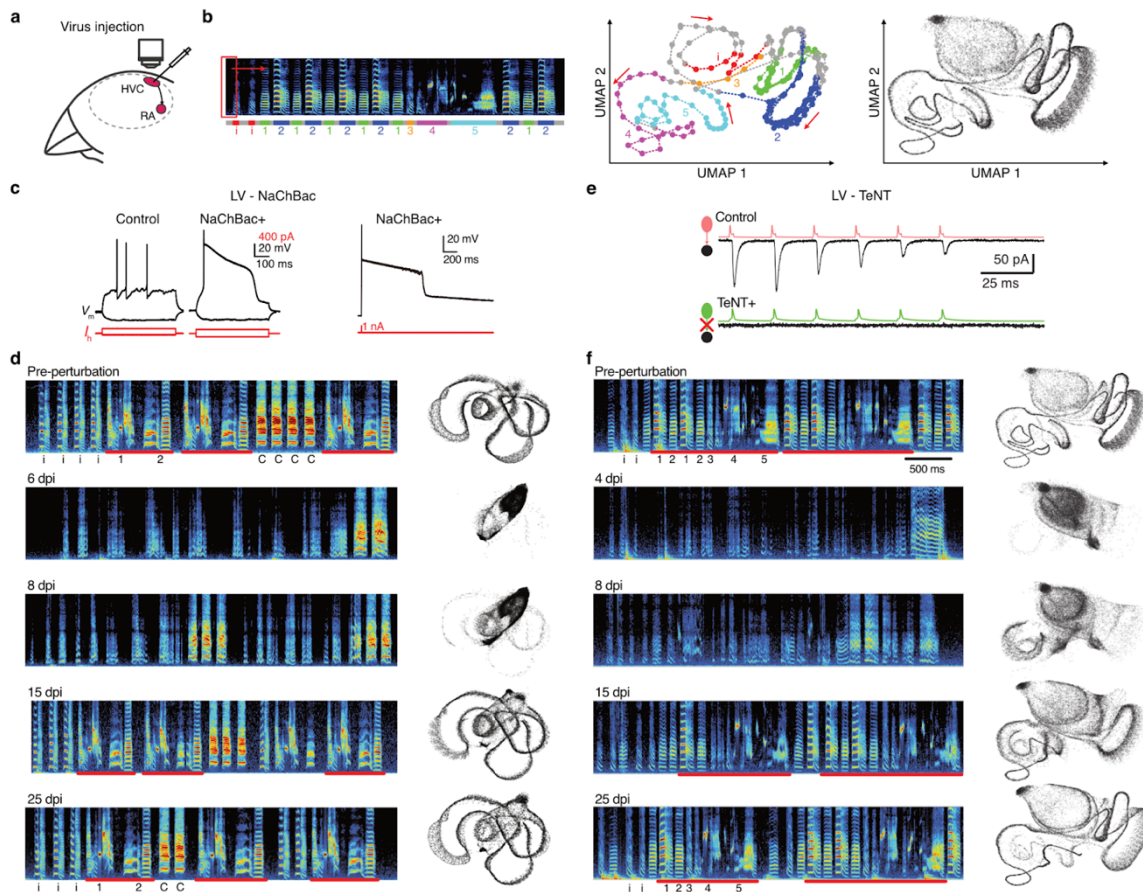
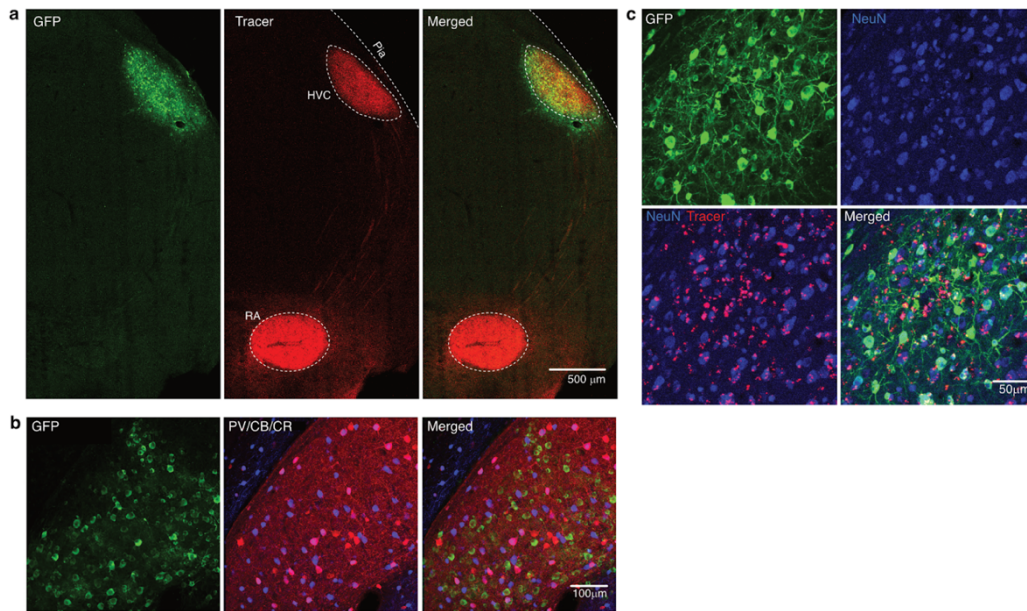


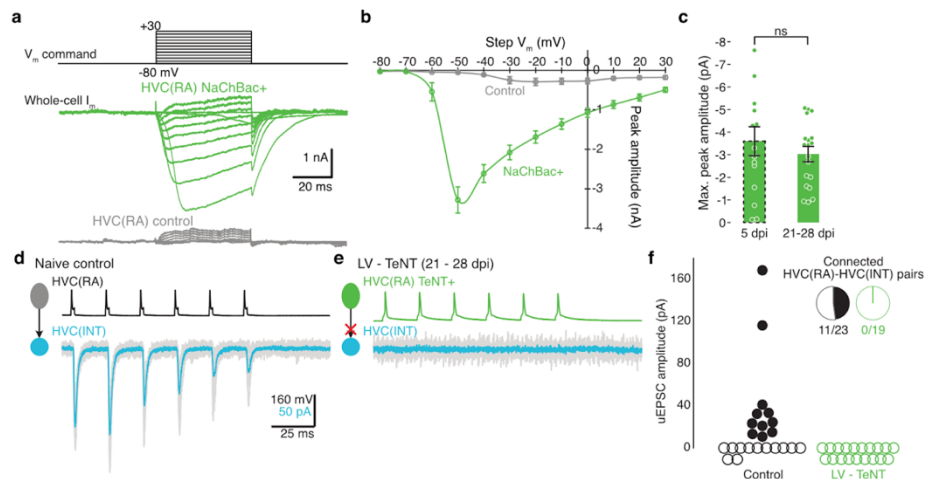
**Figure 1: Song degradation and recovery after selective large-scale perturbation of excitatory neurons**

**(a)** Schematic drawing illustrating the visual guided virus delivery into HVC (see Methods); **(b)** (Left) Spectrogram of a motif and the corresponding 2D projection (middle) using the UMAP algorithm from an unperturbed animal. The syllables are indicated by different colors and numbers in the spectrogram and UMAP plot. (Right) UMAP visualization containing ~100 songs randomly sampled one day without perturbation; **(c)** Firing pattern of RA-projecting HVC (HVC(RA)) neurons with (NaChBac+) or without NaChBac (Control); **(d)** Example spectrograms and UMAP visualizations of the song of a bird injected with LV-NaChBac; **(e)** Example dual patch clamp traces demonstrating that expression of TeNT abolishes synaptic release from excitatory neurons in HVC; **(f)** Example spectrograms and corresponding UMAP visualizations of songs of a bird at different days post injection with LV-TeNT. The song motifs containing the syllables (12345) are marked by red lines, and can be seen before perturbation and after recovery; ‘i’ stands for introductory note; ‘C’ stands for call.



Extended Data Figure 1: Specific infection of HVC projection neurons by LVs

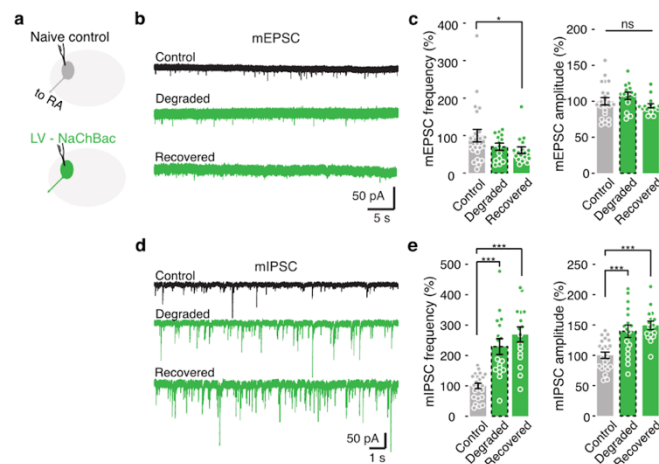
**(a)** Confocal image of a brain slice from a bird injected with LVs, showing the expression of the transgene (tagged with GFP) in HVC, which is labeled by a fluorescent retrograde tracer injected into RA; **(b)** Confocal images of a brain slice showing that LV selectively target projection neurons, where the LV transgene (tagged with GFP, seen in green) does not overlap the immunofluorescent signal of pooled antibodies against some of the standard markers of inhibitory neurons (PV, parvalbumin/CB, calbindin/CR, calretinin, seen in red, blue); **(c)** Confocal images showing the expression of delivered transgene (tagged with GFP) in the majority of HVC RA-projecting neurons (retrogradely labeled with fluorescent retrobeads from RA).



Extended Data Figure 2: Stable expression of transgenes in HVC projection neurons

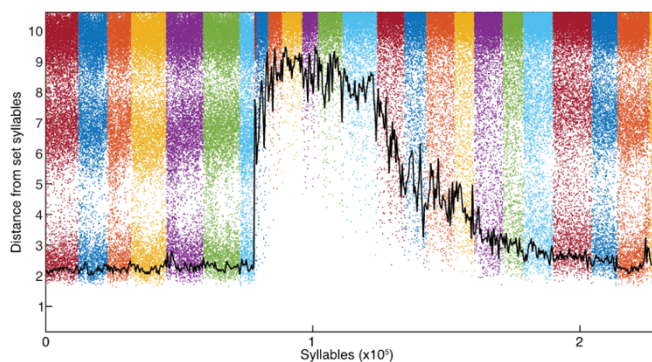
**(a)** Example traces of whole-cell NaChBac current evoked by depolarizing voltage steps (from -80 to +30 mV. increment, 10 mV.) recorded from HVC(RA) neurons infected with LV-NaChBac (NaChBac+) or control cells; **(b)** I-V curve of the NaChBac current, illustrating the peak amplitude of whole-cell current at different step voltages; **(c)** Comparison of the maximal peak amplitude of whole-cell NaChBac currents recorded at 5 dpi ( $3.6 \pm 0.6$  nA) vs. 21-28 dpi ( $3.0 \pm 0.3$  nA), demonstrating that the presence of NaChBac

is stable, as it could be detected even >3 weeks after viral injection, after the song had already recovered. Student's t-test. N = 10/3 (control), 15/2 (5 dpi), and 19/3 (21-28 dpi). Error bars represent s.e.m.; **(d)** Example traces from a dual patch clamp recording, showing that when action potentials were evoked in RA-projecting HVC (HVC(RA)) neurons (upper), excitatory postsynaptic currents (EPSCs) can be reliably detected in the connected interneuron (HVC(INT)) (below); **(e)** Example traces from dual patch clamp recording made between an HVC(RA) neuron infected with LV-TeNT and an interneuron, showing that no EPSC could be detected in the interneuron when the HVC(RA) neuron was stimulated; **(f)** Summary of dual patch clamp results from LV-TeNT neurons. In control animals, 11 out of 23 recorded pairs were connected (the amplitude of EPSCs shown in the scatter plot), but none of the 19 pairs recorded between TeNT+ projection neurons (21-28 dpi) and neighboring interneurons was connected. The block of synaptic transmission by TeNT expression is long-lasting, as it could be detected even >3 weeks after viral injection, after the song had already recovered;



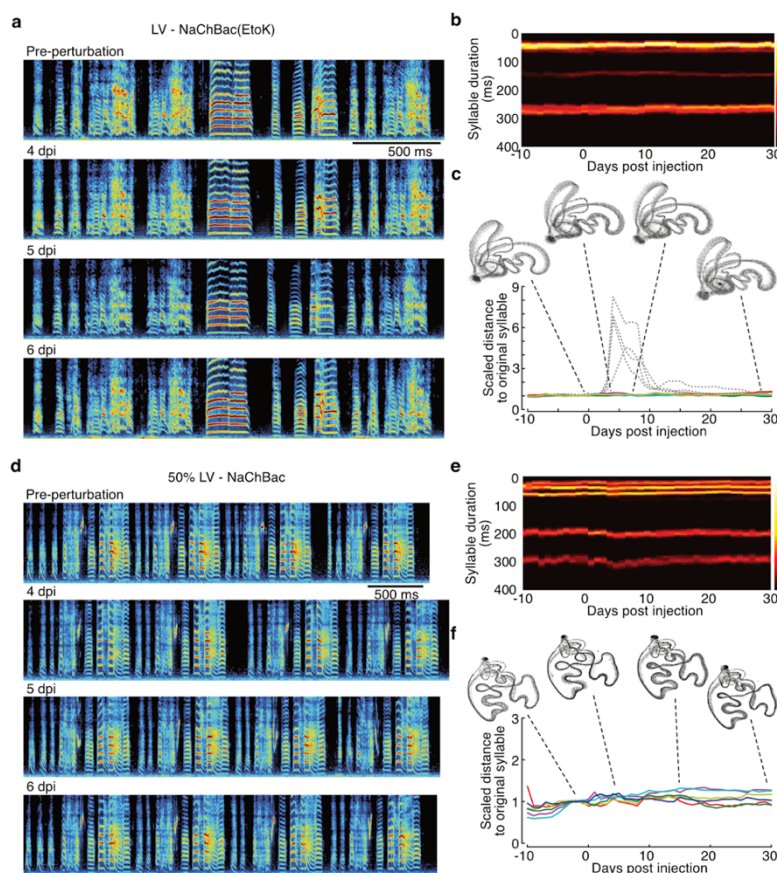
**Extended Data Figure 3:** Changes in synaptic currents in NaChBac+ HVC(RA) cells

**(a)** Schematic drawing showing whole-cell patch clamp recordings were made in HVC(RA) neurons infected with LV-NaChBac or naive controls; **(b)** Example of current traces with mEPSC events recorded in HVC(RA) neurons expressing NaChBac at different time points. “Degraded” illustrates currents at 5 dpi, when the song was highly irregular. “Recovered” illustrates currents at 25-35 dpi, after the song was fully recovered; **(c)** Group data of the frequency and amplitude of mEPSCs in HVC(RA) NaChBac+ cells. mEPSC frequency: Control,  $9.7 \pm 1.6 \text{ min}^{-1}$ , N = 22/4; Degraded,  $6.8 \pm 0.9 \text{ min}^{-1}$ , N = 14/5; Recovered,  $5.9 \pm 0.9 \text{ min}^{-1}$ , N = 17/4. mEPSC amplitude: Control,  $17.2 \pm 0.9 \text{ pA}$ ; Degraded,  $18.5 \pm 0.9 \text{ pA}$ ; Recovered,  $16.1 \pm 0.5 \text{ pA}$ ; **(d)** Example of current traces with mIPSC events recorded in HVC(RA) neurons expressing NaChBac at different times after injection; **(e)** Group data of the frequency and amplitude of mEPSCs in HVC(RA) NaChBac+ cells. mIPSC frequency: Control,  $2.7 \pm 0.2 \text{ s}^{-1}$ , N = 23/4; Degraded,  $6.1 \pm 0.7 \text{ s}^{-1}$ , N = 17/3; Recovered,  $7.2 \pm 0.7 \text{ s}^{-1}$ , N = 16/5. \*,  $p < 0.05$ , \*\*\*,  $p < 0.001$ , student's t-test. Error bars represent s.e.m.



Extended Data Figure 4: Tracking the degradation and recovery of song syllables using k-neighbor acoustic distance from set syllables

(See also the Methods for a detailed explanation). Here we plot the distance of each analyzed syllable to the set of the syllables in the original song, in a high dimensional space constructed using multiple acoustic features. Each dot represents one syllable and they are chronologically ordered on the x axis. Different colors are used to denote different days. The black line represents the average k-nearest neighbor distance of the closest song segments (2.5%) to the original syllable set, which illustrates the dynamic trajectory of song degradation and recovery. We tracked the change of songs in the same way in Figs. 2e, 4d, and Extended Data Figs. 5c, 8c.



**Extended Data Figure 5:** Songs degradation and recovery was not due to mechanical lesion or inflammation  
**(a)** Example spectrograms of songs from a bird injected with LV-NaChBac(EtoK), a dead-pore mutant of NaChBac; **(b)** Distribution of syllable durations per day of the same bird shown in panel a; **(c)** Plots of scaled acoustic distance to original syllables. Data was from the same bird as in panels a and b. The insets are UMAP visualizations of songs at selected time points. Dashed lines are generated from the syllables of the bird injected with LV-NaChBac shown in Fig. 1d, and for comparison here they were not normalized to maximum. Experiments with LV-NaChBac(EtoK) yielded consistent results,  $N = 4$ ; **(d)** Example spectrograms of songs from a bird injected with half of the volume of LV-NaChBac used for animals shown in Fig. 1; **(e)** Distribution of syllable durations per day of the same bird shown in panel d; **(f)** Plots of scaled acoustic distance to original syllables. Data was from the same bird as in panels d and e. Each line/color represents one syllable. The insets are UMAP visualizations of songs at selected time points. Experiments with reduced volume of LV-NaChBac were repeated,  $N = 2$ .

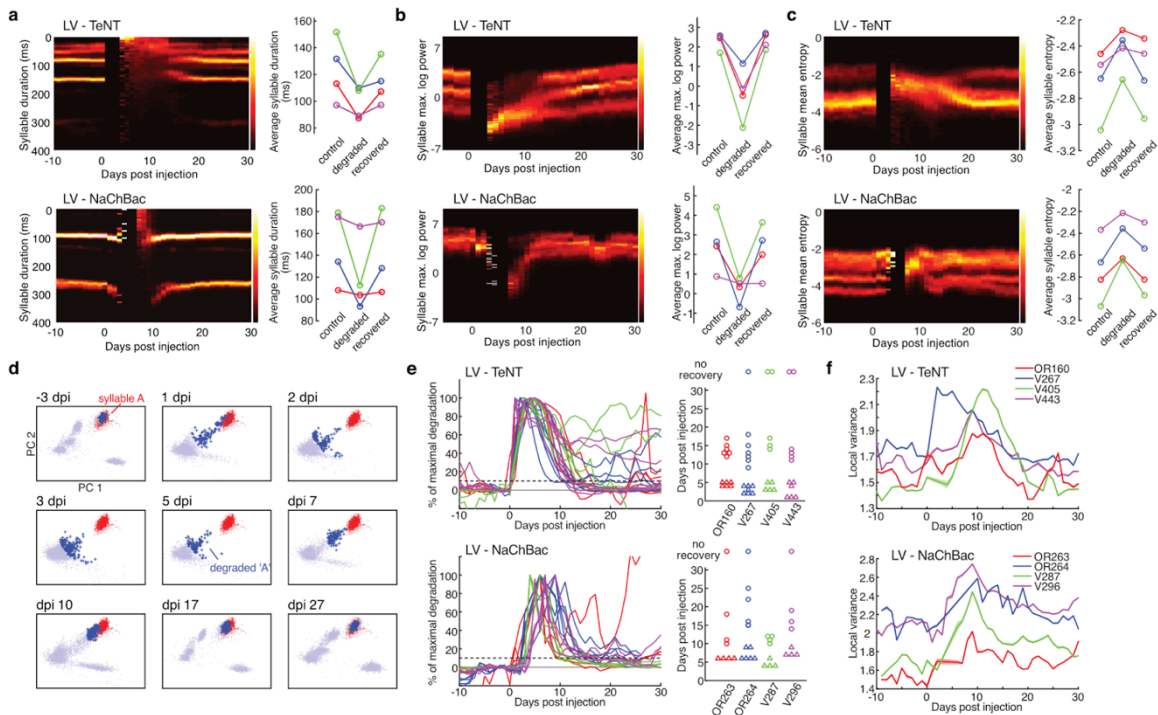


**Figure 2:** Dynamics of song degradation and recovery after large-scale perturbation of HVC excitatory neurons

**(a)** (Left) Density distribution of syllable durations day by day, for 2 birds either with LV-TeNT (upper) or LV-NaChBac (bottom). Note that the gap in the middle (between around 1-5 dpi) means the number of song bouts recorded that day was not enough for a meaningful analysis. (Right) Averaged duration of all syllables at three time points, before perturbation (control), when the song is most severely degraded (3-5 dpi), and when the song is fully recovered (25-30 dpi). Each line represents one animal; **(b)** (Left) Density distribution of the maximal log power of syllables day by day. (Right) Averaged syllable maximal log power at different time points. Animals with LV-TeNT on top and those with LV-NaChBac on bottom; **(c)** (Left) Density distribution of the mean entropy of syllables day by day. (Right) Averaged entropy of all syllables at different time points; **(d)** We tracked the change of song segments over time using acoustic features sampled from the spectrograms of the song segments (see also Methods). Here we show the trajectory of songs in the first 2 principal components of the acoustic space over a series of days after LV-TeNT injection. Each dot represents one original or degraded syllable. Red dots represent original renditions of syllable 'A' sung 1 day pre-perturbation. Blue dots represent song segments sung on each day. Dark blue dots represent the closest 2.5 % of song segments to the original syllable 'A' cluster on each day (measured using a k-nearest neighbor metric in the full acoustic parameter space), which we used to quantify the degradation of syllable 'A'; **(e)** (Left) Plots of acoustic distance (see also Methods & Fig. S4) to each original syllable, normalized so that the peak of the curve represents 100% degradation. Curves in the same color were from the same bird. (Right) Triangles represent the day when each syllable reached peak degradation (TeNT  $3.53 \pm 0.39$  vs NaChBac  $6.25 \pm 0.66$  dpi,  $p < 0.001$ , nested ANOVA), and round dots represent the day when each syllable achieved more than 90% recovery ( $13.71 \pm 0.72$  vs  $14.80 \pm 1.90$  dpi,  $p > 0.05$ , nested ANOVA). Each column represents one bird; **(f)** Plots of the local variance across days.

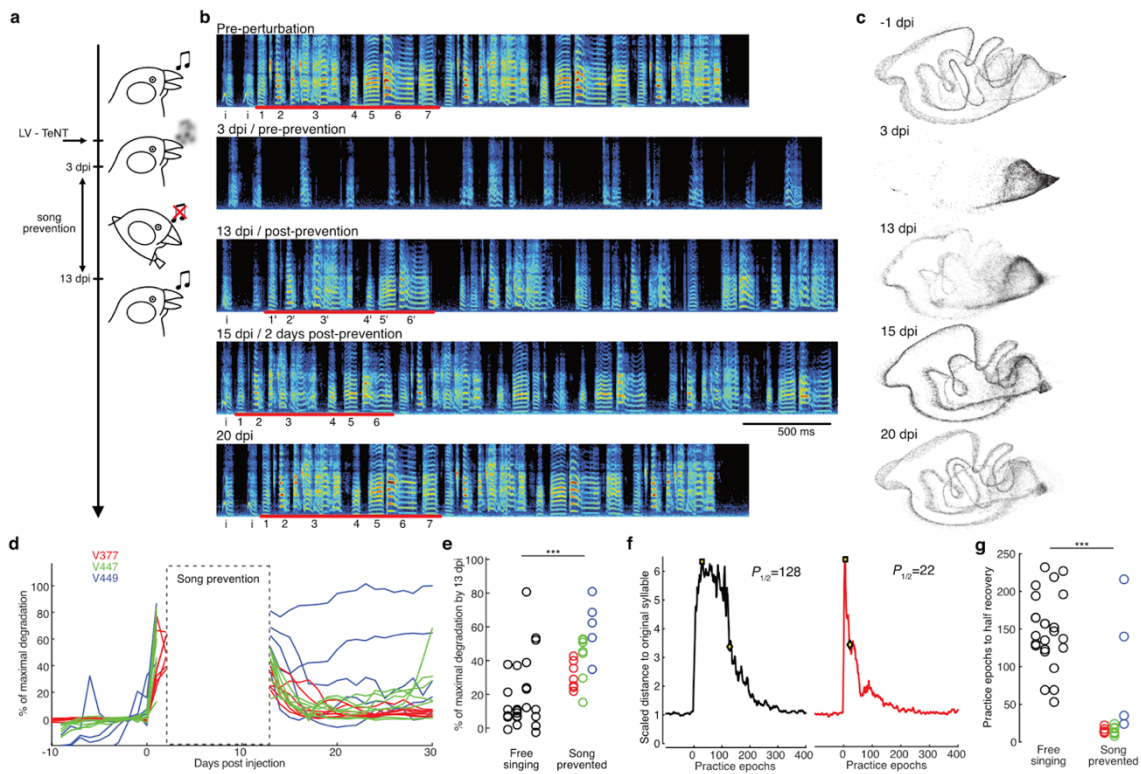
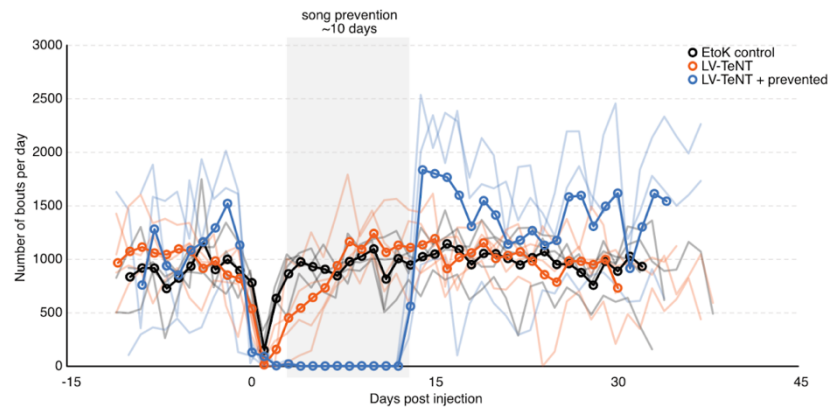


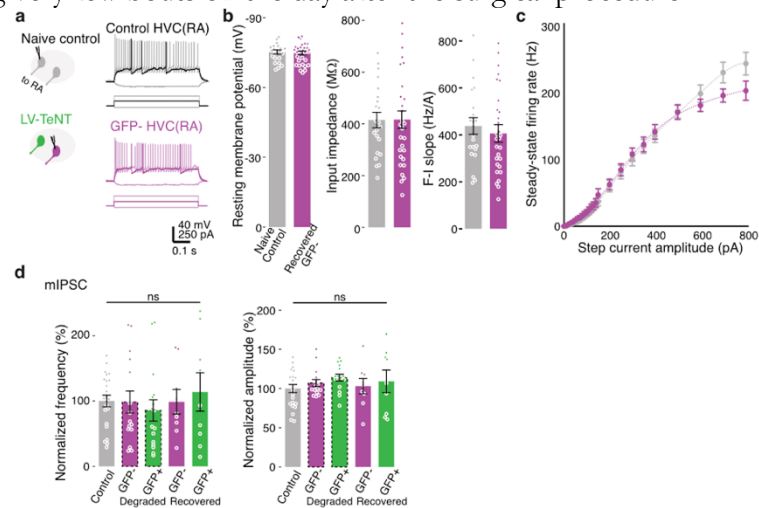
**Figure 3: Partial recovery of degraded song without practice**

(a) Schematic illustrating the experimental procedure of perturbation with LV-TeNT and song prevention; (b) Example spectrograms of a bird injected with LV-TeNT and prevented from singing for 10 days. On the first day after song prevention (“post-prevention”) the song was partially recovered and syllables were good enough to match to those of unperturbed song (“pre-perturbation”); (c) UMAP visualizations of songs of the same bird shown in B; (d) Plots of distance to original syllables (normalized to maximum) of all birds prevented from singing (gray lines). Each color represents one bird. Prevented animals sang fewer than 8 songs per day versus more than 5,000 songs per animal per day for the freely singing animals during the 10-day prevention period (marked by a gray square); (e) At 13 dpi the song of freely singing birds had mostly recovered ( $20.4 \pm 6.3\%$  of the maximal degradation remaining). At this time, when song-prevented birds were allowed to sing they also showed significant recovery ( $44.2 \pm 10.4\%$  of the maximal degradation remaining)  $p < 0.001$ , Nested ANOVA; (f) Example plots of syllable recovery vs number of practice epochs with or without prevention; (g) Group data of the number of practice epochs to reach half recovery of each syllable, each column is one bird. Free-singing,  $149.4 \pm 12.4$ ,  $N = 4$ ; Song-prevented,  $44.7 \pm 29.5$ ,  $N = 3$ . \*\*\*,  $p < 0.001$ , nested ANOVA.



**Extended Data Figure 6:** Number of song bouts sung per day in freely signing animals and individuals prevented from singing

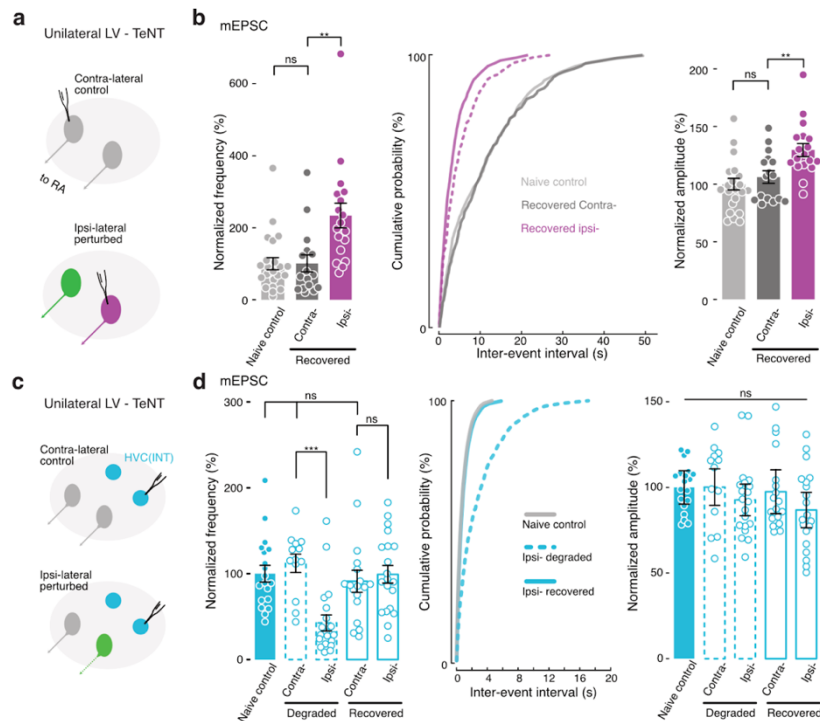
A song bout was defined as a continuous vocalization without a gap longer than 450 ms, and it usually includes several motifs. Faded lines are numbers of song bouts per day of each individual bird. Bold lines are the mean value per day of each group. Song prevention period is marked by a gray square. Notice that in cases, animals sing very few bouts on the day after the surgical procedure.



**Extended Data Figure 7:** Unperturbed cells did not change their intrinsic excitability or inhibitory synaptic inputs

**(a)** (Left) Whole-cell patch clamp recordings were made in GFP- HVC(RA) neurons in naive control birds or birds injected with LV-TeNT. (Right) Membrane potential and firing pattern of HVC(RA) neurons in response to current steps; **(b)** Group data showing that no significant difference was found in the resting membrane potential ( $-75.2 \pm 0.8$  vs.  $-74.8 \pm 0.8$  mV), input resistance ( $414.8 \pm 30.0$  vs.  $416.2 \pm 33.1$  MOhm), or initial F-I slope ( $437.9 \pm 35.5$  vs.  $406.2 \pm 37.3$  Hz/A) between neurons in naive control (N = 22/3) and in birds with LV-TeNT for more than 25 days (N = 30/4). Student's t-test; **(c)** F-I curves obtained from HVC(RA) neurons showed no difference between control or animals recovered from LV-TeNT; **(d)** Group data of mIPSC recorded in HVC(RA) neurons, showing no significant difference at any time during the experiment. “Degraded” indicates the time when the song was degraded, at 5 dpi. “Recovered” indicates the time after the song had fully recovered, at 25 dpi. mIPSC frequency: Control,  $2.7 \pm 0.2$  s<sup>-1</sup>, N = 23/4; “Degraded” GFP-negative cell,  $2.6 \pm 0.4$  s<sup>-1</sup>, N = 16/3; “Degraded” GFP-positive,  $2.3 \pm 0.4$  s<sup>-1</sup>, N = 16/3; “Recovered” GFP-,  $2.6 \pm 0.5$  s<sup>-1</sup>, N = 9/3; “Recovered” GFP+,  $3.1 \pm 0.8$  s<sup>-1</sup>, N = 9/3. mIPSC amplitude: Control,  $37.9 \pm 2.0$  pA; “Degraded” GFP-negative cell,  $40.6 \pm 1.7$  pA; “Degraded” GFP-positive cell,  $43.2$

$\pm 1.6$  pA; “Recovered” GFP- negative cell,  $39.0 \pm 3.7$  pA; “Recovered” GFP- positive cell,  $41.4 \pm 5.4$  pA. One-way ANOVA. Error bars represent s.e.m.



**Extended Data Figure 8:** Synaptic changes in unmanipulated neurons only occurred in the injected hemisphere

**(a)** Whole-cell recordings were made in GFP- HVC(RA) (“unmanipulated”) neurons in the injected and unperturbed hemispheres of birds with unilateral LV-TeNT injection; **(b)** Group data of mEPSC recorded in naive control birds and birds with unilateral LV-TeNT. The frequency (left) and amplitude (right) of mEPSC increased significantly in GFP- HVC(RA) neurons in the injected side, as compared with neurons in the contralateral side or naive animals. (Middle) Cumulative curve of inter-event intervals of mEPSCs. Dashed line represents data from GFP- neurons from animals with bilateral LV-TeNT injection for comparison and was adapted from Figure 4c. mEPSC frequency: Naive control,  $9.7 \pm 1.6$  min<sup>-1</sup>, N = 23/4; Contralateral (uninjected HVC),  $9.8 \pm 2.3$  min<sup>-1</sup>, N = 16/4; Ipsilateral (injected),  $22.8 \pm 3.3$  min<sup>-1</sup>, N = 18/3. mEPSC amplitude: Naive control,  $17.2 \pm 0.9$  pA; Contralateral,  $18.2 \pm 0.9$  pA; Ipsilateral,  $22.3 \pm 1.0$  pA; **(c)** Whole-cell recordings were made in inhibitory (HVC(INT)) neurons in birds with unilateral LV-TeNT; **(d)** Group data of mEPSC recorded in birds with LV-TeNT at 5 dpi (“Degraded”) or > 25 dpi (“Recovered”). (Left) The frequency of mEPSC in HVC(INT) neurons decreased after virus injection, but eventually recovered to a level comparable to that of controls. (Middle) Cumulative curve of inter-event intervals of mEPSCs. mEPSC frequency: Naive control,  $1.47 \pm 0.14$  s<sup>-1</sup>, N = 19/2; Degraded contralateral,  $1.56 \pm 0.16$  s<sup>-1</sup>, N = 13/3; Degraded ipsilateral,  $0.63 \pm 0.14$  s<sup>-1</sup>, N = 20/3; Recovered contralateral,  $1.34 \pm 0.19$  s<sup>-1</sup>, N = 18/4; Recovered ipsilateral,  $1.45 \pm 0.15$  s<sup>-1</sup>, N = 20/4. mEPSC amplitude: Naive control,  $38.3 \pm 1.2$  pA; Degraded contralateral,  $38.4 \pm 2.6$  pA; Degraded ipsilateral,  $35.5 \pm 1.9$  pA; Recovered contralateral,  $37.3 \pm 2.1$  pA; Recovered ipsilateral,  $33.2 \pm 2.0$  pA. \*\*, p < 0.01, \*\*\*, p < 0.001, ANOVA & student’s t-test. Error bars represent s.e.m.

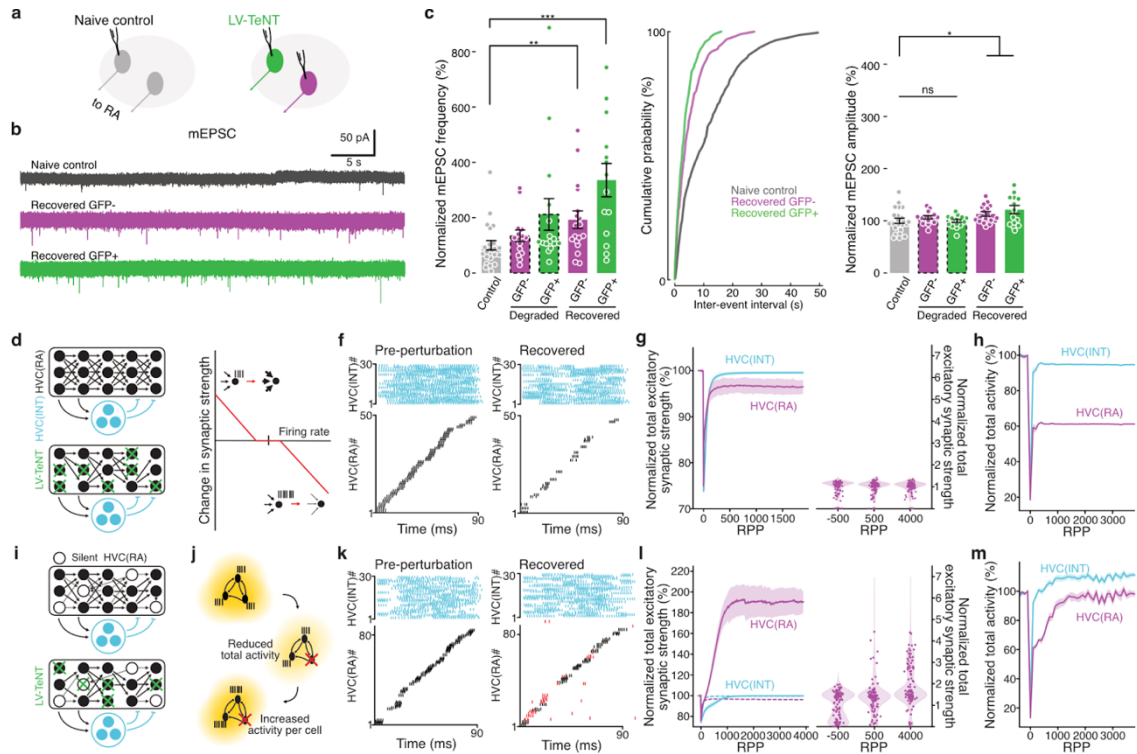


**Figure 4:** Population-level homeostatic plasticity and recruitment of silent inactive neurons in a network model contribute to the recovery of sequential activity

**(a)** Schematic illustrating whole-cell recordings from HVC(RA) neurons in birds injected with LV-TeNT or naive controls ; **(b)** Example traces of mEPSC recordings; **(c)** Group data of mEPSCs. “Degraded” indicates recordings at 5 dpi when the song was degraded. “Recovered” indicates recordings at 25 dpi, after the song had fully recovered. mEPSC frequency: Control,  $9.7 \pm 1.6 \text{ min}^{-1}$ ,  $N = 23/4$ ; Degraded GFP-,  $13.1 \pm 0.2 \text{ min}^{-1}$ ,  $N = 15/3$ ; Degraded GFP+,  $20.6 \pm 0.3 \text{ min}^{-1}$ ,  $N = 16/4$ ; Recovered GFP-,  $18.8 \pm 0.3 \text{ min}^{-1}$ ,  $N = 18/4$ ; Recovered GFP+,  $32.7 \pm 0.5 \text{ min}^{-1}$ ,  $N = 14/4$ . mEPSC amplitude: Control,  $17.2 \pm 0.9 \text{ pA}$ ; Degraded GFP-,  $18.3 \pm 0.6 \text{ pA}$ ; Degraded GFP+,  $17.1 \pm 0.5 \text{ pA}$ ; Recovered GFP-,  $19.5 \pm 0.7 \text{ pA}$ ; Recovered GFP+,  $20.8 \pm 1.4 \text{ pA}$ . \*,  $p < 0.05$ . \*\*,  $p < 0.01$ . \*\*\*,  $p < 0.001$ , One-way ANOVA & student’s t-test. Error bars represent s.e.m.; **(d)** Schematic diagram of the neuronal organization in the model; **(e)** Schematic illustrating the single-cell homeostatic plasticity rule implemented in the model; **(f)** Spike raster plots showing the sequential dynamics generated by HVC neurons before perturbation and after recovery (with only single-cell homeostatic plasticity implemented); **(g)** (Left) Plot of the normalized total excitatory synaptic input per neuron against renditions. RPP=renditions post perturbation. (Right) Scatter plot of the normalized total excitatory synaptic input received by each HVC(RA) neuron at three time points; **(h)** Plots of the normalized total firing activity of all functioning neurons; **(i)** Schematic diagram illustrating that initially inactive neurons were recruited into the network; **(j)** Schematic diagram illustrating that a population-level homeostatic plasticity, governing the summed firing activity of all neurons, was also implemented in the model; **(k)** Spike raster plots showing the sequential dynamics generated by HVC cells before perturbation and after recovery; **(l)** (Left) Plot of the normalized total excitatory synaptic input per neuron against number of renditions. (Right) Scatter plot of the normalized total excitatory synaptic input received by each HVC(RA) neuron at three time points; **(m)** Plots of the normalized total firing activity of all functioning neurons.

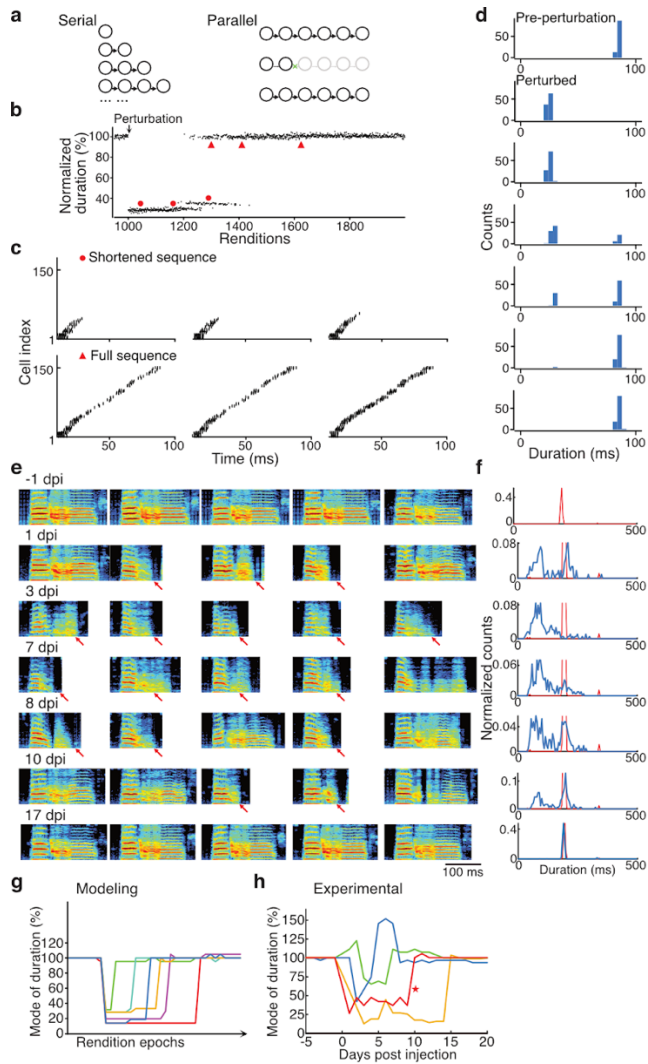


**Figure 5:** Saltatory recovery of syllables duration

(a) Schematic diagrams showing two types of potential circuit recovery mechanisms. First, the recovery of sequential firing requires building of feedforward synaptic chains step by step from the breaking point, such that the duration should regrow continuously. Second, all links in a sequence are repaired simultaneously, so that the recovery of the full sequence can be abrupt, when the broken links are fixed; (b) Plot of the normalized duration of modeled sequential firing against number of renditions. Note that the recovery of the full syllable duration was not continuous, but instead it occurred by a sudden leap from a shortened state; (c) Example raster plots showing the sequential spiking of modeled HVC(RA) neurons, picked from multiple time points indicated by red dots (shortened sequence) or triangles (full sequence) in panel b; (d) Probability density distributions of the durations of the modeled syllables at different times (before perturbation, during the degraded period, during the recovery period, and after full recovery), ordered chronologically. Note the bimodal distribution of the duration of a single syllable during the recovery phase; (e)

Example spectrograms picked from the nearest  $k$  neighbors of one syllable at multiple days before and post injection of LV-TeNT. Red arrows mark the shortened/truncated syllables found between 1 to 10 dpi; **(f)** Probability density distributions of the duration of the  $k$  neighboring syllables, ordered so that each row of panels in e and f is from the same day. Note the bimodal distribution of durations for a single syllable found during the period of song degradation and recovery; **(g)** Plots of the mode of the duration of the modeled sequences against rendition epochs, showing that the recovery of sequence duration occurs in a saltatory, rather than in a continuous, manner; **(h)** Plots of the mode of duration of actual song syllables, which shows a saltatory recovery similar to that predicted by the model. The red curve marked with a star is made from the syllable shown in panels e and f.

## Bibliography

1. Masset, P., Qin, S. & Zavatone-Veth, J. A. Drifting neuronal representations: Bug or feature? *Biol. Cybern.* **116**, 253–266 (2022).
2. Mongillo, G., Rumpel, S. & Loewenstein, Y. Intrinsic volatility of synaptic connections - a challenge to the synaptic trace theory of memory. *Curr. Opin. Neurobiol.* **46**, 7–13 (2017).
3. Nottebohm, F., Stokes, T. M. & Leonard, C. M. Central control of song in the canary, *Serinus canarius*. *J. Comp. Neurol.* **165**, 457–486 (1976).
4. Nottebohm, F., Kelley, D. B. & Paton, J. A. Connections of vocal control nuclei in the canary telencephalon. *J. Comp. Neurol.* **207**, 344–357 (1982).
5. Thompson, J. A., Wu, W., Bertram, R. & Johnson, F. Auditory-dependent vocal recovery in adult male zebra finches is facilitated by lesion of a forebrain pathway that includes the basal ganglia. *J. Neurosci.* **27**, 12308–12320 (2007).
6. Poole, B., Markowitz, J. E. & Gardner, T. J. The song must go on: resilience of the songbird vocal motor pathway. *PLoS ONE* **7**, e38173 (2012).
7. Scharff, C., Kirn, J. R., Grossman, M., Macklis, J. D. & Nottebohm, F. Targeted neuronal death affects neuronal replacement and vocal behavior in adult songbirds. *Neuron* **25**, 481–492 (2000).
8. Hahnloser, R. H. R., Kozhevnikov, A. A. & Fee, M. S. An ultra-sparse code underlies the generation of neural sequences in a songbird. *Nature* **419**, 65–70 (2002).
9. Long, M. A., Jin, D. Z. & Fee, M. S. Support for a synaptic chain model of neuronal sequence generation. *Nature* **468**, 394–399 (2010).
10. Liberti, W. A. *et al.* Unstable neurons underlie a stable learned behavior. *Nat. Neurosci.* **19**, 1665–1671 (2016).
11. Markowitz, J. E. *et al.* Mesoscopic patterns of neural activity support songbird cortical sequences. *PLoS Biol.* **13**, e1002158 (2015).
12. Ren, D. *et al.* A prokaryotic voltage-gated sodium channel. *Science* **294**, 2372–2375 (2001).
13. Sim, S., Antolin, S., Lin, C.-W., Lin, Y. & Lois, C. Increased cell-intrinsic excitability induces synaptic changes in new neurons in the adult dentate gyrus that require Npas4. *J. Neurosci.* **33**, 7928–7940 (2013).
14. Lin, C.-W. *et al.* Genetically increased cell-intrinsic excitability enhances neuronal integration into adult brain circuits. *Neuron* **65**, 32–39 (2010).
15. Xue, M., Atallah, B. V. & Scanziani, M. Equalizing excitation-inhibition ratios across visual cortical neurons. *Nature* **511**, 596–600 (2014).
16. McInnes, L., Healy, J. & Melville, J. UMAP: Uniform Manifold Approximation and Projection for Dimension Reduction. *arXiv* (2018).
17. Goffinet, J., Brudner, S., Mooney, R. & Pearson, J. Low-dimensional learned feature spaces quantify individual and group differences in vocal repertoires. *eLife* **10**, (2021).
18. Sainburg, T., Thielk, M. & Gentner, T. Q. Finding, visualizing, and quantifying latent structure across diverse animal vocal repertoires. *PLoS Comput. Biol.* **16**, e1008228 (2020).
19. Turrigiano, G. G. & Nelson, S. B. Homeostatic plasticity in the developing nervous system. *Nat. Rev. Neurosci.* **5**, 97–107 (2004).
20. Sweeney, S. T., Broadie, K., Keane, J., Niemann, H. & O’Kane, C. J. Targeted expression of tetanus toxin light chain in *Drosophila* specifically eliminates synaptic transmission and causes behavioral defects. *Neuron* **14**, 341–351 (1995).

21. Tchernichovski, O., Nottebohm, F., Ho, C. E., Pesaran, B. & Mitra, P. P. A procedure for an automated measurement of song similarity. *Anim. Behav.* **59**, 1167–1176 (2000).
22. Tchernichovski, O., Mitra, P. P., Lints, T. & Nottebohm, F. Dynamics of the vocal imitation process: how a zebra finch learns its song. *Science* **291**, 2564–2569 (2001).
23. Jun, J. K. & Jin, D. Z. Development of neural circuitry for precise temporal sequences through spontaneous activity, axon remodeling, and synaptic plasticity. *PLoS ONE* **2**, e723 (2007).
24. Egger, R. *et al.* Local axonal conduction shapes the spatiotemporal properties of neural sequences. *Cell* **183**, 537–548.e12 (2020).
25. Fiete, I. R., Senn, W., Wang, C. Z. H. & Hahnloser, R. H. R. Spike-time-dependent plasticity and heterosynaptic competition organize networks to produce long scale-free sequences of neural activity. *Neuron* **65**, 563–576 (2010).
26. Veliz-Cuba, A., Shouval, H. Z., Josić, K. & Kilpatrick, Z. P. Networks that learn the precise timing of event sequences. *J. Comput. Neurosci.* **39**, 235–254 (2015).
27. Murray, J. M. & Escola, G. S. Learning multiple variable-speed sequences in striatum via cortical tutoring. *eLife* **6**, (2017).
28. Kim, J. & Tsien, R. W. Synapse-specific adaptations to inactivity in hippocampal circuits achieve homeostatic gain control while dampening network reverberation. *Neuron* **58**, 925–937 (2008).
29. Jarvis, E. D., Scharff, C., Grossman, M. R., Ramos, J. A. & Nottebohm, F. For whom the bird sings: context-dependent gene expression. *Neuron* **21**, 775–788 (1998).
30. Kozhevnikov, A. A. & Fee, M. S. Singing-related activity of identified HVC neurons in the zebra finch. *J. Neurophysiol.* **97**, 4271–4283 (2007).
31. Hirase, H., Leinekugel, X., Czurkó, A., Csicsvari, J. & Buzsáki, G. Firing rates of hippocampal neurons are preserved during subsequent sleep episodes and modified by novel awake experience. *Proc Natl Acad Sci USA* **98**, 9386–9390 (2001).
32. Slomowitz, E. *et al.* Interplay between population firing stability and single neuron dynamics in hippocampal networks. *eLife* **4**, (2015).
33. Trouche, S. *et al.* Recoding a cocaine-place memory engram to a neutral engram in the hippocampus. *Nat. Neurosci.* **19**, 564–567 (2016).
34. Hartman, K. N., Pal, S. K., Burrone, J. & Murthy, V. N. Activity-dependent regulation of inhibitory synaptic transmission in hippocampal neurons. *Nat. Neurosci.* **9**, 642–649 (2006).
35. Beattie, E. C. *et al.* Control of synaptic strength by glial TNF $\alpha$ . *Science* **295**, 2282–2285 (2002).
36. Schinder, A. F. & Poo, M. The neurotrophin hypothesis for synaptic plasticity. *Trends Neurosci.* **23**, 639–645 (2000).
37. Wang, Y. *et al.* Astrocyte-secreted IL-33 mediates homeostatic synaptic plasticity in the adult hippocampus. *Proc Natl Acad Sci USA* **118**, (2021).
38. Stellwagen, D. & Malenka, R. C. Synaptic scaling mediated by glial TNF- $\alpha$ . *Nature* **440**, 1054–1059 (2006).
39. Schoonover, C. E., Ohashi, S. N., Axel, R. & Fink, A. J. P. Representational drift in primary olfactory cortex. *Nature* **594**, 541–546 (2021).
40. Gonzalez, W. G., Zhang, H., Harutyunyan, A. & Lois, C. Persistence of neuronal representations through time and damage in the hippocampus. *Science* **365**, 821–825 (2019).
41. Driscoll, L. N., Pettit, N. L., Minderer, M., Chettih, S. N. & Harvey, C. D. Dynamic reorganization of neuronal activity patterns in parietal cortex. *Cell* **170**, 986–999.e16 (2017).
42. Marks, T. D. & Goard, M. J. Stimulus-dependent representational drift in primary visual cortex. *Nat. Commun.* **12**, 5169 (2021).
43. Ziv, Y. *et al.* Long-term dynamics of CA1 hippocampal place codes. *Nat. Neurosci.* **16**, 264–266 (2013).
44. Duffy, A., Abe, E., Perkel, D. J. & Fairhall, A. L. Variation in sequence dynamics improves maintenance of stereotyped behavior in an example from bird song. *Proc Natl Acad Sci USA* **116**, 9592–9597 (2019).

45. Rule, M. E. & O'Leary, T. Self-healing codes: How stable neural populations can track continually reconfiguring neural representations. *Proc Natl Acad Sci USA* **119**, (2022).
46. Lois, C., Hong, E. J., Pease, S., Brown, E. J. & Baltimore, D. Germline transmission and tissue-specific expression of transgenes delivered by lentiviral vectors. *Science* **295**, 868–872 (2002).
47. Kollmorgen, S., Hahnloser, R. H. R. & Mante, V. Nearest neighbours reveal fast and slow components of motor learning. *Nature* **577**, 526–530 (2020).
48. Meehan, C., Ebrahimian, J., Moore, W. & Meehan, S. Uniform Manifold Approximation and Projection (UMAP). *MATLAB Central File Exchange*  
<https://www.mathworks.com/matlabcentral/fileexchange/71902>.
49. Mooney, R. Different subthreshold mechanisms underlie song selectivity in identified HVC neurons of the zebra finch. *J. Neurosci.* **20**, 5420–5436 (2000).

## METHODS

### Animals

All procedures involving zebra finches are approved by the Institutional Animal Care and Use Committee of the California Institute of Technology. All birds used in the current study were bred in our own colony and housed with multiple conspecific cage mates of mixed sexes and ages until use for experiments. Before any experiments, adult male birds (>120 days post hatch (dph)) were single-housed in sound isolation cages with a 14/10 hr light/dark cycle for >5 days until they were habituated to the new environment and started singing. Thereafter, birds were kept in isolation until the end of the experiment.

### Viral vectors

Lentiviral vectors were cloned using standard procedures, and were produced and titrated as described in<sup>46</sup>. All LVs contained the internal Rous sarcoma virus (RSV) promoter driving expression of different transgenes. LV-TeNT encoded the light chain of tetanus toxin fused to EGFP with a PEST domain in its C-terminus. LV-NaChBac encoded the open reading frame of NaChBac fused to EGFP.

### Stereotaxic injection

Birds were anesthetized with isoflurane (0.5% for initial induction, 0.2% for maintenance) and head-fixed on a stereotaxic apparatus. To inject a retrograde tracer in area X or RA, craniotomies were made bilaterally and fluorescent tracers (cholera toxin b 555 0.2%, fluoro-ruby 10%, or red RetroBeads, 100-300 nL) were injected through a glass capillary (tip size ~25  $\mu$ m) into the corresponding nuclei (coordinates from dorsal sinus in mm - area X: Anteroposterior (AP) 3.3-4.2, Mediolateral (ML) 1.5-1.6, Deep (D): 3.5-3.8; RA: AP 1.5, ML 2.4, D 1.8-2.1). To deliver virus into HVC, a second surgery was performed 7-10 days after retrograde tracer injection, by then HVC was strongly labeled by fluorescence and visible through a fluorescent stereoscope. Because LVs only diffuse a short distance from the injection site (~100-200  $\mu$ m), they were injected into multiple locations (up to 16 sites per hemisphere, ~100 nL each) to deliver the transgenes into as many cells as possible throughout HVC. All injections in HVC were performed ~20 nL/min to minimize physical damage. At the end of every surgery, craniotomies were covered with Kwik-Sil and the skin incision was closed with Gluture.

### Song analysis

Song analysis was performed using Matlab (Mathworks).

### **Song feature parameterization**

Continuous audio recordings (44.1 kHz) were segmented into individual bouts manually and filtered to remove low frequency noise (cutoff frequency = 500 Hz). We used the open source Matlab software package, Sound Analysis Pro 2011<sup>21</sup> to generate spectrograms and derive non-linear, time-varying song parameterizations. The time-varying features were: pitch, goodness of pitch, Wiener entropy, frequency modulation (FM), amplitude modulation (AM), amplitude, aperiodicity, mean frequency, and the maximum power in each quadrant of the frequency range 0-11 kHz (labeled power 1, power 2, power 3 and power 4). These features were computed across the entire bout every 1 ms. These time-varying features were the base from which various portions of the song were further characterized.

### **Syllable parameterization**

A high-dimensional, acoustic parameterization of individual syllables was generated by then sampling a moving average (over 10 ms) of song features (pitch, goodness of pitch, mean frequency and entropy) at 10 points across the first 50 ms of each syllable. This resulted in a 40-dimensional song feature parameterization of each syllable. If a syllable was shorter than 50 ms, the feature vectors were padded at the end with zeros. This method allowed syllables to be compared in the same parametric acoustic space despite differences in duration.

### **Syllable segmentation**

We identified syllables and silences within each bout by imposing thresholds on the time-varying, total log-power of the spectrogram. To consistently assign inter-syllable breath sounds as silence and to address minor variations in background noise during recordings across days, thresholds were defined by sampling from the background noise within each bout. We first applied a song threshold below which the recording window was defined as silence. This threshold was chosen to be high so that it would capture time windows between syllables in which soft breath sounds occur. The mean ( $\mu$ ) and standard deviation ( $\sigma$ ) of the silent regions for that bout were computed from the middle portions of the silent windows. A new threshold was defined as:  $threshold = \mu + a * \sigma$  within that bout. The multiplier,  $a$ , was selected upon inspection of the stereotyped song structure for each bird and then applied across all recorded bouts across all days. We then performed a smoothing step wherein periods of silence less than 15 ms were converted to song segments. Song segments less than 20 ms were excluded from analysis. Segmentation was further checked by eye by random sampling across both stereotyped motifs and degraded songs. We then applied these parameters to the entire course of song recordings for each bird. A note on terminology: we refer to song segments to indicate continuous periods of singing. In the unperturbed song, these song segments are termed syllables. Because this is a continuous recovery process, these terms sometimes overlap in our usage.

### **Syllable feature distributions**

Syllable features (duration, log power, and entropy) were extracted from the syllable segmentation and parameterization processes. Distributions of syllable features were computed by normalizing each distribution of all syllable features within individual days such that the sum of each daily distribution over all binned durations equaled one. Distributions for individual days were then assembled into a matrix wherein the columns represented normalized distributions for individual days. This matrix was plotted as a heat map (Fig. 2a,b,c and Extended Data Fig. 5,e).

### **Acoustic distance trajectories**

To quantify fluctuations in song, we computed k-nearest neighbor statistics of the acoustic parameterization space of song<sup>47</sup>. We computed the average k-neighbor distances of individual syllables from original, stereotyped syllables in the undistorted song. This distance was calculated from the first 20 principal components of the 40-dimensional, acoustic space described in Syllable feature parameterization. We defined a normative set of syllables from 1-3 days of recording pre-viral injection when the bird was singing undisturbed, stereotyped songs. This syllable set was labeled according to syllable identity. Syllable identity was defined using the Matlab clustering algorithm, dbSCAN. The dbSCAN clustering was performed on a reduced 2-dimensional acoustic space generated using the dimensionality reduction algorithm, Uniform Manifold Approximation and Projection (UMAP)<sup>16,48</sup>. The syllable assignments were cross checked by visual examination of a randomly selected subset of bouts and found to be in strong alignment with hand-marked syllable assignments. Syllables that did not cluster into distinct groups were excluded from this analysis. Each individual syllable was then assigned a k-nearest neighbor distance ( $k = 25$ ) from the syllables in each normative syllable cluster, which we calculated as the average distance to the 25 closest syllables within the defined cluster.

As a measure of song degradation, we tracked the acoustic distance of the syllables which most closely resemble our original syllable set, defined within a local window of singing. We quantified the k-neighbor distance of the closest syllables to each original syllable cluster in a local window of consecutively sung syllables ( $N = 400$  syllables; the 2.5% quantile of local k-neighbor distances to each syllable cluster) (Figs. 2d,e; 3d and Extended Data Figs. 4; 5c,f). When the song is highly distorted, syllables do not cluster into clearly defined groups, nor do they resemble original syllable types. This method allows us to track syllable distances even when syllables are highly distorted. We normalized the acoustic distance trajectories such that the peak acoustic distance was 100% distortion in order to compare the time course of recovery across birds and syllables.

### **Speed of recovery**

We used the acoustic distance trajectories to measure the speed with which the song recovers. We measured the point of half recovery by tracking how much time and practice respectively are required post-perturbation to achieve a 50% recovery to the pre-perturbation baseline. 50% recovery is calculated relative to the point of maximum syllable distortion for each syllable individually. The acoustic trajectory of recovery is described in the above section. This measurement is shown for the speed of recovery as a function of practice in Fig. 3f,g.

### **Song variability**

As a measure of song variability, we tracked the local variability of syllables to other syllables that have been sung within a consecutive 400 syllable window (Fig. 2f). We quantified local variability as the average k-neighbor distance of each syllable to the closest 5 syllables within the local 400 syllable window. This measure of variability quantifies how different renditions are from one another, not how similar they are to the original song.

### **Continuous representation of bout trajectory**

We generated continuous visualizations of bouts across the entire perturbation trajectory as shown in Figs. 1d,f; 3c and Extended Data Fig. 5c,f<sup>17,18</sup>. We randomly sampled 100 bouts from each day of recording to build a representative sample of the song over the course of the experiment. For each bout, we slid a 150 ms window in 3 ms steps along the bout length. We then generated a high-dimensional, acoustic

parameterization of each 150 ms song window by taking the moving average in 20 ms segments every 5 ms of seven song features (mean frequency, pitch, goodness of pitch, power 4, power 2 and summed log power of the spectrogram). We performed principal component analysis on this high-dimensional set across all bouts to normalize and reduce the feature set to 30 dimensions and applied the UMAP algorithm to project this high-dimensional representation into two dimensions<sup>16,48</sup>.

### **Duration distributions of best syllables**

Song segment duration distributions were constructed from the 2.5% of closest song segments to the original syllable cluster on individual days of singing, measured using the k-neighbor distance metric described above. In this analysis we excluded song segments which were either less than 100 ms in duration, never recovered, significantly altered their acoustic form, or did not segment cleanly into discrete clusters.

### **Song prevention**

Adult zebra finches 120-150 dph ( $n = 3$ ) were fitted with custom made fabric vests and a 20-40-gram weight attached to their vest, pulling them towards the ground to prevent them from acquiring singing posture. All birds received LV-TeNT injection bilaterally into HVC. Before we prevented the birds from singing we allowed them to sing a few renditions to confirm that their songs were degraded. Afterward, the birds were restricted from singing for ~10 days, during which they were monitored with a video camera to make sure they did not sing, although they could make calls. We confirmed that all the birds were able to move, perch, drink and eat freely and even allowed them to sing several renditions occasionally (1-3 every 2-3 days, which allowed us to track the degradation/recovery of songs). The size of the bullet weight on the birds had to be adjusted since they got accustomed to the weight in 2-3 days and attempted to sing more frequently. The weights and vest were removed daily, 1 hour prior to the light-off period while the experimenter stood next to the chamber to closely monitor that the birds were not singing. The vest and weights were put on the birds again as soon as the lights were turned back on the next day. After the prevention period, the birds were free to sing in their respective isolation chambers.

### **Electrophysiology**

Birds were first overdosed by an intramuscular injection of ketamine/xylazine (120/12 mg/kg) and after they became unresponsive to toe pinching, they were decapitated. The forebrain was quickly removed and kept in ice-cold slicing solution (in mM: sucrose 213, KCl 2.5,  $\text{NaH}_2\text{PO}_4$  1.2,  $\text{NaHCO}_3$  25, Glucose 10,  $\text{MgSO}_4$  2,  $\text{CaCl}_2$  2, pH 7.4). Sagittal slices (300  $\mu\text{m}$ ) were cut using a vibratome (Leica VT1200S) and then incubated in HEPES holding solution (in mM: NaCl 102, KCl 2.5,  $\text{NaH}_2\text{PO}_4$  1.2,  $\text{NaHCO}_3$  30, HEPES 20, Glucose 25,  $\text{MgSO}_4$  2,  $\text{CaCl}_2$  2, pH 7.35) at 34.5 °C for 30 minutes. Afterwards, slices were kept at room temperature (~ 22 °C) between 30 minutes to 5 hours before being moved to the recording chamber. Bath ACSF (in mM: NaCl 124, KCl 2.5,  $\text{NaH}_2\text{PO}_4$  1.2,  $\text{NaHCO}_3$  26, Glucose 25,  $\text{MgSO}_4$  1,  $\text{CaCl}_2$  2, pH 7.35, 33-34°C) was continuously perfused (~2 mL/min) during recording. For current clamp whole-cell recordings, glass pipettes were filled with an intracellular solution (in mM): K-gluconate 135,  $\text{MgCl}_2$  3, HEPES 10, EGTA 0.2,  $\text{Na}_2\text{-ATP}$  2, phosphocreatine 14, pH 7.25. HVC(RA) cells were identified by the presence of the retrograde fluorescent tracers injected into RA. Dual whole-cell recordings of HVC(RA) and HVC(INT) neurons were made between cells that were less than 100  $\mu\text{m}$  apart. HVC(INT) neurons were identified by their relatively big soma, not having the retrograde fluorescent tracer, and spontaneous action potential firing<sup>49</sup>. We used voltage clamp to record miniature EPSCs with the following chemicals added to the bath (in  $\mu\text{M}$ ): TTX 0.5, nimodipine 5 and picrotoxin 50, and glass pipettes were filled with (in mM)  $\text{Cs}(\text{CH}_3)\text{SO}_3$  135,  $\text{MgCl}_2$  2, HEPES 10, EGTA 0.2, QX-314.Cl 5,  $\text{Na}_2\text{-}$

ATP 2, phosphocreatine 14, pH 7.25. To record mIPSCs, the following chemicals were added to the bath (in  $\mu\text{M}$ ): TTX 0.5, nimodipine 5, CNQX 10 and APV 25, and pipettes were filled with (in mM) CsCl 120, K-Gluconate 12,  $\text{MgCl}_2$  2, HEPES 10, EGTA 0.2, QX-314.Cl 5,  $\text{Na}_2\text{-ATP}$  2, phosphocreatine 14. For whole-cell NaChBac current recording, the bath solution did not contain any  $\text{CaCl}_2$  to eliminate Calcium currents, and TTX and 4-AP were added to block currents from the endogenous  $\text{Na}^+/\text{K}^+$  channels, and glass pipettes were filled with (in mM) CsCl 135,  $\text{MgCl}_2$  3, HEPES 10, EGTA 0.2, TEA-Cl 2,  $\text{Na}_2\text{-ATP}$  2, phosphocreatine 14. We only analyzed recordings in which access resistance was always smaller than 10 percent of the membrane resistance of the cell and no compensation was applied. Membrane potential was held at -70 mV to measure mEPSCs and -60 mV for mIPSCs. Liquid junction potential was not corrected. Electric signals were amplified and sampled at 20 kHz by an EPC-10 system (HEKA). Data analysis was performed off-line using Fitmaster (HEKA), Mini-Analysis (Synaptosoft) and Matlab (Mathworks). Data were presented as mean  $\pm$  s.e.m. Statistical difference was tested using one-way ANOVA followed by two-sided student's t-test.

### Histology

After the experiments were concluded, animals were sacrificed and their brains were processed for histological analysis. Animals were first deep anesthetized by intramuscular injection of ketamine/xylazine (100/10 mg/kg) and perfused intracardially with room temperature 3.2% PFA in 1xPBS. Brains were then extracted and incubated in the same fixative for 2-4 hours at room temperature. Each brain hemisphere was cut sagittally with a vibratome into 70-100  $\mu\text{m}$  thick sections. The brain slices containing HVC were collected and incubated overnight with a rabbit anti-GFP antibody (EMD Milipore, AB3080P) in 1xPBS containing 10% donkey serum and 0.2% Triton at 4 °C. Sections were washed in 1xPBS with 0.05% Triton and incubated for 2 hours at room temperature with a secondary antibody (Abcam, ab150077). Brain slices were washed and mounted in Fluoromount (Sigma). Confocal images were taken with a LSM800 microscope. To validate the cell-type specificity of our LVs, we performed counterstaining in a subset of the brain slices, using known markers of inhibitory neurons, specifically anti-parvalbumin (Abcam, ab11427), anti-calretinin (SWANT, 7697) and anti-calbindin (SWANT, CB-300) (Extended Data Fig. 1b). Out of 1000 counted neurons, only one GFP+ cell was double-labeled with inhibitory markers.

### Modeling

We used network modeling to explore the role of different plasticity mechanisms.

#### Leaky Integrate and Fire Neurons

The membrane potentials  $V_j$  of excitatory neurons in all networks were modeled using leaky adapting integrate-and-fire dynamics:

$$C_m \frac{dV_j}{dt} = g_l(E_l - V_j) + g_i(E_i - V_j) + g_e(E_e - V_j) - w_j + I_{ext}$$

where  $E_l$ ,  $I_{ext}$  is a white noise current input. When  $V_j$  reaches the threshold  $V_{th}$ , the neuron spikes, and the voltage is reset to  $V_{re}$  after a refractory period  $t_r$ . Inhibitory neurons have the same dynamics but without adaptation. The conductances,  $g_x$ , where  $x \in \{e, i\}$  are exponentially filtered sums of spike trains from upstream neurons  $\{k\}$ :

$$\tau_x \frac{dg_x^{(j)}}{dt} = -g_x^{(j)} + \sum_k w_{k,j} \sum_{t_s^{(k)}} \delta(t - t_s^{(k)})$$

### Network Architecture

We explored two different network architectures and the resulting dynamics. In the first network, we assumed all cells actively participate in the sequential dynamics. In the second network, we assumed that only a portion of the excitatory cells initially participate in the dynamics [1] [2]. To implement this, we assumed each neuron is silent with probability  $p_s = 0.4$

### HVC Network

We modeled HVC as a feedforward, polysynchronous network composed of 200 excitatory (E) and 50 inhibitory (I) neurons. To define connectivity between E cells, each neuron is assigned an index,  $c_i$  where

$$c_i = \sum_{j=1}^{j=i} x_j$$

and each  $x_j$  is a random variable uniformly distributed on  $[0, 1]$  and a binary activity status,  $a_i$ , where  $p(a_i=1) = 1 - p_s$ . Excitatory cells are connected with weights:

$$w_{i \rightarrow j} = \begin{cases} w_f \Theta(c^* - (c_j - c_i)) \Theta(c_j - c_i) & a_i a_j = 1 \\ w_s \sim \exp(\lambda = w_f r_i) b_{i \rightarrow j} & a_i a_j = 0 \end{cases}$$

where  $w_f, c^*$  are constants,  $r_i \sim U[0,1]$ , and  $b_{i \rightarrow j}$  is a binary random variable with  $p(b_{i \rightarrow j} = 1) = 0.075$ . To implement recurrent inhibition observed in HVC [3], inhibitory neurons receive connections from excitatory cells with probability  $p_{ei} = 0.1$  ( $w_{ei} = 1e-4$ ) and vice versa with probability  $p_{ie} = 1$  ( $w_{ie} = 0.2e-4$ ).

### Axonal Delays

Following observations that axonal delays between  $HVC_{(RA)}$  projectors are relatively long (1 - 7.5 ms) [4] and that  $HVC_{(RA)}$  projectors typically synapse onto inhibitory interneurons close to their soma and other excitatory cells far from their soma, we implemented axonal delays in our model that reflected longer E-E axonal delays and relatively shorter E-I and I-E delays. The delays  $d_{i,j}$  between E cells were:

$$\delta_{i \rightarrow j} = \begin{cases} \alpha_\delta (c_j - c_i) & a_i a_j = 1 \\ \delta_s \sim U[0, \alpha_\delta c^*] & a_i a_j = 0 \end{cases}$$

where

$$\alpha_\delta = \frac{3 \text{ ms}}{\langle c \rangle}$$

so that E-E axonal delays were 3 ms on average (initializing axonal delays in this way produced a roughly uniform distribution). E→I and I→E delays were uniformly set to 0.5 ms. We found a comparatively

fast inhibitory pathway stabilized sequence dynamics by rapidly suppressing large increases in excitation and diminishing in response to decreases in excitation in analogy to an overdamped harmonic oscillator.

### Plasticity Rules

Once constructed, we allowed networks to evolve under both firing rate homeostasis and spiking timing-dependent plasticity. All synapses subject to plasticity were assumed to have lower bound  $w_{\min}$ . After each trial, synaptic strength  $w_{i \rightarrow j}$  evolved according to

$$\Delta w_{i \rightarrow j} = \beta_1 \Delta_{i \rightarrow j}^f + \beta_2 \Delta_{i \rightarrow j}^p + \beta_3 \Delta_{i \rightarrow j}^{STDP}$$

where the deltas refer to updates due to single-cell firing rate homeostasis, local activity homeostasis, and STDP, respectively, and the betas are constants. All E-E synaptic strengths had upper bound  $w_{\text{ec}}^{\max}$ .

### Firing rate homeostasis:

Single-cell firing rate homeostasis moves a neuron's firing rate toward a set point  $f_0^{(j)}$  according to:

$$\Delta_{i,j}^f = \text{Sgn} \left( f_0^{(j)} - f^{(j)} \right) \left| f_0^{(j)} - f^{(j)} \right|^{n_f} \quad (1)$$

where  $f^{(j)}$  is the average firing rate of neuron  $j$  in that trial (refer to Figure 4) and  $n_f$  regulates the strength of the homeostasis.

### Local population activity homeostasis:

Taking inspiration from literature that has shown homeostasis may operate on a network scale, we include in our final model a form of homeostasis that permits individual neurons to monitor and respond to the activity of their neighbors. We implement here one potential mechanism by which such local population activity homeostasis might be achieved based loosely on the TNF $\alpha$  pathway. We assume each E neuron emits a diffuse release in space, the concentration of which is proportional to the neuron's own activity level. All E neurons are assumed to monitor the local concentration of diffuse release and adjust their incoming excitatory synapses in order to maintain a setpoint concentration. To implement a form of local population homeostasis, each excitatory neuron was first assigned a location by uniformly sampling the space within a unit sphere. The local concentration of the diffuse release that an excitatory neuron senses is then

$$m^{(i)} = \frac{1}{\sqrt{2\pi v}} \sum_j \left[ f^{(j)} \exp -\frac{1}{2} \frac{(x_i - x_j)^2}{v} \right]$$

where  $x_j$  is the location of neuron  $j$ , and  $v$  is a parameter controlling the extent of each neuron's diffuse release. The corresponding update to local population homeostasis is

$$\Delta_{i,j}^{pop} = w_{i,j} \frac{e^{\gamma (m_0^{(i)} - m^{(i)})} - 1}{e^{\gamma (m_0^{(i)} - m^{(i)})} + 1},$$

where  $m_0^{(i)}$  is the local concentration setpoint of neuron  $i$ . Local concentration setpoints were chosen by computing the average local concentration over 50 activations of the network prior to the perturbation.

In the version of our model that included local population homeostasis and inactive neurons, we modified single-cell firing rate homeostasis in E neurons to act only to decrease input if firing exceeded a neuron's setpoint under the assumption that connectivity (and not homeostatic properties) should dictate whether a neuron was active or inactive. The modified rule is given by

$$\Delta_{i,j}^f = -\Theta \left( f^{(j)} - f_0^{(j)} \right) \left( f^{(j)} - f_0^{(j)} \right)^{n_f} \quad (2)$$

### Hebbian plasticity:

We employed a triplet STDP rule that acted on E→E and E→I synapses. We found that a triplet rule acting on synapses between excitatory neurons could maintain the relative firing times of E neurons in a sequence whereas classic pairwise STDP and burst timing dependent plasticity (BTDP) could not [5]. The update for the triplet rule for excitatory neurons was

$$\Delta_{i,j}^{STDP} = \sum_{\{t_k^{(i)}\}} \left( \sum_{\{t_l^{(j)}, t_m^{(j)}\}} A_+ (w_{ei}^{max} - w_{i,j}) K_+^{(1)}(t_m^{(j)} - t_l^{(i)}) K_+^{(2)}(t_l^{(j)} - t_k^{(j)}) + \sum_{\{t_n^{(j)}\}} A_- w_{i,j} K_-(t_n^{(j)} - t_k^{(i)}) \right)$$

where

$$K_+^{(1)}(\Delta t) = \exp \left[ \frac{-|\Delta t|}{\tau_+^{(1)}} \right] \Theta(\Delta t)$$

$$K_+^{(2)}(\Delta t) = \exp \left[ \frac{-|\Delta t|}{\tau_+^{(2)}} \right] \Theta(\Delta t)$$

$$K_-(\Delta t) = \exp \left[ \frac{-|\Delta t|}{\tau_-} \right] \Theta(-\Delta t)$$

and  $\{t_k^{(i)}\}$  are the spike times of neuron  $i$ ,  $\{t_l^{(j)}, t_m^{(j)}\}$  are spike time pairs of neuron  $j$  that satisfy

$$t_l^{(j)} = \sup \{ t \in \{t^{(j)}\} \mid t < t_k^{(i)} \}$$

$$t_m^{(j)} = \inf \{ t \in \{t^{(j)}\} \mid t > t_k^{(i)} \}$$

and  $\{t_n^{(j)}\}$  are the spike times of neuron  $j$ . The constants regulating the relative strength of potentiation and depression,  $A_+$  and  $A_-$ , and the timescales of STDP,  $\tau_-$ ,  $\tau_+^{(1)}$ , and  $\tau_+^{(2)}$ , were chosen to match the minimal, nearest spike triplet rule of Pfister and Gerstner [6]. To stabilize E→I STDP, each inhibitory neuron was assigned a total excitatory synaptic input bound, determined by the neuron's total excitatory synaptic input at the beginning of the simulation. When the bound was exceeded, E-I weight  $w_{i,j}$  was rescaled as

$$w_{i,j} \rightarrow \frac{\sum_k w_{k,j}^{(0)}}{\sum_k w_{k,j}} w_{i,j}$$

where  $w_{k,j}^{(0)}$  represents the size of the synapse prior to the first activation of the network. No plasticity takes place on I-E connections.

### Activation of Networks

At the beginning of each trial, networks were allowed to settle for 10 ms, after which each cell in the first layer of the network was driven by an independent burst (4 spikes, 660 Hz), with onset times drawn from a Gaussian (mean 10 ms, STD 1 ms). Input weights were chosen to produce reasonable spiking behavior in the first layers of the network. Networks were simulated for an additional 90 ms following the stimulus. The time step for all simulations was 0.1 ms.

### Network Initialization Procedure

To initialize networks, an activation of each network was first simulated once without plasticity. Neurons that fired during this trial were assumed to be active. Active neurons were assigned a uniform firing rate setpoint ( $f^{(0)} = 4$ ) and were subject to cell-autonomous firing rate homeostasis as given in (1) and STDP for 500 additional activations of the network. For networks with population homeostasis,  $m^{(0)}$ , the local secreted factor concentrations, were computed for activations 500-550, and then averaged to set  $m_0^{(0)}$ ; from this point, population homeostasis was permitted to act on the network if applicable, and the cell-autonomous firing rate homeostasis rule was changed to (2).

### Simulated Tetanus Toxin Perturbation of Neurons

Tetanus toxin perturbation of the network was simulated by randomly selecting a cell with probability  $p_T$  for perturbation and removing all its outgoing connections. Perturbed cells were assumed not to contribute to the population activity level. Networks were then allowed to evolve for 4000 renditions according to the plasticity rules described above. Following the observation that animals typically recovered their songs and sang consistently after ~2 weeks, we restricted our analyses of synaptic structure and network activity to networks that recovered sequential dynamics.

*A p p e n d i x D*

## PRECISION MOTOR TIMING VIA SCALAR INPUT FLUCTUATIONS

*This is a pre-print encompassing modeling work that was based on behavioral data and observations from my experiments performed in Chapter 2 and 3.*

Pang, R., Duffy, A., Bell, D., Torok, Z., Fairhall A. *Precision motor timing via scalar input fluctuations.* bioRxiv. DOI: <https://doi.org/10.1101/2022.05.18.492498>.

# Precision motor timing via scalar input fluctuations

Rich Pang<sup>1,2,\*</sup>, Alison Duffy<sup>3,4</sup>, David Bell<sup>3,4</sup>, Zsafia Torok<sup>5</sup>, and Adrienne Fairhall<sup>3,4</sup>

<sup>1</sup>Princeton Neuroscience Institute, Princeton University, Princeton, NJ, USA

<sup>2</sup>Center for the Physics of Biological Function, Princeton University, Princeton, NJ, USA and the Graduate Center at the City University of New York, New York, NY, USA

<sup>3</sup>Computational Neuroscience Center, University of Washington, Seattle, WA, USA

<sup>4</sup>Department of Physiology and Biophysics, University of Washington, Seattle, WA, USA

<sup>5</sup>Division of Biology and Biological Engineering, California Institute of Technology, Pasadena, CA, USA

\*corresponding author

**Complex motor skills like playing piano require precise timing over long periods, without errors accumulating between subprocesses like the left and right hand movements. While biological models can produce motor-like sequences, how the brain quenches timing errors is not well understood. Motivated by songbirds, where the left and right brain nuclei governing song sequences do not connect but may receive low-dimensional thalamic input, we present a model where timing errors in an autonomous sequence generator are continually corrected by one-dimensional input fluctuations. We show in a spiking neural network model how such input can rapidly correct temporal offsets in a propagating spike pulse, recapitulating the precise timing seen in songbird brains. In a reduced, more general model, we show that such timing correction emerges when the spatial profile of the input over the sequence sufficiently reflects its temporal fluctuations, yielding *time-locking attractors* that slow advanced sequences and hasten lagging ones, up to the input timescale. Unlike models without fluctuating input, our model predicts anti-correlated durations of adjacent segments of the output sequence, which we verify in recorded zebra finch songs. This work provides a bioplausible picture of how temporal precision could arise in extended motor sequences and generally how low-dimensional input could continuously coordinate time-varying output signals.**

Complex motor sequences like playing the piano often require precision timing over extended periods. If small timing errors accumulated over long sequences, this could lead to substantial variability in sequence duration or desynchronize different subprocesses like a sequence's left and right motor components, if their errors accumulated independently. While robust sequence generation by biological neural network models has been studied extensively (1–9), how the nervous system could prevent the accumulation of timing errors remains largely unexplored.

Brain regions associated with sequence generation do not operate in isolation but receive input from other areas. Mammalian motor cortex receives ongoing input from thalamus during movement, which if inhibited disrupts cortical patterning and limb kinematics (10). Feed-forward thalamic inputs are also implicated in preserving temporal information in sensory pathways (11). Although external inputs to a sequence-generating network may play multiple roles, such as initiating cortical state or movement (12–15), or gating signal transmission (16), one role relevant to timing control is modulating the speed at which the sequence-generating network's dynamics unfold (17). It was shown that the level of external input to a recurrent neural network could adjust the interval from task start to output by smoothly scaling the indi-

vidual response time-courses of its internal units (17). If fluctuating external input slowed or accelerated a network's dynamics opposite their internal noisy temporal variations this might compensate for ongoing timing errors.

One of the most well-studied precision motor sequences is birdsong. Adult zebra finch song, a highly stereotyped vocalization sequence, lasts up to 2 seconds but varies only about 1.5% in total duration across renditions (18); other birds like canaries can sing for tens of seconds (19). Accompanying zebra finch song is a sparse, extremely precise spike sequence in premotor area HVC (proper name); many neurons burst during every song within a few-millisecond window surrounding a single song timepoint (20). While HVC is thought to be the central sequence generator underlying song timing (6), it requires input from the thalamic Uvaeform nucleus (Uva), which if lesioned abolishes or substantially distorts song (21). Uva activity is dynamic during song but highly correlated across the nucleus (21), suggesting it does not bequeath to HVC the complete sequential information guiding song but acts instead a global modulation signal, although its precise role is unknown. As songbirds have no corpus callosum, left and right HVC do not directly communicate (22); Uva inputs could in principle help them remain coordinated throughout song by dynamically controlling how fast each HVC's spike sequence unfolds.

Here we introduce a model in which timing in an autonomous sequence generator is corrected purely via a one-dimensional external input, inspired by Uva, that dynamically modulates the sequence's propagation speed. In an HVC-like model network, we show how this input corrects timing errors in a propagating spike pulse even without access to the errors. Formulating the problem more generally we show this error correction occurs when the 1-D input is spread nonuniformly over the sequence so as to reflect the input's time-derivative spatially, which yields "time-locking attractors" (fixed-point attractors (23) in a constant-velocity moving reference frame) that slow advanced sequences and hasten lagging ones. A key prediction of this model is an anti-correlation between durations of adjacent output segments, which we confirm in recorded zebra finch songs.

**Significance.** Complex motor skills like playing piano require precision timing over long periods, often among multiple components like left and right muscle groups. Although brain-like network models can produce motor-like outputs, timing regulation is not well understood. We introduce a model, inspired by songbird brains, where imprecise timing

in a cortical-like system is corrected by a single thalamic input regulating the sequential propagation, or tempo, of cortical activity. This model illuminates a relation between the input's spatial structure and temporal variation that lets lagging activity hasten and advanced activity slow, which makes a prediction about output timing that we verify in real bird-song. This work reveals a simple, neuroplausible mechanism that may play a role in precision cortical or motor timing.

## Results

**Timing correction in a biological network model.** To illustrate our proposed timing control mechanism we modeled a chain-organized neural network supporting the stable propagation of a spike pulse, in line with previous HVC models (5, 6, 24), but additionally modulated by an external 1-D input (Fig 1A). The chain comprised small recurrent clusters of adaptive spiking neurons connected via feed-forward excitatory synapses, with additional connections from the external input covering the whole chain, although nonuniformly. When the first cluster, or "link", is stimulated, a brief spike pulse emerges that travels down the chain, which we take as our output sequence. Given that we will only consider sequences of a fixed order, the network state can be characterized during pulse propagation by  $x(t)$ , the index (or "position") of the sequence element active at time  $t$  (i.e. the chain link whose neurons are spiking at  $t$ ) (Fig 1A-C). A spike pulse propagating at a constant speed, for example, would be described by  $x(t) = vt$ .

The propagation speed of the spike pulse when passing over a given link in the chain is determined by (1) the "intrinsic" chain speed (governed by the feed-forward connection strengths to and from that link), (2) the input weight at that link, and (3) the (scalar) activation level of the input when the pulse is passing over that link. Strong feed-forward weights and active excitatory input hasten propagation; weak feed-forward weights and active inhibitory input slow propagation. Active excitatory input can also cancel the speed decrease from weak feed-forward weights, and active inhibitory input can cancel the speed increase from strong feed-forward weights. Here we assume a binary external input level (on or off) oscillating at 10 Hz, in line with observed Uva rhythms (21), although neither the specific frequency nor periodicity are essential to our mechanism. Because the input is 1-D, at any given time external inputs to the chain are all active or all silent, reflecting the putative low-dimensional nature of Uva (21). We let the spatial input profile alternate between excitation and inhibition and the intrinsic speed profile between weak, medium, and strong feed-forward weights (Fig 1A). For simplicity we modeled our Uva-inspired input as directly exciting or inhibiting different parts of the chain, but real Uva-HVC projections could be purely excitatory, although this is not yet known. It may thus be more realistic that any effective Uva-HVC inhibitory modulation is mediated through Uva projections to inhibitory interneurons in HVC, which in turn project to HVC excitatory neurons (25).

Given this network configuration we sought conditions under which large offsets in spike pulse initiation times were

corrected by fluctuating input. An example solution is shown in Fig 1B. Given a 100 ms temporal modulation period and appropriate spatial variation (discussed shortly) in both the feed-forward weights in the chain and the input weight profile, spike pulses initialized either 40 ms before or after a "correct" start time cleanly hastened or slowed, respectively, after just a few hundred ms to approximately match the timing of the correct pulse. In an unmodulated chain network with spatially constant feed-forward weights supporting the same average propagation speed as the modulated chain, timing correction did not occur – spike pulses initiated 40 ms before or after a correct pulse remained about 40 ms behind or ahead (Fig 1C). Varying spike pulse initiation time across several hundred milliseconds confirmed that the temporal basin of error correction matched the 100 ms period of the external input (Fig 1D), while spike pulse timing in the unmodulated chain remained uncorrected regardless of start time (Fig 1E). One-dimensional but appropriately shaped external input can thus cause the network dynamics to follow the temporal structure of the input signal, while their sequential ordering is determined by the network's internal connectivity (the ordered chain links, here).

**Sequence evolution through a spatiotemporal speed landscape.** To understand theoretically how timing correction, intrinsic speed, and external input interact we analyzed a simplified, more general model of sequence propagation. For an evolving sequence whose instantaneous position is given by  $x(t)$  (the position of the propagating spike pulse in our network model), let its speed be given by:

$$v(x,t) \equiv \frac{dx}{dt}(x,t) = v_0(x) + u(t)w(x). \quad (1)$$

where  $v_0(x)$ ,  $u(t)$ , and  $w(x)$  are the intrinsic propagation speed profile, time-varying scalar input level, and spatial input weight profile. When  $u(t) = 0$  (input is off) propagation speed depends only on  $x$  and equals the intrinsic speed  $v_0(x)$ . When  $u(t) = 1$  (input on) the propagation speed evaluated at  $x$  is the sum of the intrinsic speed  $v_0$  and input weight  $w$  at  $x$ . Under what conditions does such a system cause sequences with perturbed start times to converge to the same timecourse?

To gain intuition we first examine how to stabilize the constant-speed sequence  $x(t) = t$  via the spatiotemporal "speed landscape" given in (1). Arbitrary sequences  $\mathbf{z} = \mathbf{f}(t)$  can be constructed by finding a map  $\mathbf{z} = \mathbf{g}(x)$  that transforms the  $x$  coordinate into an arbitrary value or vector (akin to activating sets of motor neurons (26)), so that the stability of  $\mathbf{z}(t)$  follows the stability of  $x(t)$ . As the input timecourse and spatial profiles of the intrinsic speed and input weights and are all 1-D, the speed landscape will have a rank-2 structure, the key bio-inspired constraint on the problem we seek to solve.

Fig 2 shows a temporal square-wave input  $u(t)$  oscillating between 0 and 1 and example  $v_0(x)$  and  $w(x)$  that stabilize  $x(t) = t$ . The contributions of each term to the full speed landscape  $v(x,t)$  can be understood geometrically (Fig 2A-C). As the intrinsic speed  $v_0(x)$  has no temporal dependence it admits variation only along the vertical  $x$  direction (Fig

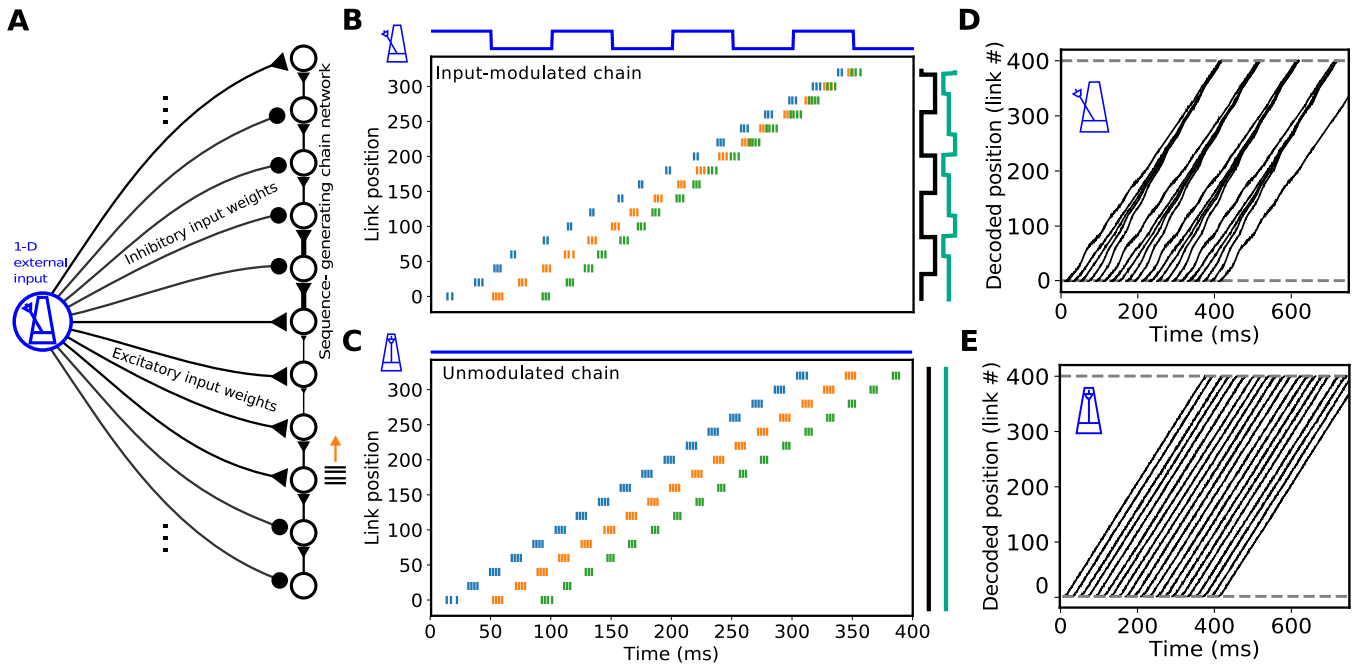


**Fig. 1. Timing correction via 1-D input in a simple spiking network model.** A. Network architecture: A chain-organized network supporting the propagation of a spike pulse (right) is modulated by a 1-D input signal (blue) via either excitatory (triangles) or inhibitory (circles) weights that fall on distinct zones of the chain. When the input is on spike pulses propagate more quickly through excited zones and more slowly through inhibited zones. Momentary propagation speed is determined by the absence/presence and sign of the input and by the intrinsic chain speed governed by the feed-forward weights. B. Evolution of spike pulses in three separate trials, initiated at different start times in the input-modulated network. Only spikes from an evenly spaced subset of neurons are shown, labeled by the neurons' chain link. Blue line shows input timecourse, black contour shows spatial modulation profile (left-inhibition, right-excitation), cyan contour shows three levels of intrinsic speed variation as a function of link position (slow, medium, fast from left to right). C. Propagation of three spike pulses in an unmodulated chain network with constant intrinsic speed. D. Evolution of spike pulse position (decoded from link positions of neurons spiking in a 2 ms window surrounding time point  $t$ ) for a range of start times in the modulated network. E. As in D, but for the unmodulated network.

2A), with certain horizontal bands corresponding to an intrinsic speed greater than 1 (purple) and others to an intrinsic speed less than 1 (orange) (Fig 2A). The input-modulation term  $u(t)w(x)$  admits both spatial and temporal variation, yielding a rank-1 contribution to the speed landscape (Fig 2B); certain regions correspond a positive modulation that increases propagation speed (purple) and others to a negative modulation that decreases propagation speed (orange). Summing the contributions of the intrinsic speed  $v_0(x)$  (Fig 2A) and input modulation  $u(t)w(x)$  (Fig 2B) yields the full speed landscape  $v(x,t)$  under the fluctuating input (Fig 2C). In this example,  $v(x,t) = 1$  can arise in regions with unity intrinsic speed and no modulation, regions with increased intrinsic speed but negative input modulation, or regions with decreased intrinsic speed but positive input modulation. Regions corresponding to  $v(x,t) < 1$ , which slow sequences down, or  $v(x,t) > 1$ , speeding sequences up, can each arise from either the intrinsic speed term  $v_0(x)$  or the input modulation  $u(t)w(x)$ . The temporal evolution of the output sequence is given by how  $x(t)$  moves through this landscape.

Sequences that begin at different times or positions take different paths through the speed landscape. In our example in Fig 2 the sequence  $x(t) = t$  travels at constant speed, as desired, whereas sequences instantiated at slightly advanced or delayed positions pass through more slow or fast zones, respectively (Fig 2D). After a short time perturbed sequences will approach the sequence  $x(t) = t$  if the perturbation lies within a small enough window. This attractive effect in our

example is robust to small changes in the speed landscape (Fig 2E), which only changes the basin of attraction. Thus the external input corrects, or stabilizes, the timing of perturbed sequences.

To identify formal conditions enabling timing correction we define a *time-locking attractor*  $x(t) = t$  as a stable fixed point in a constant-velocity moving reference frame. Letting the position coordinate in the moving frame be  $y(t) \equiv x - t$ , the function  $dy/dt = f_y(y)$  describes the attraction or repulsion of the system toward the target sequence  $x(t) = t$ . Since  $v(x,t)$  is rank-2,  $dy/dt$  must also change over time because the local speed landscape surrounding  $y = 0$  changes throughout the sequence (Fig 2H-J). In our example the time average  $\langle dy/dt \rangle = \langle f_y(y) \rangle$  has a downward zero-crossing at  $y = 0$ ; thus, points  $y < 0$  will hasten and points  $y > 0$  will slow, on average, stabilizing  $x(t) = t$  and yielding the desired timing correction (Fig 2K). Crucially, for such a fixed point to exist, neither the input timecourse  $u(t)$  nor weight profile  $w(x)$  can be constant. When either is constant, all sequences spend the same total time in either slow or fast zones and thus have the same average speed and do not converge (Fig 2F, G);  $\langle dy/dt \rangle$  lacks a downward-crossing zero at  $y = 0$  so no correction occurs (Fig 2K). Thus, a scalar-valued external input can correct timing errors only if it fluctuates in both time and space. As shown in Fig 2-Supp-fig-1 and Fig 2-Supp-fig-2, time-locking attractors can also emerge under constant intrinsic speed and either purely excitatory or purely inhibitory modulation (reflecting the possible case that Uva

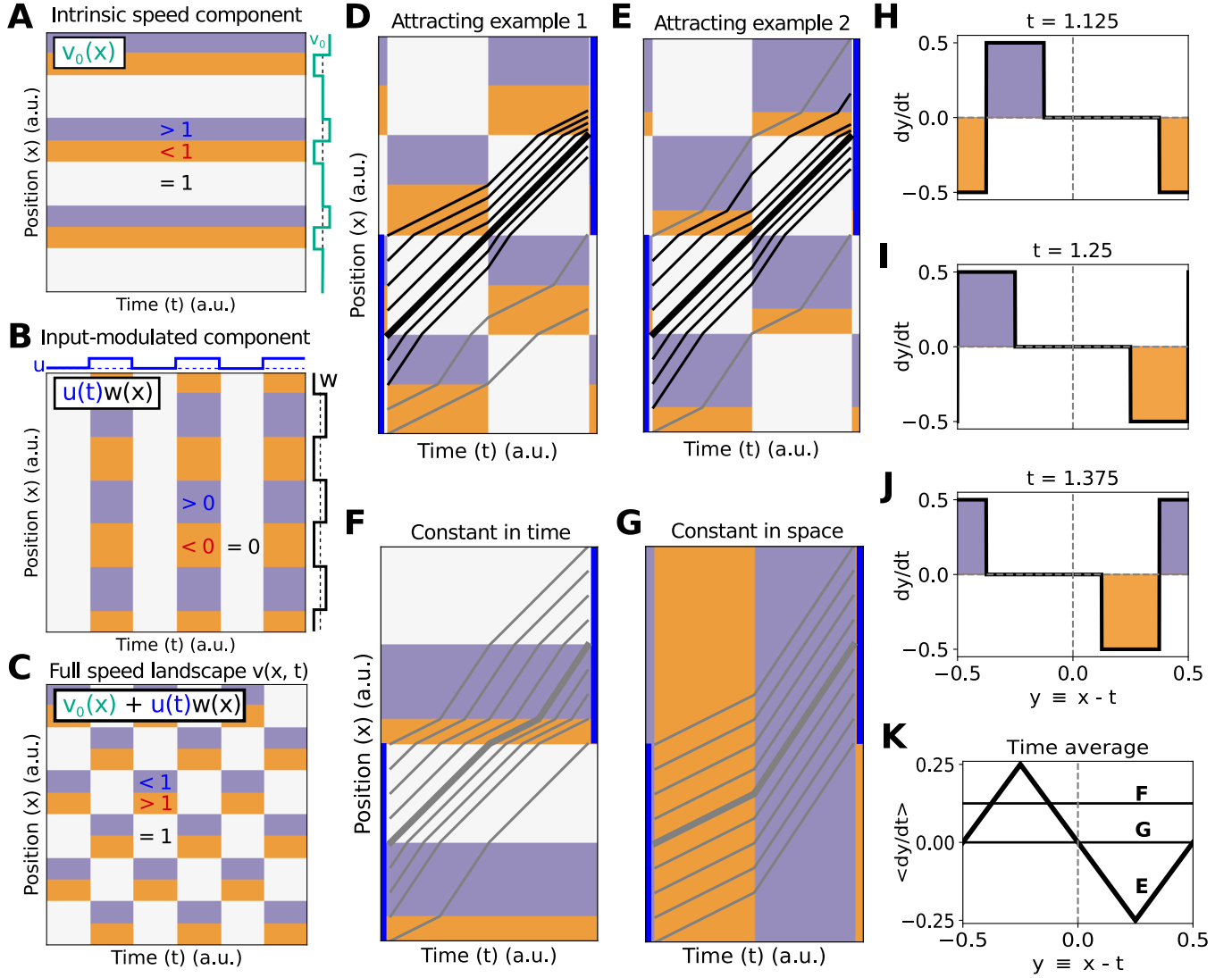


**Fig. 2. Time-locking attractors in example speed landscapes.** A. Contribution of the position-dependent intrinsic speed profile to the speed landscape. Orange and purple indicate zones of slowed and hastened speeds, respectively. B. Contribution of spatiotemporal input modulation profile to the speed landscape. C. Full speed landscape with intrinsic speed and input modulation. Purple (fast) zones in input modulation profile cancel orange (slow) zones in intrinsic speed profile and vice versa, yielding a rank-2 checkerboard-like pattern. D. Multiple example sequences with different starting positions moving through speed landscape in C for one temporal period. Blue bars provide reference positional ranges offset by one spatial period. Black trajectories are within the basin of attraction. E. As in D but for a slightly different speed landscape. F. As in E but without temporal modulation. G. As in D/E/F but for a speed landscape without spatial modulation. H-J. Time-derivative of sequence position in a moving reference frame  $y \equiv x - t$  at different time points corresponding to E. K. Time-average of  $dy/dt$  over one temporal period for examples in E, F, and G.

provides a single sign of modulation onto HVC), so long as this modulation still fluctuates appropriately in both time and space. The resulting stable trajectories are more complex, however, since their propagation speed is not constant.

**Conditions for time-locking attractors.** For a time-locking attractor to emerge generally, we found that it suffices for the relationship among the input timecourse and spatial profiles of the input weights and intrinsic speed to satisfy two conditions. First, the propagation speed  $v(x, t)$  should equal 1 when  $x(t) = t$ : using (1) we require

$$v_0(x) + u(t)w(x) \Big|_{t=x} = 1 \quad \forall x. \quad (2)$$

This condition creates a fixed point  $\langle dy/dt \rangle = 0$  corresponding to  $x(t) = t$ . Taking the spatial derivative of (2) yields

$$\frac{dv_0}{dx} + u(t) \frac{dw}{dx} \Big|_{t=x} = - \frac{du}{dt} w(x) \Big|_{t=x} \quad (3)$$

For  $x(t) = t$  to be stable, we require from (1) that

$$\frac{dv}{dx} \Big|_{t=x} = \frac{dv_0}{dx} + u(t) \frac{dw}{dx} \Big|_{t=x} < 0 \quad (4)$$

so that lagging trajectories  $x(t) = t - \delta$  experience an increased propagation speed, whereas advanced trajectories  $x(t) = t + \delta$  experience a decrease. Substituting (3) into (4) yields the sufficient condition

$$\frac{du}{dt} w(x) \Big|_{t=x} > 0 \quad (5)$$

which requires  $w(x)$  to have the same sign as  $u(t)$  evaluated at  $t = x$ . Thus, when  $u(t)$  is increasing,  $w(x)|_{x=t}$  should be positive, and when  $u(t)$  is decreasing  $w(x)|_{x=t}$  should be negative. A simple (although not unique) solution is to let  $w(x)$  be proportional to the time-derivative of  $u(t)$  evaluated at  $t = x$ , and to then solve (2) to find  $v_0(x)$  so that the stable trajectory has a uniform speed.

Time-locking attractors thus emerge when the input weight profile  $w(x)$  "reflects" spatially (has the same sign as) the input's time derivative. As an input  $u(t)$  is not likely to continually increase for an arbitrarily long period in a real system, but will instead fluctuate in time, its spatial profile  $w(x)$  must accordingly fluctuate in space, although (5) implies that as long as the signs of  $du/dt$  and  $w$  match, their relationship need not be fine-tuned.

This rule allows us to construct input timecourses and weight profiles that propagate stable sequences. As an example, for  $u(t) = \cos(t) + 1$  we can use (5) to choose  $w(x) = -\sin(x)$  and (2) to choose  $v_0(x) = 1 + (\cos(x) + 1)\sin(x)$ . Sequences initiated across several start times and positions reveal that these  $u(t)$ ,  $w(x)$ , and  $v_0(x)$  indeed yield a time-locking attractor  $x(t) = t$  (Fig 3A). Periodicity is not required, however. Choosing  $w(x)$  and  $v_0(x)$  via the above rule when  $u(t)$  was a sample from a smoothed noise process also yielded the attractor  $x(t) = t$  (Fig 3B). Plotting  $dy/dt$  in the moving reference frame with  $y = x - t$  reveals that although the momentary phase portrait in each example is highly variable, its time average  $\langle dy/dt \rangle$  yields a 1-D flow with a fixed point at  $y = 0$  (Fig 3C-F), thereby stabilizing  $x(t) = t$ . Thus, given an arbitrary fluctuating 1-D input, there exist accompanying spatial profiles of the input weights and intrinsic speed that stabilize the evolution of the sequence  $x(t) = t$ , with the local temporal basin of attraction depending on the timescale of the input fluctuations.

**Correlated fluctuations in motor output timing.** Due to the timing correction our model imposes, in the face of noise we expect durations of adjacent segments of the output sequence near the timescale of the external input to be anti-correlated. Segments shortened by noise will tend to be followed by segments slowed by the input's correction effect, and vice versa for segments dilated by noise. We verified this by generating noisy sequences over the range  $x \in [0, 1]$  atop an input-driven speed landscape according to

$$v(x, t) \equiv \frac{dx}{dt}(x, t) = v_0(x) + u(t)w(x) + \eta(t) \quad (6)$$

where  $\eta(t)$  is an Ornstein-Uhlenbeck process (exponentially filtered Gaussian white noise) with timescale  $\tau_\eta = 1/30$ . Fig 4A shows example output sequences modulated by a periodic speed landscape. Whereas unmodulated sequences ( $v(x, t) = 1 + \eta(t)$ ) diffuse freely, modulation by the input-dependent speed landscape constrains the spread (Fig 4A,B).

To investigate temporal structure in the output sequences we split the output into even segments and examined the durations over which they unfolded. Durations of sufficiently short adjacent segments (noiseless duration  $\ll \tau_\eta$ ) were positively correlated, regardless of modulation by the speed land-

scape, as they were likely to receive similar noise. In the input-modulated sequences, however, sufficiently long segments became anti-correlated, a sign of timing correction that was not present without the modulation (Fig 4C-E).

We tested our model's prediction that durations of certain segments of motor output sequences should be anti-correlated by analyzing real zebra finch songs. Songs were produced by adult males in isolation ("undirected" song), with the recorded audio converted to spectrograms using a short-time Fourier transform (Fig 4F). Due to the imprecision in determining exactly when an arbitrary moment  $x$  in a song occurred (and spurious anti-correlations introduced by jitter in such a labeling process), instead of splitting the song into even segments we examined segments bounded by peaks and valleys in the power of the spectrogram, retaining only segment boundaries that could be reliably identified in every song (Fig 4F-G). Indeed, durations of adjacent segments of zebra finch song were anti-correlated (Fig 4H-I), as predicted by and dependent on the input-modulation in our model, a finding that held up across multiple birds (Fig 4-Supp-fig-1, A-H). This suggests the neural song circuit in songbirds may recruit a similar mechanism for timing control as the input-dependent time-locking attractors we have investigated.

## Discussion

We introduced a model of precision motor timing via scalar input fluctuations and validated a key prediction in recorded zebra finch songs. When a scalar input locally and dynamically controls how fast a sequence unfolds and the input's spatial structure reflects its time derivative, time-locking attractors emerge that continually correct timing errors without requiring knowledge of the errors. Although timing errors could accumulate in the input itself, they do not additionally accumulate in the downstream sequence generator. This allows multiple motor processes receiving the same input fluctuations to stay coordinated for long periods, reflecting how left and right HVC may receive similar input from left and right Uva. Our work builds on previous observations of spatiotemporal inhomogeneities in songbird HVC (27), providing new insight into how spatial and temporal signals may be linked to temporally coordinate ongoing neural activity.

While neural spike time coordination has been explored at length in "synfire" chain models (1, 3, 24, 28, 29), where synchrony arises through extensive excitatory coupling among neurons between network layers, our work addresses the distinct problem of quenching timing errors via external input. For instance, HVC-inspired computational work showed that zones of inhibitory feedback triggered by a propagating spike pulse could keep the spikes within the pulse synchronized without redundant excitatory connections (29). Our model expands on this picture by explaining how a propagating spike pulse or other sequential activity pattern could be kept synchronized with an external input, and in turn with other sequential activity patterns receiving the same input, all without requiring feedback about timing errors. A separate input-based model of neural timing showed how external oscillatory inputs matched to spike latencies in a feed-forward

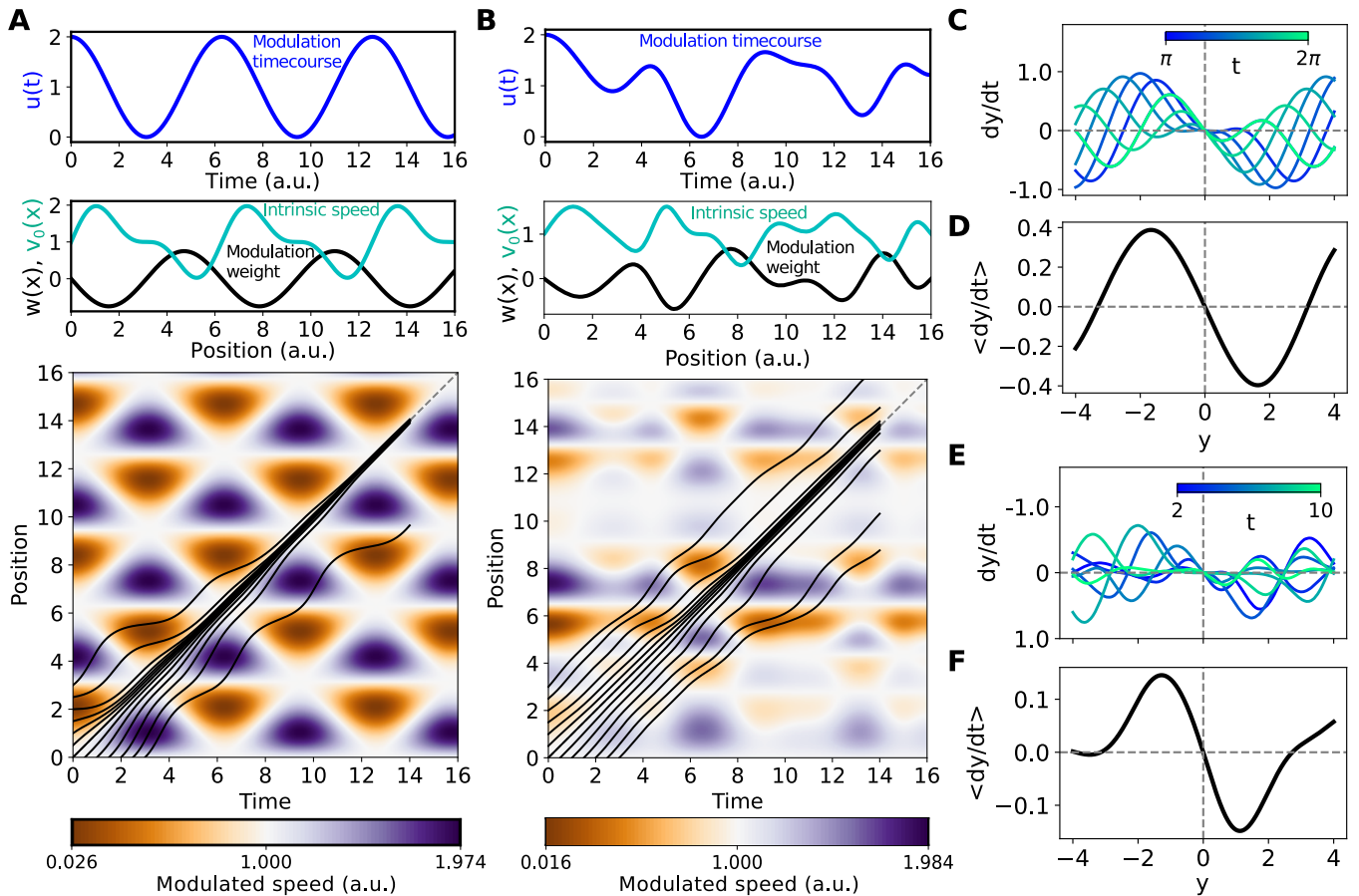


**Fig. 3. General conditions for a time-locking attractor to emerge from 1-D input.** A. Example intrinsic speed and modulation weight profile (middle) derived from a periodic input timecourse (top), with  $w(x) \propto du/dt|_{t=x}$ . Examples of sequence evolution through modulated speed landscape for various start times and positions (bottom). B. As in C but for an aperiodic input timecourse. C. Phase portrait of A in the moving reference frame  $y = x - t$  evaluated at several timepoints. D. Time average of momentary phase portraits in C (corresponding to speed landscape in A). E. Phase portrait of B in the reference frame  $y = x - t$  at several timepoints. F. Time averaged of phase portraits in E (corresponding to speed landscape in B). The time-averaged dynamics in D and F each exhibit a stable fixed point at  $y = 0$  corresponding to the sequence  $x(t) = t$ .

network could entrain the propagation of a spike pulse by imposing specific windows at which spikes can occur (16), suggestive of hippocampal spike sequences that are locked to high-frequency "ripple" events (30). Our work presents a distinct input-based mechanism grounded in speed control rather than neuronal properties (although still applicable to spiking networks [Fig 1]) and which requires time-varying but not necessarily oscillating input.

Our model effectively splits each motor process into a dynamical system specifying sequence order and a scalar input controlling timing. This is a simple and perhaps biologically favorable alternative to directly coupling multiple motor networks, which for long sequences would require coupling at many points over the sequence. During the course of development allocating timing precision to an external input could allow other features of the output sequence, such as syntax or instantaneous spectral content (19, 31) to be learned independently of timing, which might simplify and hasten learning.

How might the match between our input's time-derivative  $du/dt$  and spatial profile  $w(x)$  emerge or be maintained over time, for instance in the face of random synaptic fluctuations (32–34)? Recalling that  $w(x)$  in our spiking network model (Fig 1) represents the synaptic weight from the ex-

ternal input onto the neurons at position  $x$  in the chain, the relationship between  $du/dt$  and  $w(x)$  could potentially be stabilized by local spike-timing-dependent synaptic plasticity (STDP) rules (e.g. (35–39)). For instance, to keep the input synaptic weight  $w(x)$  sufficiently positive when  $du/dt|_{t=x}$  is positive (following the constraint in Eqn. 5), it could suffice to increase  $w(x)$  whenever a spike pulse passing through the chain link at position  $x$  at time  $t$  is accompanied by accelerating presynaptic spikes from the external input onto that chain link at  $t$ . One average, one might expect such a scenario to yield more postsynaptic-followed-by-presynaptic spike pairs—if the presynaptic spike rate is increasing, then in a small window around  $t$  there will be more presynaptic spikes in the later part of the window. An anti-Hebbian STDP rule (38) might then suffice to increase  $w(x)$  in response to the repeated occurrence of these spike pairs. Conversely, when  $du/dt|_{t=x}$  is negative, so that  $w(x)$  should also be sufficiently negative to satisfy (5), one might expect more presynaptic-followed-by-postsynaptic spike pairs. If  $w(x)$  were represented by an inhibitory synapse, a Hebbian STDP rule (35, 36, 39) could increase the weight of that synapse to make  $w(x)$  more negative. While more work will be required to illuminate the details of how such plasticity mech-

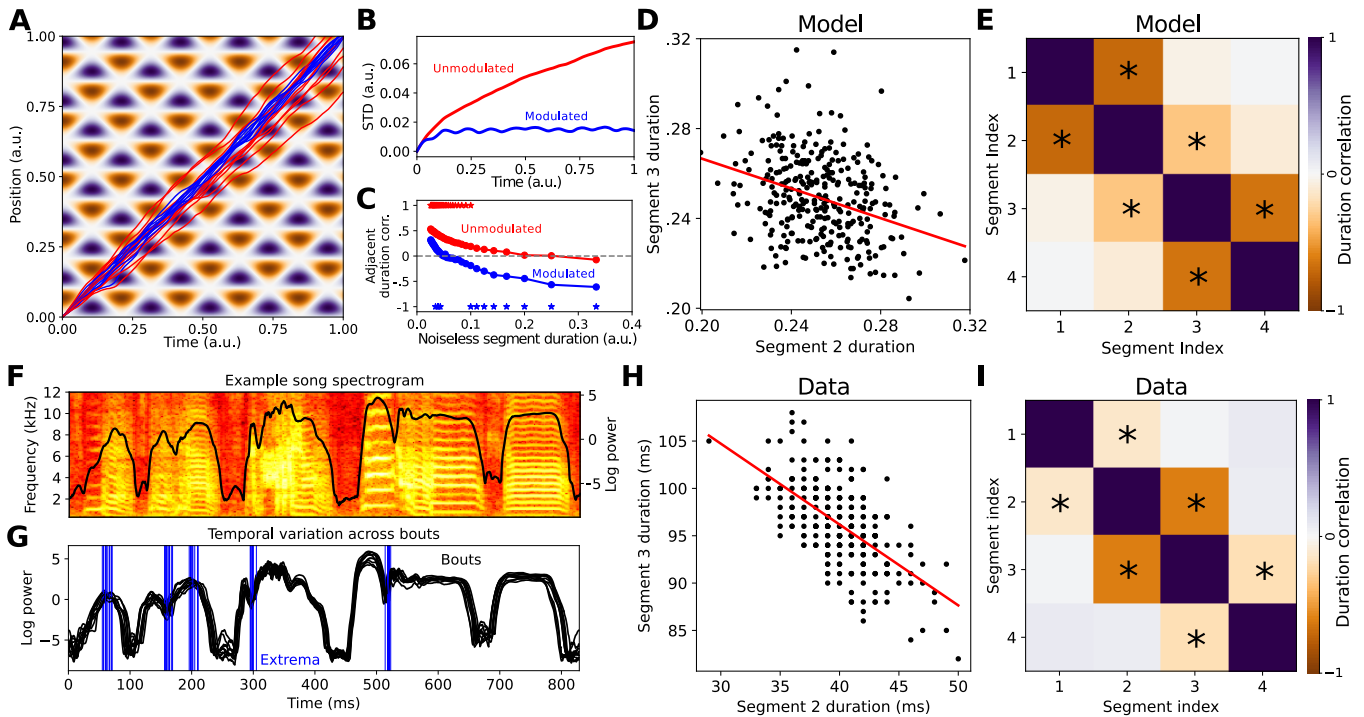


**Fig. 4. Correlated fluctuations in motor output timing.** A. Example noisily propagating output sequences while modulated (blue) or not modulated (red) by underlying speed landscape (background) generated by 1-D input fluctuations. B. Growth of standard deviation of sequence position over time for modulated and unmodulated sequences, corresponding to 300 sample sequences as demonstrated in A. C. Pearson correlation (across trials) between durations of adjacent segments (averaged across segment pairs) of the output sequence vs the noiseless segment duration, for modulated (black) and unmodulated (orange) trials. Stars indicate an average  $p < .05$  (two-sided t-test for zero-valued correlation coefficient) across segment pairs. D. Durations of second and third segments (given 4 equal segments total, each with a noiseless duration of .25) across trials, and best fit line ( $R = -.324, p < 10^{-8}$ ). E. Correlation matrix between durations of all segment pairs in simulated motor output. Stars indicate correlations with  $p < .05$ . F. Spectrogram of example zebra finch song motif, with log power overlaid in black. G. Log power of the same song motif across several bout renditions in one bird. Blue lines show extrema used to define song segment boundaries before quantifying variation across renditions. H, I. As in D, E but for real zebra finch song segments ( $N = 292$ ). ( $R = -.62, p < 10^{-31}$  for best fit line in H.)

animals could stabilize or even give rise to the spatial input profile suggested by our model, the local nature of the plasticity required along with the lack of fine-tuning in our model suggest a bioplausible maintenance or development process that could achieve this.

We expect the role of thalamocortical inputs we have proposed to co-exist with other thalamic functions and multi-area interactions. Baseline Uva input to HVC, for instance (21), may be required for song production regardless of temporal precision; thalamic inputs also likely contribute to setting movement preparatory states in cortex (12–15). Thus, one may expect to observe multiple functions superimposed in thalamocortical input dynamics measured experimentally. In birds Uva and HVC are embedded within a larger brainstem-thalamocortical loop (22) that indirectly couples the two hemispheres, which may be involved in the slowing of song when HVC is only cooled unilaterally (40). Our model posits that such coupling is nonetheless strictly gated by low-dimensional Uva inputs to HVC, with Uva sending predominantly timing signals, while all ordering and spectral information is contained within HVC’s recurrent and downstream connectivity (although other HVC inputs may contain additional syntactic information, i.e. influencing the order in which HVC neurons fire (19)). Our work thus contrasts with models of birdsong neurophysiology in which the network connections encoding sequence order are coiled around the brainstem-thalamocortical loop

(41, 42); we instead ascribe sequence ordering and timing functions predominantly to HVC and Uva, respectively.

Although not easily dissociated from the multi-functional system it is embedded in, our model makes additional predictions. First, it predicts that Uva inputs onto HVC should exhibit significant spatial structure relative to song position. Specifically, HVC neurons that spike during Uva increases should receive more excitation from Uva, and those that spike during decreases more inhibition (possibly via HVC interneurons). Although technically challenging, one could test this by tracing Uva-HVC projections and recording which HVC neurons spike at different points during song. More generally, our model predicts that removing temporal fluctuations from thalamic input to motor cortex should preclude timing error correction. This could be tested by silencing thalamus and directly activating thalamocortical axon terminals (10) with constant or ramping stimulation, which should increase variability in the total durations of the accompanying cortical and motor sequences, relative to stimulation matched to real thalamic fluctuations.

The central mechanism in our model applies to sequence generators beyond chain networks. One only requires a sufficiently ordered sequence to support a notion of time-varying position  $x(t)$ , and a fluctuating input that modulates  $dx/dt$  differently at different  $x$ . The first condition is met, for instance, by neural activity that evolves along a time-ordered manifold, a topology hypothesized to underlie dy-

namics in several cortical areas (43), or through a sequence of metastable network attractors (9). To model timing control in such a system one could extend work on input-dependent speed control of recurrent network dynamics (17) by making the input itself (presumably coming from another brain area) dynamic and localizing its slowing and/or accelerating effects to different regions of the sequence. Finally, time-locking attractors from scalar input fluctuations may have applications outside neuroscience, for instance in coordinating cellular processes via fluctuating molecular concentrations or synchronizing growth processes across a population of organisms via fluctuating temperature or sunlight.

## Methods

**Neuron and synaptic dynamics.** Our spiking network used integrate-and-fire neurons, which receive conductance inputs from excitatory and inhibitory neurons, and in which adaptation is modeled as a self-inhibitory synaptic current:

$$\frac{c_m}{g_m} \frac{dv^i}{dt} = -(v^i - E_L) + g_E^i(t)(E_E - v^i) + g_I^i(t)(E_E - v^i) + g_A^i(t)(E_A - v^i) + \eta(t), \quad (7)$$

where

$$g_Q^i(t) = \sum_j \sum_k w_{ij}^Q h(t) * \delta(t - t_k^j) \quad (8)$$

and  $v^i$  is the  $i$ -th neuron's membrane voltage;  $\eta$  is a white noise current;  $c_m = 1\mu F/cm^2$  and  $g_m = 100\mu S/cm^2$  are the membrane leak capacitance and conductance, yielding a membrane time constant of  $\tau_m = c_m/g_m = 10ms$ ;  $E_L = -60mV$ ,  $E_E = 0mV$ ,  $E_I = -80mV$ ,  $E_A = -100mV$  are the leak, excitatory, inhibitory, and adaptation reversal potentials;  $g_Q^i$ ,  $Q \in \{E, I, A\}$  are the relative excitatory, inhibitory, and adaptation conductances;  $w_{ij}^Q$  is the weight of synapse type  $Q$  onto neuron  $i$  from  $j$ ;  $t_k^j$  is the  $k$ -th spike time of neuron  $j$ ; and  $h(t)$  is an exponential filter with time constants  $\tau_E = \tau_I = 2ms$ ,  $\tau_A = 10ms$ . Neurons spiked when  $v^i \geq v_{th} = -50mV$  and were reset to  $E_L = -60mV$  for a  $2ms$  refractory period. The simulation timestep was  $\Delta t = .5ms$ , and  $\eta\Delta t \sim \mathcal{N}(0, \sigma^2 = .01nA^2s)$ .

**Network architecture.** Our spiking network comprised 321 chain "links", each containing 30 excitatory neurons. Recurrent (within a link) weights were only excitatory and equal to  $w_{ij}^E = 1.4 \times 10^{-5}$  with probability .6 and 0 otherwise. Feed-forward weights were excitatory and all-to-all from each link to its successor with  $w_{ij}^E = .65, 1.0$ , or  $1.4 \times 10^{-5}$ , corresponding to weak, medium or strong connections (Fig 1B). Adaptation "weights" for all neurons were  $w_{ii}^A = 6 \times 10^{-5}$ . All feed-forward weights being set to "medium" supported a self-sustained spike burst (approx. 3-5 spikes over 5-10 ms in each neuron) propagating from link to link. Last, neurons received E and I synapses capable of transmitting Uv-like input spikes, with  $w_{ij}^E = 6 \times 10^{-6}$  and  $w_{ij}^I = 2 \times 10^{-5}$  for E or I external inputs. In Fig 1B, contiguous sets of 58

chain links alternated between receiving external E or I input synapses, and feed-forward weights alternated between 58 medium weights, 29 weak weights, 29 strong weights, etc. (black). In Fig 1C,  $w_{ij}^E = w_{ij}^I = 0$  for all external inputs, and all feed-forward weights were medium. In Fig 1B, external inputs alternated between a 50 ms "on" state and a 50 ms "off" state corresponding to 800 Hz and 0 Hz input spike frequencies, and in Fig 1C were off throughout the whole simulation.

**Time-locking attractor simulations.** Example output sequences in Fig 2D-G began at 9 evenly spaced start positions spanning one spatial period of the shown speed landscape. In Fig 3, simulations used an integration timestep of  $\Delta t = .001$ . In Fig 3D,  $u(t)$  was sampled from a white-noise process smoothed with a Gaussian kernel with width  $.9/\Delta t$ ;  $w(x)$  was chosen to be  $.65du/dt|_{t=x}$ , and  $v_0(x) = 1 - u(x)w(x)$ .

**Data analysis.** Song renditions were recorded from adult male zebra finches during an "undirected" song context (no female present) and transformed into spectrograms using a short-time Fourier transform. The power of the logarithm of the spectrogram was computed at each timepoint to get a scalar representation of song, from which peaks were identified and used to define song segment boundaries (only peaks that could be reliably identified across renditions were used as boundaries). Durations of each segment were then extracted and correlations among resulting segment durations computed across song renditions.

## Acknowledgments

We would like to acknowledge Nader Nikbakht and Jonathan Pillow for helpful discussions regarding the preparation of this manuscript. This work was supported by the Simons Foundation's Simons Collaboration for the Global Brain and by NIH 1R01NS104925.

1. Moshe Abeles. *Local cortical circuits: An electrophysiological study*, volume 6. Springer Science & Business Media, 1982.
2. David Kleinfeld. Sequential state generation by model neural networks. *Proceedings of the National Academy of Sciences*, 83(24):9469–9473, 1986.
3. Moshe Abeles, Gaby Hayon, and Daniel Lehmann. Modeling compositionality by dynamic binding of synfire chains. *Journal of computational neuroscience*, 17(2):179–201, 2004.
4. David Sussillo and Larry F Abbott. Generating coherent patterns of activity from chaotic neural networks. *Neuron*, 63(4):544–557, 2009.
5. Ila R Fiete, Walter Senn, Claude ZH Wang, and Richard HR Hahnloser. Spike-time-dependent plasticity and heterosynaptic competition organize networks to produce long scale-free sequences of neural activity. *Neuron*, 65(4):563–576, 2010.
6. Michael A Long, Dezhe Z Jin, and Michale S Fee. Support for a synaptic chain model of neuronal sequence generation. *Nature*, 468(7322):394–399, 2010.
7. Rodrigo Laje and Dean V Buonomano. Robust timing and motor patterns by taming chaos in recurrent neural networks. *Nature neuroscience*, 16(7):925–933, 2013.
8. Kanaka Rajan, Christopher D Harvey, and David W Tank. Recurrent network models of sequence generation and memory. *Neuron*, 90(1):128–142, 2016.
9. Stefano Recanatesi, Ulises Pereira-Oblinovic, Masayoshi Murakami, Zachary Mainen, and Luca Mazzucato. Metastable attractors explain the variable timing of stable behavioral action sequences. *Neuron*, 110(1):139–153, 2022.
10. Britton A Sauerbrei, Jian-Zhong Guo, Jeremy D Cohen, Matteo Mischiati, Wendy Guo, Mayank Kabra, Nakul Verma, Brett Mensh, Kristin Branson, and Adam W Hantman. Cortical pattern generation during dexterous movement is input-driven. *Nature*, 577(7790):386–391, 2020.
11. Hsi-Ping Wang, Jonathan W Garcia, Carl F Sabotke, Donald J Spencer, and Terrence J Sejnowski. Feedforward thalamocortical connectivity preserves stimulus timing information in sensory pathways. *Journal of Neuroscience*, 39(39):7674–7688, 2019.
12. Julien Catanese and Dieter Jaeger. Premotor ramping of thalamic neuronal activity is modulated by nigral inputs and contributes to control the timing of action release. *Journal of Neuroscience*, 41(9):1878–1891, 2021.
13. Matthew T Kaufman, Mark M Churchland, Stephen I Ryu, and Krishna V Shenoy. Cortical activity in the null space: permitting preparation without movement. *Nature neuroscience*, 17(3):440–448, 2014.

14. Afsheen Afshar, Gopal Santhanam, M Yu Byron, Stephen I Ryu, Maneesh Sahani, and Krishna V Shenoy. Single-trial neural correlates of arm movement preparation. *Neuron*, 71(3):555–564, 2011.
15. Laureline Logiacco, LF Abbott, and Sean Escola. Thalamic control of cortical dynamics in a model of flexible motor sequencing. *Cell Reports*, 35(9):109090, 2021.
16. Sven Jahnke, Raoul-Martin Memmesheimer, and Marc Timme. Oscillation-induced signal transmission and gating in neural circuits. *PLoS computational biology*, 10(12):e1003940, 2014.
17. Jing Wang, Devika Narain, Eghbal A Hosseini, and Mehrdad Jazayeri. Flexible timing by temporal scaling of cortical responses. *Nature neuroscience*, 21(1):102–110, 2018.
18. Christopher M Glaze and Todd W Troyer. Temporal structure in zebra finch song: implications for motor coding. *Journal of Neuroscience*, 26(3):991–1005, 2006.
19. Yarden Cohen, Jun Shen, Dawit Semu, Daniel P Leman, William A Liberti, L Nathan Perkins, Derek C Liberti, Darrell N Kotton, and Timothy J Gardner. Hidden neural states underlie canary song syntax. *Nature*, 582(7813):539–544, 2020.
20. Richard HR Hahnloser, Alexay A Kozhevnikov, and Michale S Fee. An ultra-sparse code underlies the generation of neural sequences in a songbird. *Nature*, 419(6902):65–70, 2002.
21. Husain H Danish, Dmitry Aronov, and Michale S Fee. Rhythmic syllable-related activity in a songbird motor thalamic nucleus necessary for learned vocalizations. *PLoS one*, 12(6):e0169568, 2017.
22. Marc F Schmidt. Pattern of interhemispheric synchronization in hvc during singing correlates with key transitions in the song pattern. *Journal of neurophysiology*, 90(6):3931–3949, 2003.
23. Steven H Strogatz. *Nonlinear dynamics and chaos with student solutions manual: With applications to physics, biology, chemistry, and engineering*. CRC press, 2018.
24. Dezhe Z Jin, Fethi M Ramazanoğlu, and H Sebastian Seung. Intrinsic bursting enhances the robustness of a neural network model of sequence generation by avian brain area hvc. *Journal of computational neuroscience*, 23(3):283–299, 2007.
25. Georg Kosche, Daniela Vallentin, and Michael A Long. Interplay of inhibition and excitation shapes a premotor neural sequence. *Journal of Neuroscience*, 35(3):1217–1227, 2015.
26. Alison Duffy, Elliott Abe, David J Perkel, and Adrienne L Fairhall. Variation in sequence dynamics improves maintenance of stereotyped behavior in an example from bird song. *Proceedings of the National Academy of Sciences*, 116(19):9592–9597, 2019.
27. Jeffrey E Markowitz, William A Liberti III, Grigori Guitchounts, Tarciso Velho, Carlos Lois, and Timothy J Gardner. Mesoscopic patterns of neural activity support songbird cortical sequences. *PLoS biology*, 13(6):e1002158, 2015.
28. Markus Diesmann, Marc-Oliver Gewaltig, and Ad Aertsen. Stable propagation of synchronous spiking in cortical neural networks. *Nature*, 402(6761):529–533, 1999.
29. Jonathan Cannon, Nancy Kopell, Timothy Gardner, and Jeffrey Markowitz. Neural sequence generation using spatiotemporal patterns of inhibition. *PLoS computational biology*, 11(11):e1004581, 2015.
30. Shantanu P Jadhav, Caleb Kemere, P Walter German, and Loren M Frank. Awake hippocampal sharp-wave ripples support spatial memory. *Science*, 336(6087):1454–1458, 2012.
31. Fernando Nottebohm. The neural basis of birdsong. *PLoS biology*, 3(5):e164, 2005.
32. Gianluigi Mongillo, Simon Rumpel, and Yonatan Loewenstein. Intrinsic volatility of synaptic connections—a challenge to the synaptic trace theory of memory. *Current opinion in neurobiology*, 46:7–13, 2017.
33. Noam E Ziv and Naama Brenner. Synaptic tenacity or lack thereof: spontaneous remodeling of synapses. *Trends in neurosciences*, 41(2):89–99, 2018.
34. Lee Susman, Naama Brenner, and Omri Barak. Stable memory with unstable synapses. *Nature communications*, 10(1):1–9, 2019.
35. Guo-qiang Bi and Mu-ming Poo. Synaptic modifications in cultured hippocampal neurons: dependence on spike timing, synaptic strength, and postsynaptic cell type. *Journal of neuroscience*, 18(24):10464–10472, 1998.
36. Henry Markram, Joachim Lübke, Michael Frotscher, and Bert Sakmann. Regulation of synaptic efficacy by coincidence of postsynaptic apss and epsps. *Science*, 275(5297):213–215, 1997.
37. Katherine Buchanan and Jack Mellor. The activity requirements for spike timing-dependent plasticity in the hippocampus. *Frontiers in synaptic neuroscience*, 2:11, 2010.
38. Claire Piochon, Peter Kruskal, Jason MacLean, and Christian Hansel. Non-hebbian spike-timing-dependent plasticity in cerebellar circuits. *Frontiers in Neural Circuits*, 6:124, 2013.
39. Tim P Vogels, Robert C Froemke, Nicolas Doyon, Matthieu Gilson, Julie S Haas, Robert Liu, Arianna Maffei, Paul Miller, Corette Wierenga, Melanie A Woodin, et al. Inhibitory synaptic plasticity: spike timing-dependence and putative network function. *Frontiers in neural circuits*, 7:119, 2013.
40. Michael A Long and Michale S Fee. Using temperature to analyse temporal dynamics in the songbird motor pathway. *Nature*, 456(7219):189–194, 2008.
41. Leif Gibb, Timothy Q Gentner, and Henry DI Abarbanel. Brain stem feedback in a computational model of birdsong sequencing. *Journal of neurophysiology*, 102(3):1763–1778, 2009.
42. Kosuke Hamaguchi, Masashi Tanaka, and Richard Mooney. A distributed recurrent network contributes to temporally precise vocalizations. *Neuron*, 91(3):680–693, 2016.
43. Sue Ann Koay, Adam S Charles, Stephan Y Thiberge, Carlos D Brody, and David W Tank. Sequential and efficient neural-population coding of complex task information. *Neuron*, 110(2):328–349, 2022.